THE DESIGN AND SYNTHESIS OF POLYMERIC ASSEMBLIES FOR MATERIALS APPLICATIONS: CHEMOSENSING, LIQUID CRYSTAL ALIGNMENT AND BLOCK COPOLYMERS

by

Jason R. Cox

B.S. (with Distinction), Chemistry
Worcester Polytechnic Institute, 2005

M.S., Chemistry
Worcester Polytechnic Institute, 2009

Submitted to the Department of Chemistry
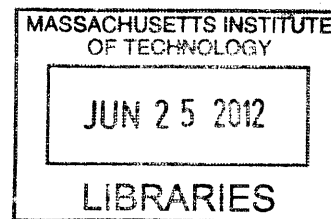in Partial Fulfillment of the Requirements for the Degree of
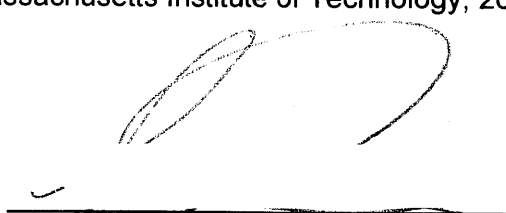
Doctor of Philosophy

at the

Massachusetts Institute of Technology

June 2012

Signature of Author: _____

Department of Chemistry
May 24, 2012

Certified by: _____

Timothy M. Swager
Thesis Supervisor

Accepted by: _____

Robert W. Field
Chairman, Departmental Committee on Graduate Studies

This doctoral thesis has been examined by a Committee of the
Department of Chemistry as follows:

Professor Stephen L. Buchwald: _____

Thesis Committee Chair

Professor Timothy M. Swager: _____

Thesis Supervisor

Professor Gregory C. Fu: _____

Department of Chemistry

THE DESIGN AND SYNTHESIS OF POLYMERIC ASSEMBLIES FOR MATERIALS APPLICATIONS: CHEMOSENSING, LIQUID CRYSTAL ALIGNMENT AND BLOCK COPOLYMERS

by

Jason R. Cox

ABSTRACT

Conjugated polymers are an indispensable class of materials that have advanced the development of optoelectronic device architectures; in part, due to their outstanding electronic and mechanical properties. This thesis explores the utility of rationally designed energy transfer cascades involving conjugated polymers that can be used in applications such as chemosensing and liquid crystal alignment.

We begin by describing the design and development of a new transduction mechanism for the detection of cyclic ketones – molecules that are found in plasticized explosives. We discuss the synthesis of a new reporter dye bearing a receptor for cyclic ketones that is capable of undergoing efficient energy transfer with conjugated polymers. We further describe the optimization of a thin-film sensor comprised of these two components as well as its performance and selectivity.

In the next chapter we describe the design and synthesis of two new polymers that are capable of undergoing the di-π-methane rearrangement. We begin by describing the synthesis and photochemistry of the polymers as well as a model compound. The polymers contain triplet sensitizers built into the polymer backbone thereby creating an energy transfer cascade that facilitates the di-π-methane rearrangement. These materials are then evaluated as liquid crystal alignment layers for optoelectronic applications.

In the final chapter, we describe the end-capping of cross-coupling polymerizations using the hydroarylation of norbornadiene. This reaction is shown to be an efficient approach to generating macroinitiators which can be further polymerized using ring opening metathesis polymerization. These end-capped materials can also be crosslinked into hybrid materials that show promise as thin-film sensors for volatile organic compounds.

Dedicated to my girls-Maegan and Norah Faith –

for their unwavering support and understanding

TABLE OF CONTENTS

LIST OF ABBREVIATIONS

AFP	amplifying fluorescent polymer
CP	conjugated polymer
DART	direct analysis in real time
DMF	dimethylformamide
DMSO	dimethyl sulfoxide
DNT	2,4-dinitrotoluene
EET	electronic energy transfer
E_T	triplet energy
FRET	Förster resonance energy transfer
GRIM	Grignard metathesis reaction
HOMO	highest occupied molecular orbital
HRMS	high-resolution mass spectra
IC	internal conversion
IMS	ion mobility spectrometry
ISC	intersystem crossing
k_{ET}	rate of energy transfer
LCD	liquid crystal display
LCM	liquid crystal material
LOD	limit of detection
LUMO	lowest unoccupied molecular orbital
M_n	number-average molecular weight
MS	mass spectroscopy
NIR	near infrared
NMR	nuclear magnetic resonance
OLED	organic light emitting diode
OPV	organic photovoltaics
PDI	polydispersity index
PET	photoinduced electron transfer
PETN	pentaerythritol tetranitrate
POM	polarized optical microscopy
QCM	quartz crystal microbalance
RDX	1,3,5-trinitro-1,3,5-triazacyclohexane
ROMP	ring-opening metathesis
SEC	size-exclusion chromatography
T_g	glass transition temperature
THF	tetrahydrofuran
THz-TDS	terahertz time domain spectroscopy
TNT	2,4,6-trinitrotoluene
UV	ultraviolet
VOC	volatile organic compound

LIST OF FIGURES FROM MAIN TEXT

emission of **SQ1** is suppressed (top, left). The film is then sparged with a stream of N_2 and a subsequent spectrum recorded (top, middle). The same film is heated to 120 °C for 10 minutes and an additional spectrum recorded (top, right). The resulting film is then re-exposed to the saturated vapor of cyclohexanone (bottom, middle) (λ_{ex} = 400 nm).

LIST OF SCHEMES FROM MAIN TEXT

in this work (bottom).

Scheme 4.6. Conditions and monomers used for the formation of triblock
copolymers.   **111**

LIST OF TABLES FROM MAIN TEXT

Chapter 1

Introduction to Electronic Energy Transfer in Conjugated Systems

1.1 Introduction

In 1953, Hermann Staudinger received the Nobel Prize for his role in the development of macromolecular chemistry,[1] a field that was surprisingly underdeveloped despite the ubiquity of polymers in naturally occurring systems. During his lecture he stated, "I sincerely hope that this great distinction will be the means whereby macromolecular chemistry will undergo further fruitful development."[2] This wish was undoubtedly fulfilled as exemplified by the impact of polymeric materials in every aspect of human life.[3] A second Nobel Prize was awarded to Alan J. Heeger, Alan G. MacDiarmid, and Hideki Shirakawa in 2000 for their pioneering work with conductive (conjugated) polymers whereby a new sub-field of macromolecular chemistry was born.[4] Conjugated polymers; that is, polymeric materials that contain alternating single and multiple bonds, occupy a venerable role in device architectures as they combine the optoelectronic properties of semiconductors with the mechanical properties of organic polymers.[5] These materials are readily synthesized using standard carbon-carbon bond forming techniques and are typically soluble materials that can be processed into thin-films over large areas.[6] Initially, these materials found utility in devices such as organic light emitting diodes (OLEDs) due to their excellent luminescent properties and have since matured into materials for organic photovoltaics (OPV) and sensing applications.[7] The latter two applications take advantage of the electronic and photophysical properties of conjugated polymers, namely exciton migration, which will be described in the following sections.

1.2 Photophysical Processes of Organic Materials

In order to fully understand the photophysical properties of conjugated polymers, it is first necessary to understand the various transitions that are available to organic molecules when they interact with electromagnetic radiation. The different transitions are best explained with the

aid of a Jablonski diagram (Figure 1.1). The generation of an excited stated is a direct result of the interaction of electrons in the highest occupied molecular orbital (HOMO) with the oscillating electric and magnetic fields of a photon. The oscillating electric field couples with the electron and if certain energetic (band gap) and geometric (field is oscillating in the same direction as the transition dipole moment) considerations are met, the electron will be promoted to the lowest unoccupied molecular orbital (LUMO) or higher unoccupied orbitals.[8]
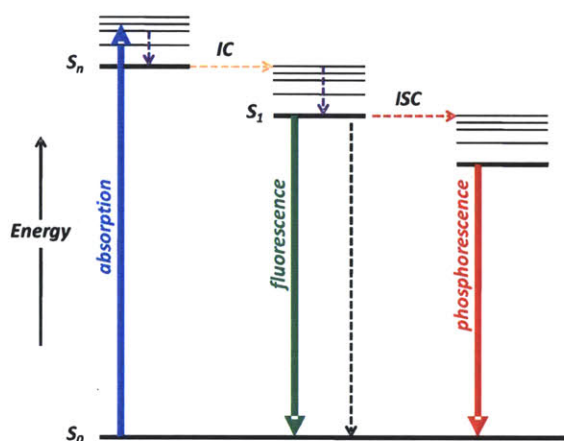
Figure 1.1 Jablonski diagram depicting the photophysical pathways available to an organic molecule after excitation with a photon. Photochemical transformations have been omitted; however, in many cases reactivity initiated from the excited state is the dominant pathway.

After excitation, the molecule will rapidly relax to the lowest vibrational level of the first excited singlet state in a process known as internal conversion (IC). From here, a number of pathways are possible including fluorescence, non-radiative decay, intersystem crossing (ISC) and phosphorescence.[9] An additional deactivation process is called electronic energy transfer (EET) whereby the excited state of a molecule (donor) transfers its energy non-radiatively to a

nearby molecule (acceptor) (Figure 1.2). There are two possible mechanisms for energy transfer – Förster resonance energy transfer (FRET)[10] and Dexter energy transfer.[11]
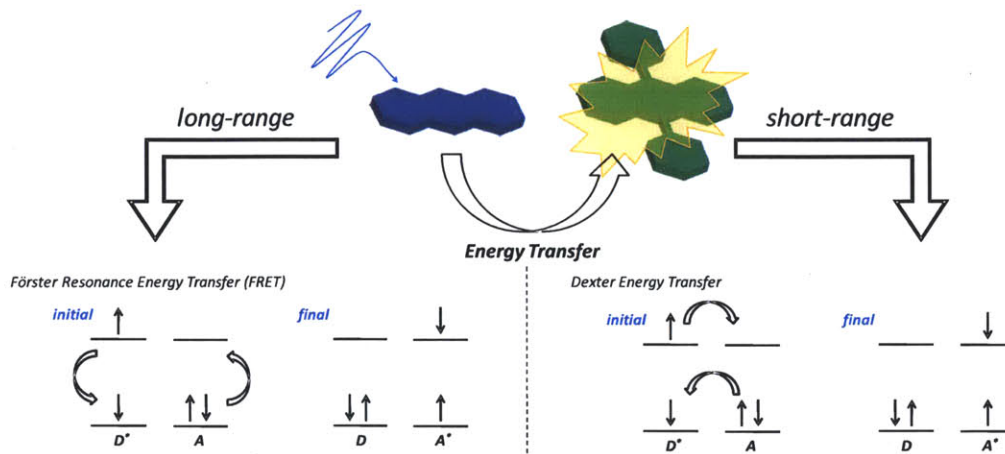
Figure 1.2 Schematic depiction of electronic energy transfer between a donor and acceptor. Both modes of non-trivial EET are described – FRET (left) and exchange transfer (right).

1.3 Mechanisms for Electronic Energy Transfer – FRET and Electron Exchange

The excited state of an organic chromphore is itself an oscillating dipole; as such, it is capable of inducing a resonant interaction with nearby molecules whereby the excitation energy is transferred from the donor molecule to the acceptor molecule (Figure 1.2 left). This type of energy transfer is known as FRET and is the dominant form of energy transfer between organic compounds.[12] It is not to be confused with trivial modes of energy transfer whereby the emission of a photon from a donor chromophore is reabsorbed by an acceptor molecule followed by emission. In the case of FRET, the transfer process results in a diminished lifetime of the donor which would not be observed in the trivial case. The rate of energy transfer (k_{ET}) is described by Equations 1-3 where τ_D is the lifetime of the donor, R_0 is the Förster radius, R is the distance between donor and acceptor molecules, κ^2 is an orientation factor, $F_D(\lambda)$ describes the

22

normalized fluorescence intensity of the donor, $\varepsilon_A(\lambda)$ represents the molar extinction coefficient

of the acceptor, and J is the spectral overlap integral.

$$k_{ET} = \frac{1}{\tau_D} \cdot \left(\frac{R_0}{R}\right)^6 \qquad (1)$$

$$R_0{}^6 = \frac{9000ln10}{128\pi^5 N_A} \frac{\kappa^2 Q_D}{n^4} J \qquad (2)$$

$$J = \int_0^\infty F_D(\lambda)\ \varepsilon_A(\lambda)\ \lambda^4 d\lambda \qquad (3)$$

These equations describe a system in which the efficiency of EET is directly proportional

to the spectral overlap integral and inversely proportional to R^6. These predictable dependencies

have made FRET an indispensable analytical tool for measuring sub-nanometer intermolecular

separations.

The exchange, or Dexter mechanism, describes a situation where the donor and acceptor

molecules formally exchange electrons (Figure 1.2 right). This implies that the two components

exist at intermolecular separations small enough to permit overlap of the involved orbitals. The

rate constant for the exchange mechanism is described by Equation 4 where K describes specific

orbital interactions, J' is the normalized spectral overlap integral, R is the intermolecular

separation between donor and acceptor, and L is the sum of the van der Waals radii.

$$k_{ET} = KJ' \exp\left(-\frac{2R}{L}\right) \qquad (4)$$

Implicit in this description is the steep dependency of k_{ET} on the intermolecular

separation of donor and acceptor. The exponential drop-off in exchange efficiency with

increasing separation results in a process that can only occur over distances of 1 or 2 molecular

diameters – a point that is central to the work described here.

It is worth summarizing the key differences between these two forms of EET: (i) the

efficiency of energy transfer is dependent on the oscillator strength for the transitions $D^* \rightarrow D$ and

$A \rightarrow A^*$ in the case of Förster energy transfer unlike the exchange mechanism, (ii) the distance dependence for Dexter energy transfer ($\exp(-2R/L)$ is much stronger than for FRET ($1/R^6$) and (iii) only for exchange interactions are triplet states allowed to transfer. The first difference highlights an important distinction between the two mechanisms – the spectral overlap integral for the exchange mechanism is not dependent on the intensity of the overlapping transitions. Conversely, the Förster mechanism is strongly dependent on the oscillator strength of the $A \rightarrow A^*$ transition.

1.4 Photophysical Processes in Conjugated Polymers

In many ways, the processes that have been described for small organic molecules thus far also pertain to larger systems such as conjugated polymers (CPs). Events such as absorption/emission of a photon, internal conversion, intersystem crossing and energy transfer have all been observed with CPs.[13] However, there are some subtle differences between these two classes of materials that are a result of the extended conjugation in such systems.

As shown in Figure 1.3, the sequential addition of unsaturated centers results in a narrowing of the band gap (E_g) until the electronic system more closely resembles an inorganic semiconductor possessing valence and conduction bands.[14] Absorption of a photon generates a strongly bound electron-hole pair (exciton) that is capable of diffusing along the polymer backbone as well as hopping from one polymer chain to another.[15] The diffusion length of an exciton, ranging from 5 to 14 nm,[16] means that a single excitation can sample many different polymer subunits prior to a photophysical process taking place. In Figure 1.3 (right) we have illustrated a process where the exciton is quenched by two sequential electron transfer events with an analyte – a process known as photoinduced electron transfer (PET). It is important to note that the diffuse nature of the exciton increases sensory gain as a single analyte molecule is

capable of quenching an entire polymer chain.[7] The Swager group has devised a number of sensing applications that exploit this characteristic including a system that boasts the highest sensitivity for the detection of trinitrotoluene (TNT) vapor.[17]
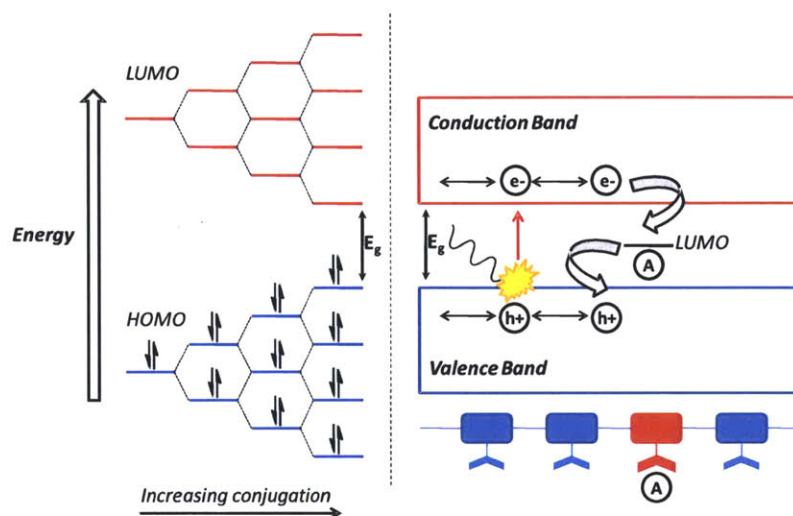
Figure 1.3 Schematic depiction of the band gap (E_g) of extended conjugated systems (left) and the relationship between semiconductor band structure and conjugated polymers (right).

In addition, the Swager group has shown that exciton migration is greatly increased when the polymer molecules are aggregated.[18] The condensed nature of an aggregated system gives rise to decreased interpolymer separations thereby facilitating multidimensional exciton transport. Figure 1.3 depicts an idealized situation that assumes the polymer subunits are coplanar thus enforcing the band gap perturbations that result from extended conjugation. In practice, polymer molecules are typically coiled or aggregated to some degree, especially high molecular weight materials. The result is that there is a collection of chromophores within each polymer strand that differ in effective conjugation length and hence band gap. This point is illustrated schematically in Figure 1.4.

25

emission

exciton migration

exciton formation

longer effective conjugation length
smaller E_g
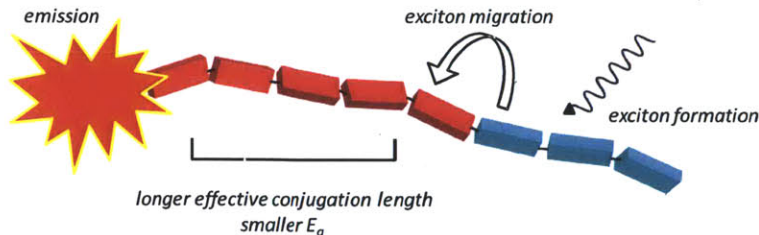
Figure 1.4 Schematic depiction of conformational effects on band gap structure and photophysical properties of conjugated polymers. At the interface of the light blue and red subunits is a 90 □ twist in the polymer chain, this generates two separate chromophoric subunits.

As shown in Figure 1.4, initial excitation of a smaller (larger band gap) conjugated subunit generates an exciton that rapidly diffuses to the lower energy (smaller band gap) subunit and then radiatively decays to the ground state. This exemplifies why conjugated polymers often exhibit broad structureless absorbance spectra yet also exhibit well structured emission spectra. This seemingly paradoxical situation arises from the fact that a coiled CP chain possesses a variety of different chromophoric subunits – each with a different bad gap that can absorb a photon – while the emission spectra is controlled by exciton diffusion to the smallest band gap subunit in the chain.

Thus far we have described situations where an analyte may quench CP emission as well as how excitons will diffuse to and emit from small band gap subunits; however, we have not described the situation where a small band gap analyte acts as an emissive quencher. If we consider the fact that excitons readily diffuse to small band gap defects in CP chains then we would expect that amplified emission from an emissive quencher doped into a CP film should also occur. Indeed, the Swager group has shown that covalently attached emissive defects will emit strongly when the CP is excited[19] as well as films that have been doped with small molecule dyes.[20] This work showed that the CP unit can behave as a light-harvesting antennae which

26

funnels excitons to the small band gap traps and actually amplifies their emission via energy transfer (Figure 1.5).
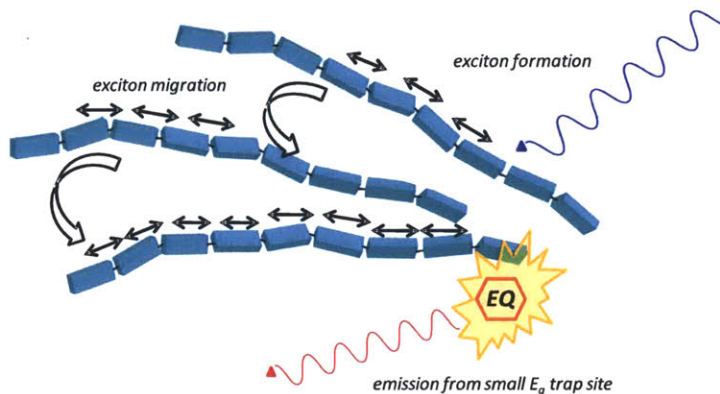
Figure 1.5 Schematic depiction of energy migration to an emissive defect in a CP thin film.

1.5 Summary

In summary, the photphysical processes available to the excited states of organic molecules and conjugated polymers have been described. Behavioral distinctions between the two classes of materials are governed by excition diffusion and energy transfer processes. This brief introduction highlights the essential characteristics of electronic energy transfer in order to be described in subsequent chapters including the detection of ketone molecules in the vapor phase (Chapter 2), alignment of liquid crystalline materials (Chapter 3) and the photophysical properties of crosslinked CP materials (Chapter 4).

1.6 References

(1) (a) Staudinger, H. *Ber. Deut. Chem. Ges.* **1920**, *53*, 1073. (b) Staudinger, H. *Chem. Ztg.* **1953**, *77*, 679.

(2) Staudinger, H. *Nobel Lectures, Chemistry 1942-1962*, Elsevier Publishing Company:

Amsterdam, 1964.

(3) Polymers exhibit a wide range of properties that can be tuned for a given application ranging from high-strength materials to biopolymers. From elastomers to polyamides and conjugated polymers, polymer science has advanced nearly every scientific discipline.

(4) (a) Shirakawa, H.; Louis, E. J.; MacDiarmid, A. G.; Chiang, C. K.; Heeger, A. J. *J. Chem. Soc. Chem. Commun.* **1977**, 578. (b) Shirakawa, H. *Angew. Chem. Int. Ed.* **2001**, *40*, 2575. (c) MacDiarmid, A. G. *Angew. Chem. Int. Ed.* **2001**, *40*, 2581. (d) Heeger, A. J. *Angew. Chem. Int. Ed.* **2001**, *40*, 2591.

(5) (a) *Conjugated Polymers: The Novel Science and Technology of Highly Conducting and Nonlinear Optically Active Materials*; Brédas, J.-L.; Silbey, R. J., Eds.; KluwerAcademic Publishers: Boston, 1991. (b) *Conjugated Conducting Polymers*; Kiess, H. G.; Baeriswyl, D., Eds.; Springer-Verlag: New York, 1992. (c) Barashkov, N. N.; Gunder, O. A. *Fluorescent Polymers*; Ellis Horwood: NewYork, 1993. (d) *Conjugated Polymers and Related Materials: The Interconnection of Chemical and Electronic Structure*; Salaneck, W. R.; Lundström, I.; Rånby, B. G., Eds.;Oxford University Press: New York, 1993. (e) *Advances in Synthetic Metals: Twenty Years of Progress in Science and Technology*; Bernier, P.; Lefrant, S.; Bidan, G., Eds.; Elsevier: New York, 1999. (f) Roth, S.; Carroll, D. *One-Dimensional Metals: Conjugated Polymers, Organic Crystals, Carbon Nanotubes*, 2nd ed.; Wiley-VCH: Weinheim, 2004. (g) *Handbook of Conducting Polymers*, 3rd ed.; Skotheim, T. A.; Elsenbaumer, R. L.;Reynolds, J. R., Eds.; CRC Press: New York, 2007.

(6) Cheng, Y.-J.; Yang, S.-H.; Hsu, C.-S. *Chem. Rev.* **2009**, *109*, 5868.

(7) Many of these applications are referenced in Ref. 6, for more recent reviews the reader is directed to the following publications. For OLED applications: (a) Grimsdale, A. C.; Chan, K. L.; Martine, R. E.; Jokisz, P. G.; Holmes, A. B. *Chem. Rev.* **2009**, *109*, 897. (b) Beaujuge, P. M.; Reynolds, J. R. *Chem. Rev.* **2010**, *110*, 268. For OPV applications: Günes, S.; Neugebauer, H.; Sariciftci, N. S. *Chem. Rev.* **2007**, *107*, 1324. For chemical sensing: (a) McQuade, D. T.; Pullen, A. E.; Swager, T. M. *Chem. Rev.* **2000**, *100*, 2537. (b) Swager, T. M. *Acc. Chem. Res.* **1998**, *31*, 201. (c) Thomas III, S. W.; Joly, G. D.; Swager, T. M. *Chem. Rev.* **2007**, *107*, 1339.

(8) Turro, N. J. *Modern Molecular Photochemistry*; University Science Books:Sausalito, CA, 1991.

(9) Lakowicz, J. R. *Principles of Fluorescence Spectroscopy*, 2nd ed.; Kluwer Academic/Plenum:

New York, 1999.

(10) Förster, T. *Ann. Phys.* **1948**, *2*, 55.

(11) Dexter, D. L. *J. Chem. Phys.* **1953**, *21*, 836.

(12) Anslyn, E. V.; Dougherty, D. A. *Modern Physical Organic Chemistry;* University Science Books: Sausolito, CA, 2006.

(13) These photophysical processes are observed in a variety of applications, the reader is directed to Refs 5, 6 and 7 for more information.

(14) Moliton, A.; Hiorns, R. C. *Polym. Int.* **2004**, *53*, 1397.

(15) Yan, M.; Rothberg, L.; Hsieh, B. R.; Alfano, R. R. *Phys. Rev. B* **1994**, *49*, 9419-9422.

(16) (a) Theander, M.; Yartsev, A.; Zigmantas, D.; Sundstrom, V.; Mammo, W.; Andersson, M. R.; Inganas, O. *Phys. Rev. B* **2000**, *61*, 12957. (b) Haugeneder, A.; Neges, M.; Kallinger, C.; Spirkl, W.; Lemmer, U.; Feldmann, J.; Scherf, U.; Harth, E.; Gugel, A.; Mullen, K. *Phys. Rev. B* **1999**, *59*, 15346. (c) Halls, J. J. M.; Pichler, K.; Friend, R. H.; Moratti, S. C.; Holmes, A. B. *Appl. Phys. Lett.* **1996**, *68*, 3120. (d) Stubinger, T.; Brutting, W. *J. Appl. Phys.* **2001**, *90*, 3632.

(17) (a) Yang, J. S.; Swager, T. M. *J. Am. Chem. Soc.* **1998**, *120*, 5321-5322. (b) Yang, J. S.; Swager, T. M. *J. Am. Chem. Soc.* **1998**, *120*, 11864-11873.

(18) (a) McQuade, D. T.; Hegedus, A. H; Swager, T. M. *J. Am. Chem. Soc.* **2000**, *122*, 12389. (b) Levitsky, I. A.; Kim, J.; Swager, T. M. *J. Am. Chem. Soc.* **1999**, *121*, 1466.

(19) Swager, T. M.; Gil, C. J.; Wrighton, M. S. *J. Phys. Chem.* **1995**, *99*, 4886.

(20) Levine, M.; Song, I.; Andrew, T. L.; Kooi, S. E.; Swager, T. M. *J. Polym. Sci. A* **2010**, *48*, 3382.

Chapter 2
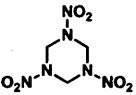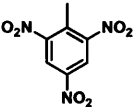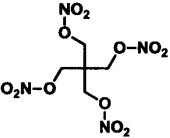
Interrupted Energy Transfer: Highly Selective Detection of Cyclic Ketones in the Vapor Phase

2.1 Introduction and Motivation for Ketone Detection

Plasticized explosives such as Composition C-4 and Semtex have drawn consiberable interest from government agencies due to the worldwide increase in terrorism related events.[1] These materials are typically comprised of approximately 90% energetic compounds and 10% binders/plasticizers.[2] The molecular structures and relevant physical properties of some expolsives and related materials are depicted in Table 2.1. In the case of C-4, the energetic material is 1,3,5-trinitro-1,3,5-triazacyclohexane (RDX). This compound exhibits an extremely low equilibrium vapor pressure – approximately 6 ppt at 25 °C.[3] Approaches to the detection of RDX rely upon mass spectroscopic (MS) techniques,[4] ion mobility spectrometry (IMS),[5] terahertz time domain spectroscopy (THz-TDS)[6] and various colorimetric and fluorescence techniques.[7]

Table 2.1. Names, molecular structures and equilibrium vapor pressures of explosives and related compounds.

Name	Molecular structure	Equilibrium vapor pressure at 20 °C (Torr)	Purpose
1,3,5-trinitro-1,3,5-triazacyclohexane (RDX)		4.1×10^{-9}	Energetic component C-4
2,4,6-trinitrotoluene (TNT)		1.1×10^{-6}	High explosive
Pentaerythritol tetranitrate (PETN)		3.8×10^{-10}	Energetic component of Semtex
Cyclohexanone		5 (25 °C)	Solvent used in the recrystallization of RDX

Each of these approaches carries with it a unique collection of advantages and limitations. Mass spectroscopic techniques, while providing excellent sensitivity and exquisite selectivity, requires the use of equipment that is not amenable to field-portable settings such as military operations. Canines have also proven effective in this regard; however, they require special handling and cannot be employed for long periods of time without significant rest periods. The Swager group recently reported an enzyme inspired approach to RDX detection using acridine-based hydride donors.[7b]

As outlined previously, amplifying fluorescent polymers (AFPs) are excellent materials for chemosensing applications including the detection of trace energetic materials such as TNT.[8] Despite the success of PET-based transduction mechanisms using AFPs in nitroaromatics detection, RDX cannot easily be detected. This is primarily due to the extremely low equilibrium vapor pressure and unfavorable reduction potential of this compound. In order to create a favorable electron transfer event for PET, a larger band gap AFP is required.[7a] The increase in driving force for electron transfer also brings with it a loss in selectivity as many other analytes could potentially quench the AFP.

Plasticized explosives contain a percentage of binders and plasticizers that increase the stability of the energetic component while simultaneously enhancing favorable mechanical properties such as malleability. A recent study using solid-phase microextraction (SPME) techiques coupled with IMS reported the identities of the various additives in different samples of C-4.[9] The two most prevalent compounds present in the air above these samples are cyclohexanone and 2-ethylhexanol. Cyclohexanone, whose molecular structure is depicted in Table 2.1, is used as a solvent in the production of RDX.[4] Residual quantities of this compound survive the binding process and are present in C-4 samples in varying quantities. The branched

alcohol, 2-ethylhexanol, is used in the synthesis of a diester phthalate plasticizer known as DEHP and also finds its way into commercial C-4 samples. These two compounds exhibit much larger equilibrium vapor pressures than RDX and are speculated to be the compounds that trained canines actually smell when identifying C-4.[10] Cyclohexanone is less prevalent than 2-ethylhexanol in non-explosives materials (present in plastic bottles/bags, glue etc.) thus limiting the number of false positives if using these components for an early warning detection system. These points served as inspiration for the development of an AFP-based sensor to detect cyclic ketones such as cyclohexanone in the context of plasticized explosives detection.

2.2 Proposed Transduction Mechanism

The detection of simple ketones using an AFP-based transduction mechanism has not been described in the literature. This is due, in part, to the lack of a favorable PET event between conjugated organic materials and unconjugated ketone moieties. This called for the formulation of an alternative transduction mechanism that does not rely on any electron transfer events involving the ketone. As described in previous sections, the efficiency of Dexter energy transfer is governed largely by the extent of orbital overlap between the donor and acceptor.[11] The proposed transduction mechanism, outlined in Figure 2.1, is predicated on interrupted Dexter energy transfer. An AFP thin-film is used as a light-harvesting unit that can amplify the luminescence of a near-infrared (NIR) emitting receptor through the synergy of exciton migration and Dexter energy transfer. In the absence of any analytes, the selective excitation of the AFP component should yield fluorescence from both the AFP and the NIR fluorophore. In the presence of an analyte that is capable of interacting with the receptor, the interaction is thought to disturb the distance between the receptor and the AFP backbone thereby perturbing the efficiency of energy transfer and signaling the presence of the analyte.
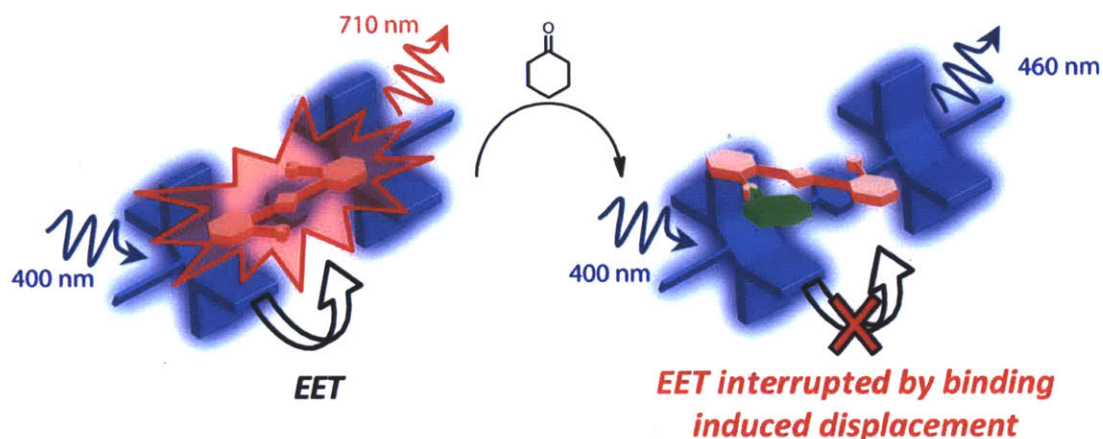
Figure 2.1. Schematic depiction of the proposed transduction mechanism (blue barbed structure = AFP, red structure = NIR-emitting receptor, green structure = cyclohexanone).

2.3 Design Considerations and Synthesis of Emissive Receptor

Realization of the aforementioned transduction mechanism requires the exclusion of any EET via the FRET pathway due to the fact that FRET can operate over very large distances.[12] Condensed phases such as thin-films yield exceedingly small intermolecular distances; and as such, favor both the FRET and Dexter pathways. In order to favor the exchange mechanism, a chromophore with an absorbance spectrum that does not overlap with the emission spectrum of an AFP was necessary. Squaraine dyes are highly luminescent materials with narrow bandwith absorbance spectra typically in the 650 – 700 nm range.[13] Synthetic access to substituted squaraines is facile, making this class of molecules an excellent choice for interrupted energy transfer. Our proposed sensing scheme also requires that the squaraine dye possess a molecular recognition unit for the ketone moiety of cyclohexanone. Bifurcated hydrogen bond donors such as diaryl ureas and thioureas have been widely used as activators of carbonyl functionalities and serve as inspiration for our molecular recognition unit.[14]

Our synthetic route towards **SQ1** is displayed in Scheme 2.1. The synthesis begins with the formation of an unsymmetrical diaryl urea via the reaction of a phenylenediamine and 3,5-bis(trifluoromethyl)phenyl isocyanate. This compound underwent an electrophilic aromatic substitution/condensation reaction with squaric acid to afford **SQ1** in good yield.

(i): 3,5-Bis(trifluoromethyl)phenyl isocyanate, CH$_2$Cl$_2$, rt, 12 h.
(ii): Squaric acid, toluene/*n*-butanol (3:1), reflux, 6 h.
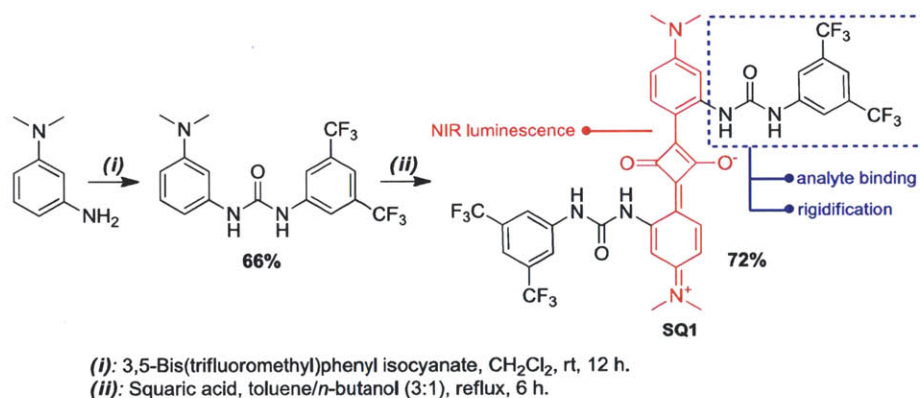
Scheme 2.1. Synthetic route to emissive receptor **SQ1**.

The resulting emissive receptor contains two strong intramolecular hydrogen bonds between the urea amide protons and the two oxygen atoms of the central four-membered ring. These interactions rigidify the dye scaffold thereby red shifting the absorbance spectrum (relative to unfunctionalized squaraine dyes) and also increasing the quantum yield of luminescence by removing rotational modes that could promote internal conversion. We chose to use pentiptycene containing **PPE1** (structure displayed in Scheme 2.2) as the light harvesting unit for two reasons: (1) the pentiptycene unit reduces interpolymer π-π interactions that could compete as low energy trap sites and (2) the pentiptycene units increase the porosity of the polymer film thereby facilitating analyte diffusion into the film and also providing ample space for **SQ1** to interact with the polymer backbone.[15]
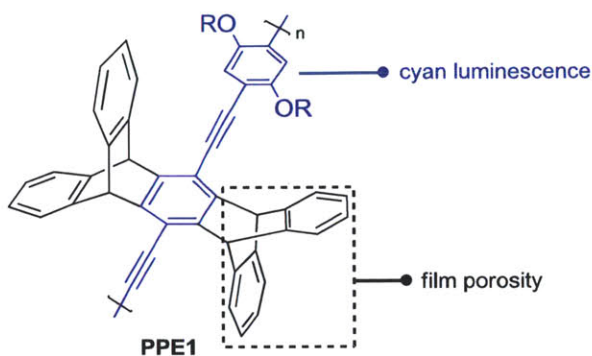
Scheme 2.2. Molecular structure of **PPE1**.

The photophysical properties of **SQ1** and **PPE1** are displayed in Figure 2.2. The emission

spectrum of **PPE1** exhibits relatively little spectral overlap with the absorbance spectrum of **SQ1**

– an ideal scenario for the promotion of Dexter energy transfer. However, **SQ1** does exhibit a

small absorbance at approximately 415 nm which is due to a $S_0{\rightarrow}S_n$ transition as the $S_0{\rightarrow}S_2$

transition is symmetry forbidden.[16] This low oscillator strength transition displays finite spectral

overlap with the emission maximum of **PPE1** and is believed to contribute to the energy transfer

cascade. As mention previously, the efficiency of Dexter energy transfer is not dependent on the

oscillator strength of the acceptor transition whereas FRET is strongly dependent on this

variable; and as such, points towards Dexter energy transfer as the dominant mechanism.[17]

36
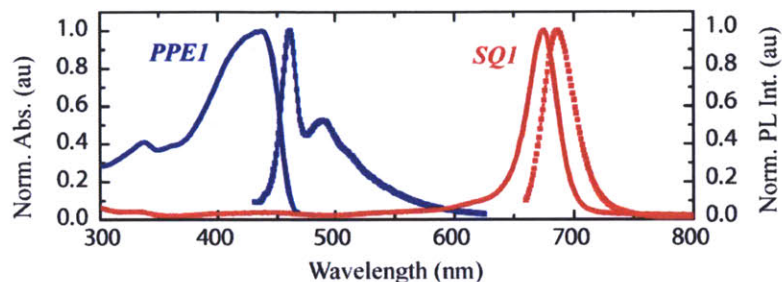
Figure 2.2. Absorbance (solid line) and emission (line with squares) spectra of **PPE1** (blue) and **SQ1** (red). Spectra were taken in CHCl$_3$, using the absorbance maximum for each component as the excitation wavelength for emission collection.

2.4 Optimization of Dye Loading, Energy Transfer Efficiency and Ketone Detection

The efficiency of energy transfer was found to vary according to the dye-loading of **SQ1** within thin-films of **PPE1**. Figure 2.3 displays the results of this study. Surprisingly, dye-loadings greater than approximately 0.5 wt% resulted in a decrease in the effieciency of energy transfer. We hypothesize that this seemingly counter intuitive result is due to the insolubility of **SQ1** in films of **PPE1** thereby causing phase separation of the two components and a net loss of energy transfer. Indeed, **SQ1** was sparingly soluble in all organic solvents tested including chloroform, dichloromethane, DMSO and ethanol. In addition, dye loadings less than 0.5 wt% also resulted in decreased energy transfer. Given that excitons created in AFP thin-films have a finite migration sphere, and that the energy transfer efficiency drops off precipitously at dye loadings below 0.5 wt%, we hypothesize that a dye loading of 0.5 wt% results in a film where the average dye-dye distance is less than the radius of the exciton sphere.

Once the optimum dye-loading was established, the films were exposed to the saturated vapor of both cyclohexanone and acetone to ascertain whether the thin-films would elicit a

37

response. Interestingly, exposure to acetone vapor yielded no change in the emission spectra whereas cyclohexanone caused a dramatic shift in the ratio of emission of the two components as shown in Figure 2.4.
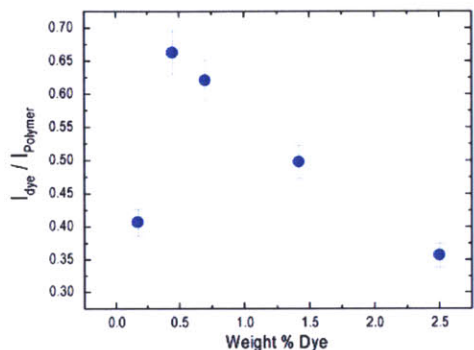
Figure 2.3. Plot expressing the relationship between dye-loading (wt%) and energy transfer efficiency. Thin-films containing both components were excited in a spectral region where only **PPE1** absorbs (400 nm) and the ratio of **SQ1:PPE1** was compared.
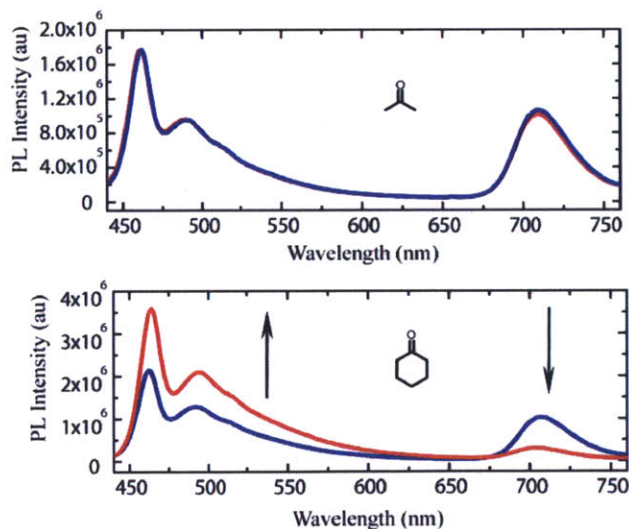
Figure 2.4. Thin-film fluorescence spectra before (blue) and after (red) exposure to the saturated vapor of acetone (top) and cyclohexanone (bottom) for 30 s (λ_{ex} = 400 nm).

Given the large disparity in equilibrium vapor pressure between cyclohexanone and acetone (acetone exhibits an equilibrium vapor pressure approximately 40 fold larger than cyclohexanone) and the small size of acetone relative to cyclohexanone, it was surprising to observe the results depicted in Figure 2.4. In order to further probe the selectivity of the sensor system, a number of other acyclic and cyclic ketones were screened. The ketone dependent responses of the sensor system are depicted in Figure 2.5.
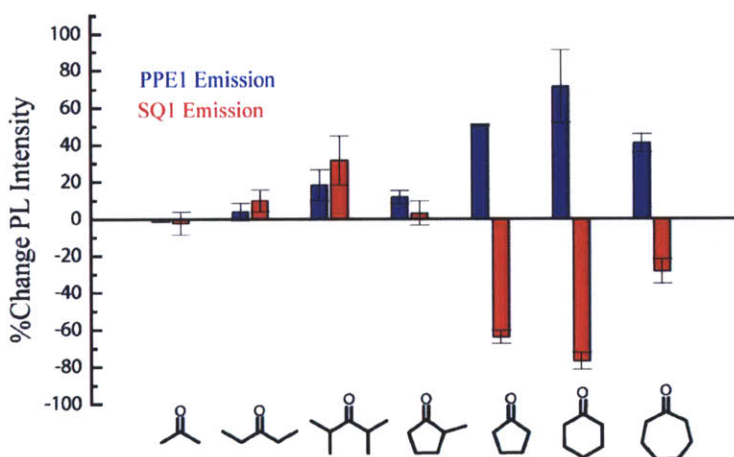
Figure 2.5. Change in thin-film fluorescence intensity of polymer (blue) and squaraine dye (red) after 30 s exposure to the saturated vapor of the indicated ketone (λ_{ex} = 400 nm) (mean of three different films).

Close inspection of Figure 2.5 reveals two important trends. The most intriguing of the two trends lies in the sensor response to cyclic ketones. The three cyclic ketones elicited a ratometric response of the sensor system whereby the emission intensity of **SQ1** decreased with a concomitant increase in the emission intensity of **PPE1**. This particular response matches the expected response if the transduction mechanism described in Figure 2.1 is operating. Conversely, exposure to acyclic ketones such as diisopropyl ketone, acetone, and 3-pentanone

yielded increases in the emission intensity of both components. The second trend is the overall increase in the magnitude of the response as a function of increasing alkyl character. This trend suggested that the hydrophobicity of the analyte may be a contributing factor to the observed selectivity.

To probe whether the observed selectivity was a function of the partition coefficient of the analytes, a quartz crystal microbalance (QCM) study was undertaken. The QCM instrument allows for high precision measurments of changes in mass by measuring the fluctuation of the resonant frequency of an oscillating quartz crystal.[18] The results of this study are depicted in Figure 2.6. Each measurment was performed in a manner identical to the method used to produce the results in Figure 2.5.
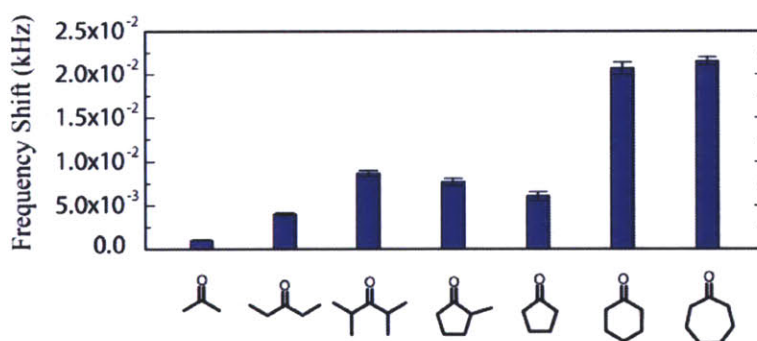
Figure 2.6. Mean frequency shift of a QCM crystal coated with a thin-film of the sensor formulation after 30 s exposure to the saturated vapor of the indicated ketone (mean of three sequential measurements).

In general, the results of the QCM study corroborate the hypothesis that the partition coefficient of the analytes is a contributing factor to the observed selectivity of the sensor. However, there are three important observations that suggest **SQ1** is intrinsically selective for cyclic ketones over acyclic ketones. The first point is that the results from Figure 2.6 suggest that

40

the partition coefficient of diisopropyl ketone is within an order of magnitude of the partition coefficient of cyclopentanone. Interestingly, despite the ability of both analytes to permeate the film, only cyclopentanone elicits a ratiometric response. Along similar lines, the partition coefficients of the cyclic ketones increase with increasing ring size – most likely a result of increased hydrophobicity. Despite this trend, cyclopentanone and cyclohexanone yield a greater response than cycloheptanone. This result suggests that **SQ1** may be exhibiting some intrinsic structure-property selectivity; specifically, that the binding area in **SQ1** cannot accommodate larger rings. The third point involves the response of the sensor to 2-methylcyclopentanone. This compound partitions into the films as efficiently as cyclopentanone; yet, it does not yield the expected ratiometric response thereby supporting the hypothesis that **SQ1** possesses some degree of intrinsic selectivity.

Further supporting evidence comes from the cocrystal structure of **SQ1** with dimethylformamide (DMF) shown in Figure 2.7. The structure displays the strong intramolecular hydrogen bonds that exist between the proximal urea protons and the central carbonyl functionalities of the central four membered ring as well as an intramolecular hydrogen bond between the distal urea protons and the amide carbonyl of DMF. The DMF molecules form intermolecular hydrogen bonds with two **SQ1** molecules which are situated face to face due to strong π-π interactions. Attempts to produce cocrystals of **SQ1** with cyclic ketones such as cyclohexanone failed due to the limited solubility of this compound.
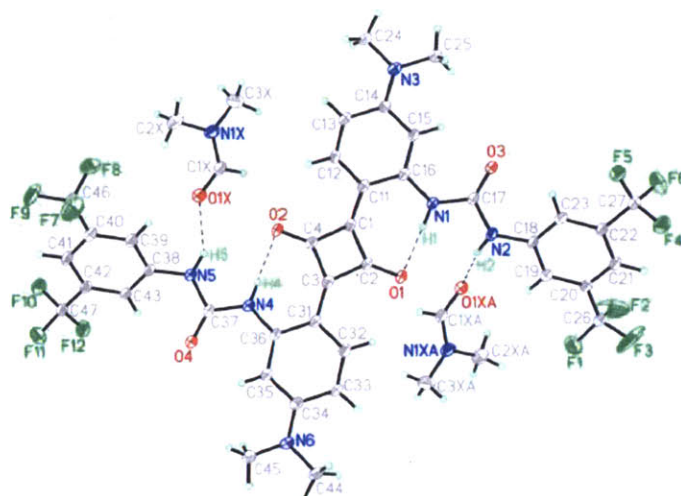
Figure 2.7. Thermal ellipsoid representation of the X-ray structure of **SQ1** (1:1 cocrystal with DMF). The displacement ellipsoids are drawn at the 50% probability level, hydrogen atoms are represented by a sphere of arbitrary radius (gray = carbon, green = fluorine, blue = nitrogen, red = oxygen, light blue = hydrogen, black dashed lines = hydrogen bonds).

To further understand the observed selectivity, we sought to investigate what causes the emission intensity of **PPE1** to increase when exposed to acyclic ketones such as diisopropyl ketone. Thin-films solely comprised of **PPE1** are known to elicit an increase in emission intensity when exposed to 'good' solvents such as toluene.[19] This effect is due to solvent induced swelling of the film which removes low energy trap sites (π-π stacking) in the polymer film that act as quenching sites. To verify that solvent induced swelling was indeed the origin of the increase in **PPE1** emission in the presence of acyclic ketones we exposed the sensor formulation to the saturated vapor of toluene (Figure 2.8).
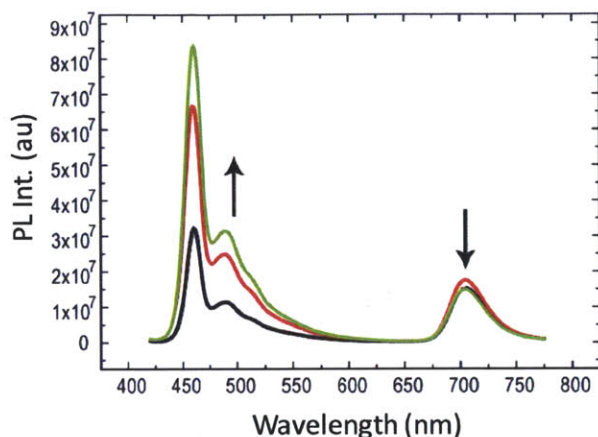
Figure 2.8. Thin-film fluorescence spectra taken in the presence of the saturated vapor of toluene. The black trace represents the first collected spectrum with red and green traces following at intervals of approximately 30 s (λ_{ex} = 400 nm).

The results in Figure 2.8 are consistent with the notion that 'good' solvents such as toluene are capable of swelling thin-films of **PPE1**, as demonstrated by the large increase in the emission intensity of **PPE1** during the exposure. Interestingly, the emission intensity of **SQ1** remains relatively constant (slight decrease) during the exposure indicating that **SQ1** maintains a small intermolecular distance with the backbone of **PPE1** despite the surge of solvent molecules into the film. This result lends credence to the hypothesis that swelling, in the absence of any molecular recognition event, is not capable of eliciting a ratiometric response.

2.5 Development of a Reversible, Field-portable Detection System Using Interrupted Energy Transfer

In order to develop a truly field-portable sensor it is advantageous to use a reversible sensing system as this increases the lifetime of the sensor, decreases the number of consumables

and defrays some of the cost of the sensing element.[20] Initially, our sensing system did not display reversibility as shown in Figure 2.9.
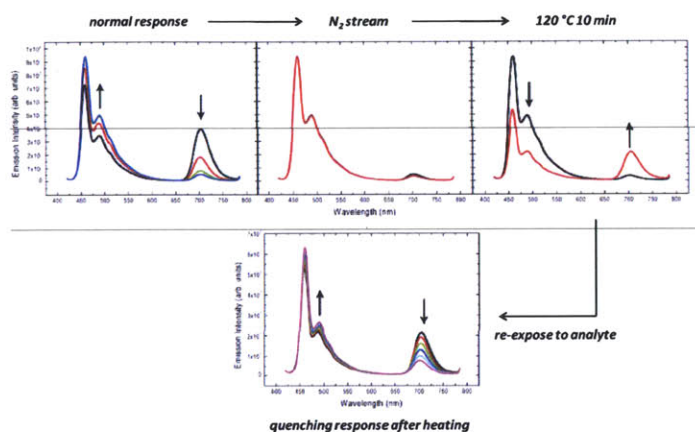
Figure 2.9. Sequential fluorescence spectra of sensor formulation. The film is first exposed to the saturated vapor of cyclohexanone until the emission of **SQ1** is suppressed (top, left). The film is then sparged with a stream of N$_2$ and a subsequent spectrum recorded (top, middle). The same film is heated to 120 °C for 10 minutes and an additional spectrum recorded (top, right). The resulting film is then re-exposed to the saturated vapor of cyclohexanone (bottom, middle) (λ_{ex} = 400 nm).

The results displayed in Figure 2.9 show that the lack of reversibility was not due to residual cyclohexanone bound to the receptor site of **SQ1** as sparging with an N$_2$ stream did not regenerate the emission from **SQ1**. However, annealing the film at 120 °C for 10 minutes restored the emission from **SQ1** and the resulting film was capable of responding to additional cyclohexanone vapor. This result indicated that the initial exposure to cyclohexanone vapor may have displaced the dye molecules from the polymer backbone and heating (annealing) was necessary to restore the equilibrium positions of the dye molecules within the scaffold.

As discussed previously, chemosensing technology utilizing AFPs have been incorporated into a portable device known as FIDO®. This instrument allows for heating of the sensing element and, in principle, should interface easily with our sensing mechanism to create a field-portable, reversible sensor for cyclohexanone vapor. Unfortunately, despite continuous heating of the thin-film, the sensor did not exhibit any significant reversibility when exposed to cyclohexanone vapor as depicted in Figure 2.10.
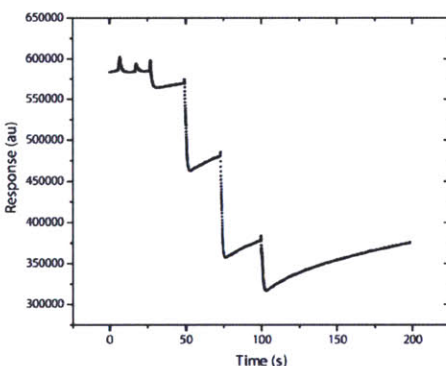
Figure 2.10. Uncorrected response of FIDO® to the saturated vapor of acetone (first three reversible peaks) followed by saturated cyclohexanone vapor (four consecutive exposures). Note the 'staircase' structure of the data indicating that it is an irreversible response.

We surmised that lowering the glass transition temperature (T_g) of the polymer would increase the reversibility of the sensor formulation. Dioctyl phthalate was employed as a plasticizer, and at loadings of approximately 1 wt%, successfully increased the fluidity of the film. Gratifyingly, the plasticized film responded to cyclohexanone in a reversible manner as shown in Figure 2.11.

45
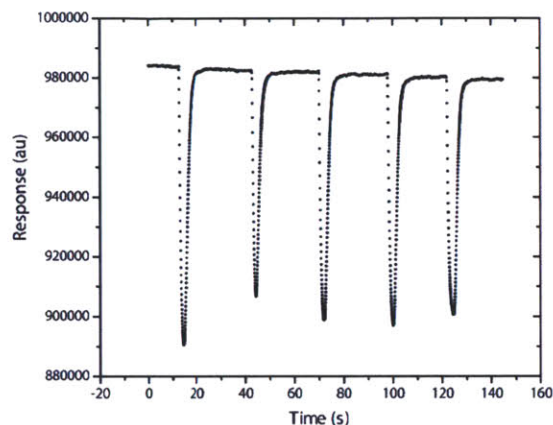
Figure 2.11. Uncorrected response of FIDO® to the saturated vapor of cyclohexanone using a plasticized film.

With a reversible sensor in hand, we focused our efforts on determining the analytical capabilities of the new system. Using a calibrated vapor delivery system, we generated precious concentrations of cyclohexanone vapor to challenge our new system.[21] The resulting data was used to construct a calibration curve (Figure 2.12) and to determine the limit of detection (LOD). It is noteworthy that all measurements were collected in ambient air with (or without) 48% relative humidity – conditions that mimic those that would be encountered outside the laboratory. The LOD obtained under these conditions was 5 ppm cyclohexanone, a value that is significantly larger than what would be necessary for trace explosives detection. Despite this apparent drawback, we exposed the FIDO® system to the headspace above a sample of C-4 explosive. The instrument recorded small 'hits' in response to the headspace as shown in Figure 2.13. Using the calibration data from Figure 2.12 we estimated that the magnitude of the FIDO® response correlated to a concentration of approximately 17 ppm of cyclohexanone vapor. In order to verify this result, the headspace above the same sample of C-4 was sampled using SPME techniques and the concentration of cyclohexanone in the headspace was obtained using GC/MS. The obtained value of 27 ppm was very similar to the value reported by the FIDO® and lends

46

credence to the notion that the response of the sensor system was indeed due to cyclohexanone vapor in the headspace. The headspace GC/MS analysis also showed no traces of TNT or 2,4-dinitrotoluene (DNT) contaminants which could potentially interfere with the signal.
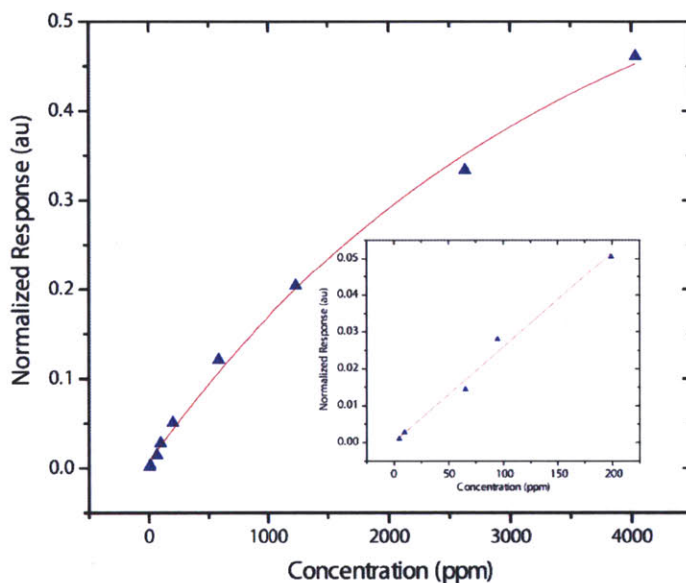
Figure 2.12. Calibration curve showing the response of the sensor system to different concentrations of cyclohexanone vapor (exponential fit). Inset figure is an expansion of the 0 – 200 ppm concentration range (linear fit).
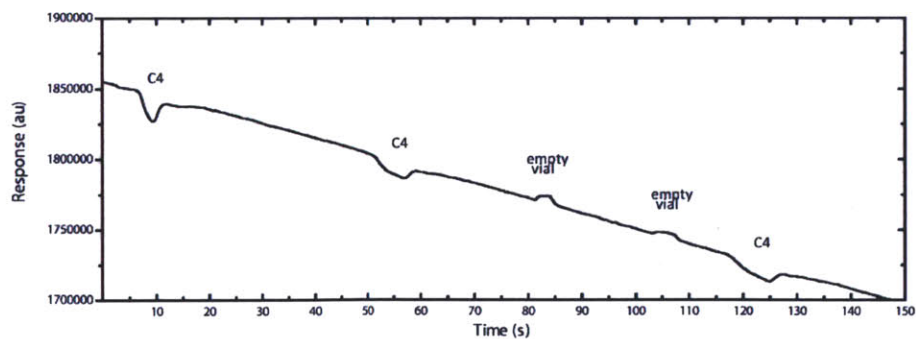
Figure 2.13. Uncorrected response of the FIDO® instrument to the headspace of C-4 explosive.

47

2.6 Conclusion

In summary, we have developed a highly selective detection system for cyclic ketones. The transduction mechanism leverages the unique spatial requirements of Dexter energy transfer to generate a selective detector that does not require any type of PET in order to function. In addition, the synthesis and photophysical properties of emissive receptor **SQ1** were described as well as the optimization of the energy transfer cascade utilizing this new fluorophore. The sensor was effectively interfaced with the FIDO® system and was shown to reversibly respond to concentrations of cyclohexanone vapor down to 5 ppm. The sensor also showed promise for the detection of cyclohexanone vapor in the headspace of the plasticized explosive C-4.

2.7 Experimental Section

MATERIALS AND METHODS: All chemicals were of reagent grade, purchased from Sigma-Aldrich and used as received. All solvents used for photophysical experiments were of spectral grade. **PPE1** was a gift from IC_x® Technologies (Lot#: BD15267). ^1H and ^{13}C NMR spectra were obtained on either a Varian Mercury (500 MHz) or Varian Mercury (501 MHz) spectrometer. NMR chemical shifts are referenced to either THF-d_8 or DMSO-d_6 and reported in units of δ (ppm). All ^{13}C spectra are proton decoupled. All NMR experiments were conducted at room temperature. High-resolution mass spectra (HRMS) were obtained at the MIT Department of Chemistry using a peak-matching protocol to determine the mass and error range of the molecular ion. Electrospray or direct analysis in real time (DART), operating in negative ion mode, were used as the ionization techniques. UV-vis spectra were measured on an Agilent 8453 diode array spectrophotometer and corrected for background signal with a solvent filled cuvette. Fluorescence spectra were obtained using a SPEX Fluorolog-τ3 fluorimeter using right-angle detection (solution measurements) or front-face detection (thin film measurements). Thin films

containing **PPE1** and **SQ1** were fabricated by spin-coating (5000 RPM for 1 min) chloroform solutions of the appropriate concentrations (Specialty Coating Systems™ G3P-8 Spincoat). The films were then placed under vacuum to ensure complete removal of the residual solvent. Thin-film quenching experiments were conducted by taking an initial photoluminescence spectrum (λ_{ex}= 400 nm, entrance/exit slits 2 nm) of the thin film, placing the surface over a glass vial loaded with 2 mL of the appropriate ketone for 30s, and taking an additional photoluminescence spectrum immediately after exposure. Quartz crystal microbalance measurements were performed with a home-built quartz crystal microbalance setup with crystals (10 MHz, Au electrodes) and oscillator from the International Crystal Manufacturing Co. Films were applied by spin-coating chloroform solutions of **PPE1** and **SQ1** on both sides of the crystal (5000 RPM for 1 min). Exposure of the QCM crystals to analyte was performed analogous to the photoluminescence experiments with data collection running continuously during the exposure. Film thicknesses were obtained according to previously published procedures. LOD measurements and experiments involving C-4 explosive were carried out at the Edgewood Chemical Biological Center and the methods are described in a subsequent section.

SYNTHETIC PROCEDURES AND CHARACTERIZATION:
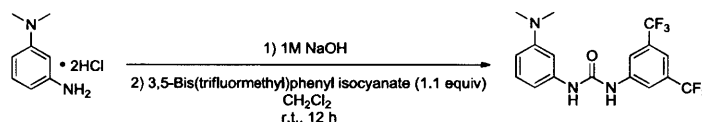
1-(3,5-bis(trifluoromethyl)phenyl)-3-(3-dimethylamino)phenyl)urea. *N,N*-Dimethyl-*m*-phenylenediamine dihydrochloride (2.0 g, 9.56 mmols) was dissolved in 10 mL of methylene chloride and washed with 1M NaOH (aq). The resulting organic layer was isolated, dried over anhydrous MgSO$_4$, and added directly to a 25 mL round-bottom flask containing a stirred solution of 3,5-Bis(trifluoromethyl)phenyl isocyanate (2.68 g, 10.52 mmols) in 5 mL methylene

49

chloride. The mixture was stirred at room temperature for 12 h during which the precipitation of a white solid was observed. The precipitate was isolated by filtration, washed with cold methylene chloride and dried under vacuum to yield 2.47 g (66%) of a white solid. ^{1}H NMR (501 MHz, DMSO-d_6): δ 9.29 (s, 1H), 8.80 (s, 1H), 8.10 (s, 2H), 7.61 (s, 1H), 7.07 (t, J = 8.21 Hz, 1H), 6.90 (s, 1H), 6.74 (d, J = 8.21 Hz, 1H), 6.40 (d, J = 8.21 Hz, 1H), 2.87 (s, 6H). ^{13}C NMR (501 MHz, DMSO-d_6): δ 153.5, 152.1, 143.1, 140.9, 131.9 (q, $J_{C\text{-}CF3}$ = 32.3 Hz), 130.3, 125.6 (q, $J_{C\text{-}F}$ = 272.8 Hz), 119.0, 115.4, 108.3, 108.3, 104.0, 41.3. MS (DART) calc for $C_{17}H_{15}F_6N_3O$ [M − H]$^-$: 390.10, found 390.10.
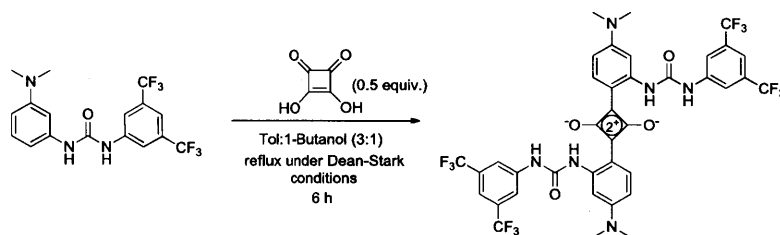
SQ1. A 50 mL round-bottom flask, equipped with a magnetic stir bar, Dean-Stark trap and reflux condenser, was charged with 1.0 g (2.56 mmols) 1-(3,5-bis(trifluoromethyl)phenyl)-3-(3-dimethylamino)phenyl)urea, 0.15 g (1.28 mmols) 3,4-dihydroxycyclobut-3-ene-1,2-dione, and 30 mL of a 3:1 mixture of toluene and n-butanol. The resulting mixture was refluxed under azeotropic distillation conditions for 6 h. During the reaction a color change from light yellow to dark green was observed with concomitant precipitation of a metallic green solid. The vessel was cooled to r.t. and allowed to sit overnight. The resulting metallic green solid was filtered, washed with methanol and hexanes, and dried under vacuum to yield 0.8 g (72%) of squaraine **2**. ^{1}H NMR (500 MHz, THF-d_8): δ 11.87 (s, 2H), 8.42 (m, 6H), 8.29 (s, 4H), 7.99 (s, 2H), 7.60 (s, 2H), 6.58 (d, J = 9.1 Hz, 2H), 3.21 (s, 6H). Due to the limited solubility of the compound satisfactory ^{13}C spectra could not be obtained even after acquiring for 24 h. Anal. calc for

$C_{38}H_{28}F_{12}N_6O_4 \cdot 1H_2O$: %C 51.94, %H 3.44, %N 9.56, %F 25.95; found %C 51.56, %H 3.27, %N 9.24, %F 26.90.
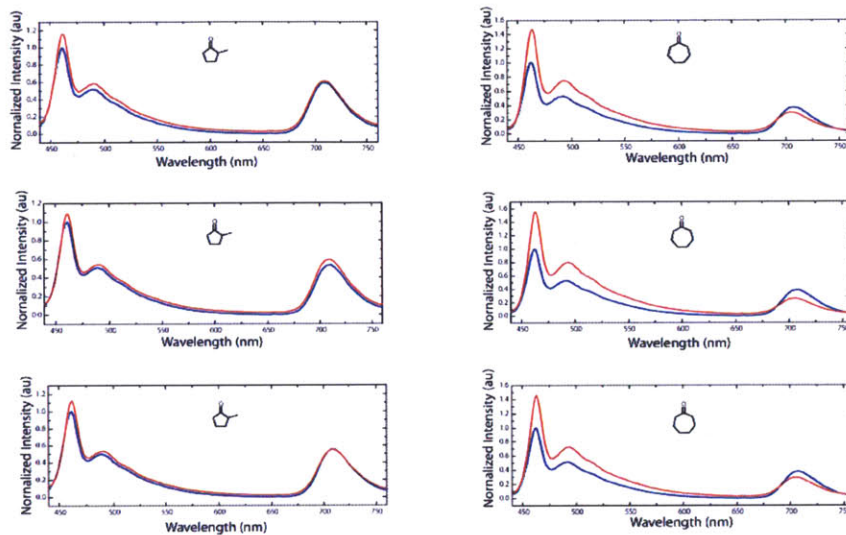
Figure 2.7.1 Photoluminescence spectra of thin films before (blue) and after (red) 30 second exposure to the headspace of the indicated ketone (λ_{ex} = 400 nm).
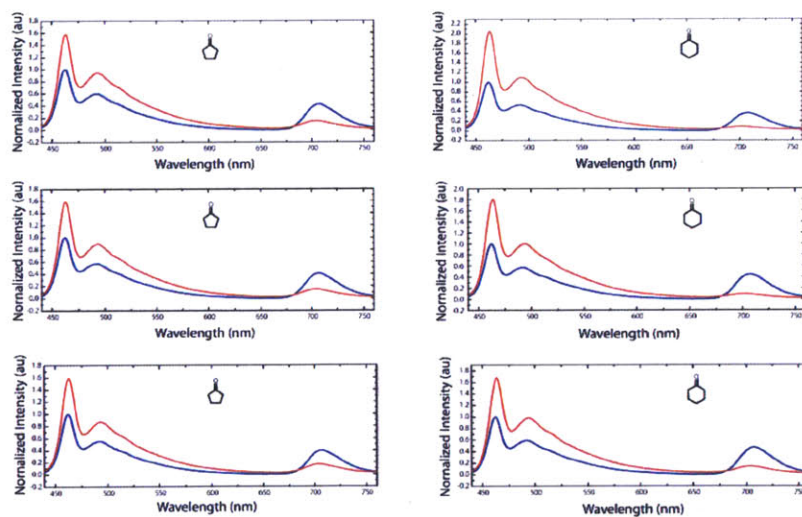
Figure 2.7.2. Photoluminescence spectra of thin films before (blue) and after (red) 30 second exposure to the headspace of the indicated ketone (λ_{ex} = 400 nm).
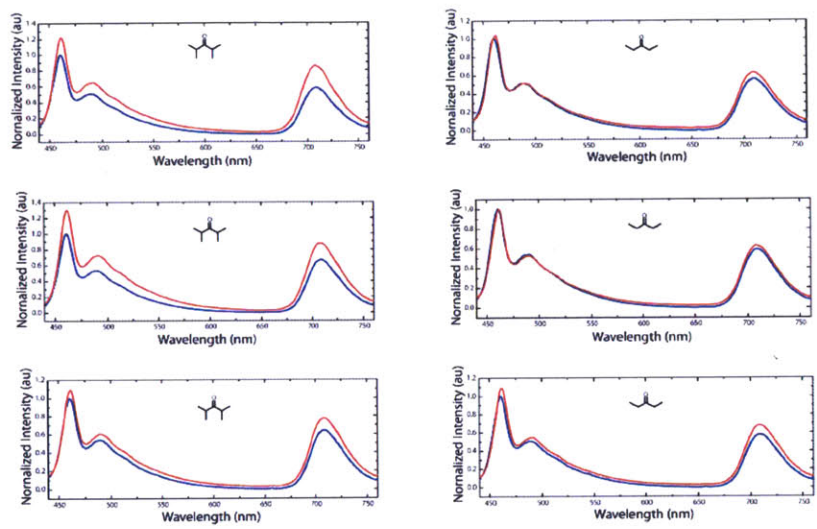
Figure 2.7.3. Photoluminescence spectra of thin films before (blue) and after (red) 30 second exposure to the headspace of the indicated ketone (λ_{ex} = 400 nm).
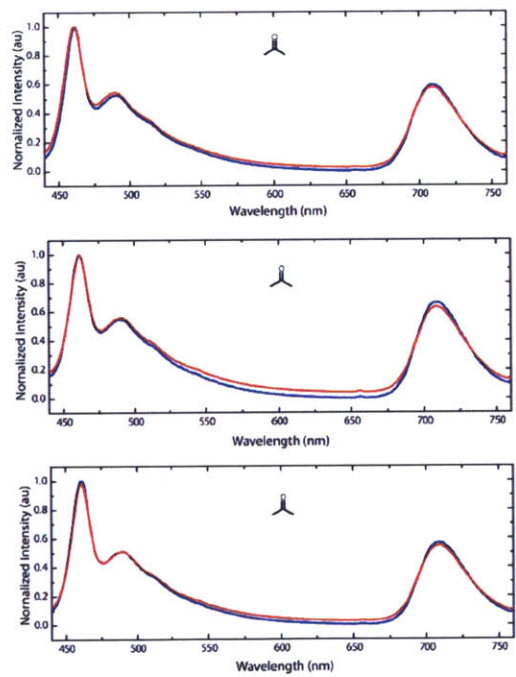
Figure 2.7.4. Photoluminescence spectra of thin films before (blue) and after (red) 30 second exposure to the headspace of acetone (λ_{ex} = 400 nm).
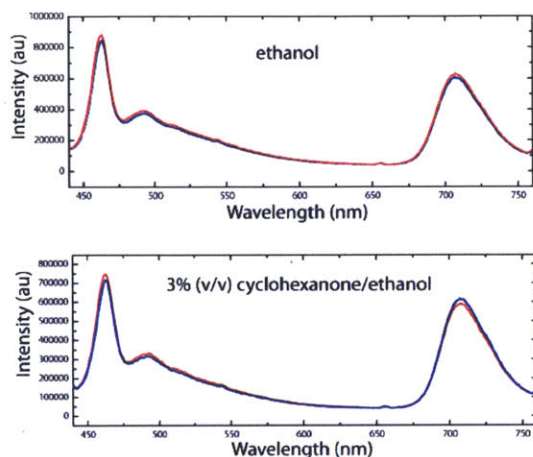
Figure 2.7.5. Photoluminescence spectra before (blue) and after (red) exposure to the headspace of the indicated solvent mixture. Note that both components exhibit an increase in emission intensity when exposed to pure ethanol and exhibit a small ratiometric response when exposed to a 3% (v/v) cyclohexanone/ethanol mixture.
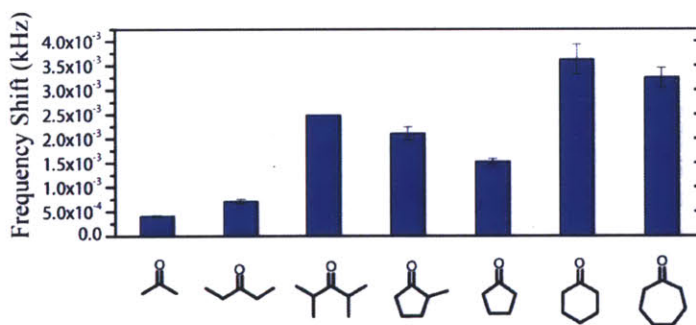
Figure 2.7.6. Mean frequency shift of a QCM crystal coated with a thin-film of PPE **2** after 30 second exposure to the headspace vapor of cyclohexanone (mean of three sequential measurements).

54
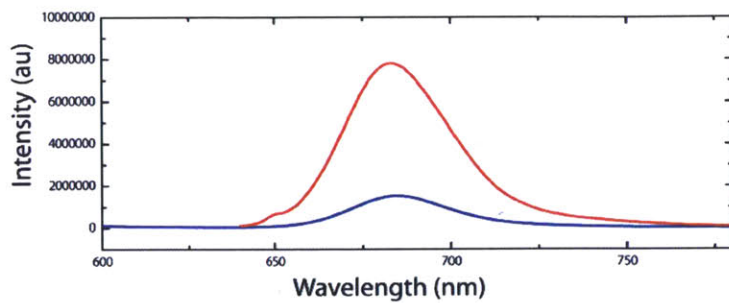
Figure 2.7.7. Photoluminescence spectra of squaraine **1** in $CHCl_3$ (O.D. = 0.1 au) with excitation wavelength at 650 nm (red) and 400 nm (blue). The small bump at 650 nm in the red spectrum is due to the excitation wavelength.
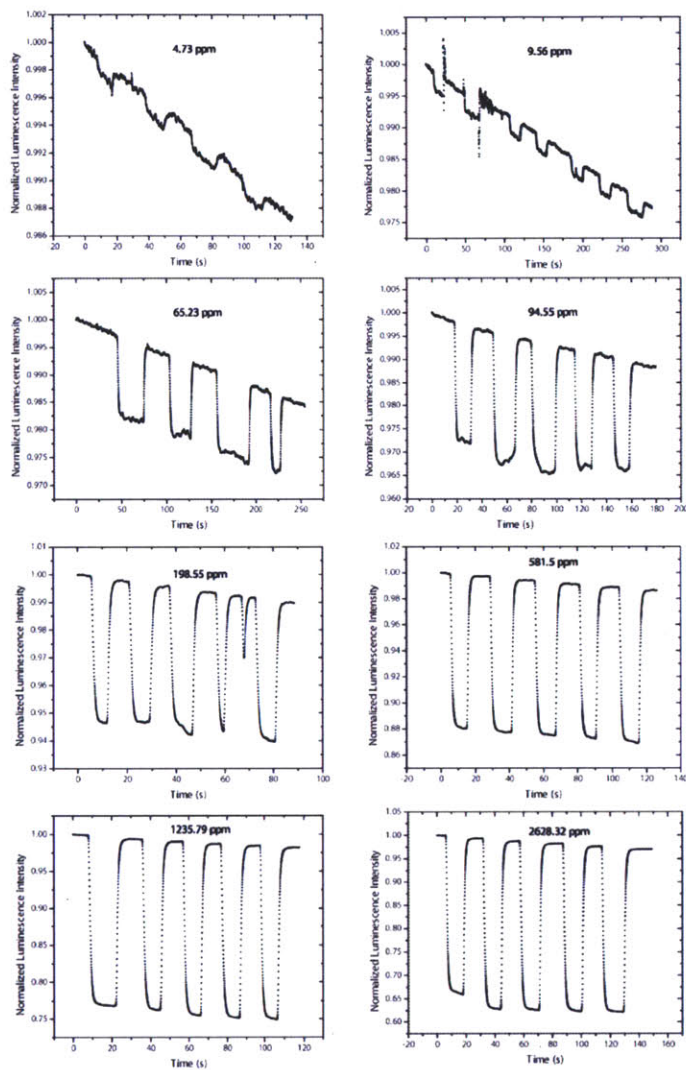
Figure 2.7.9. Normalized responses of the FIDO® system to the indicated concentration of cyclohexanone vapor.
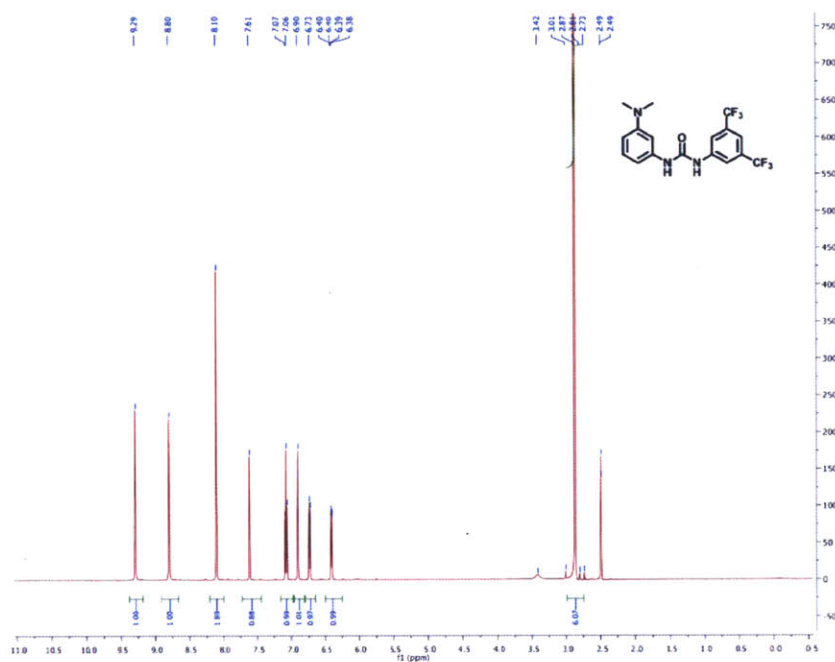
Figure 2.7.10. ¹H NMR spectrum of 1-(3,5-bis(trifluoromethyl)phenyl)-3-(3-dimethylamino)phenyl)urea (DMSO-d_6).
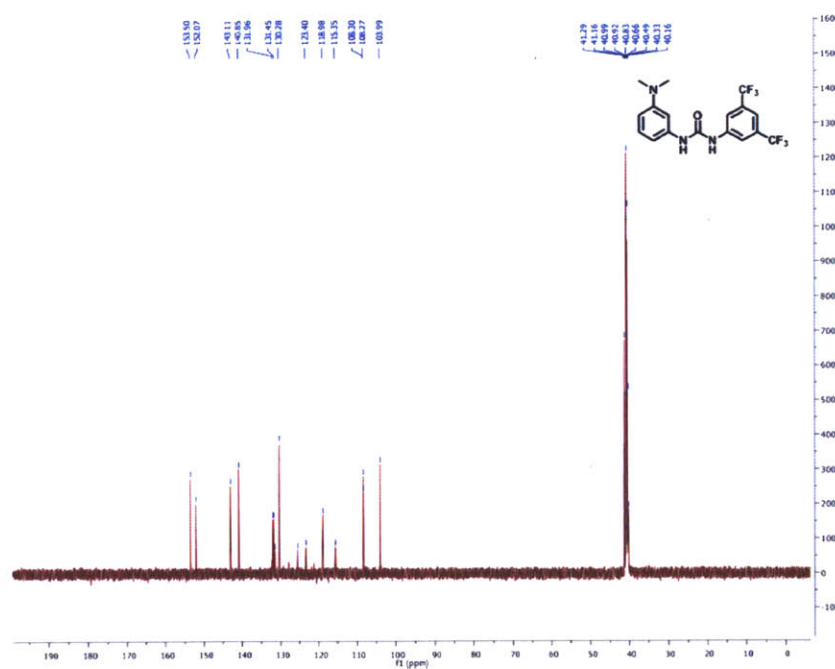
Figure 2.7.11. ¹³C NMR spectrum of 1-(3,5-bis(trifluoromethyl)phenyl)-3-(3-dimethylamino)phenyl)urea (DMSO-d_6).

57
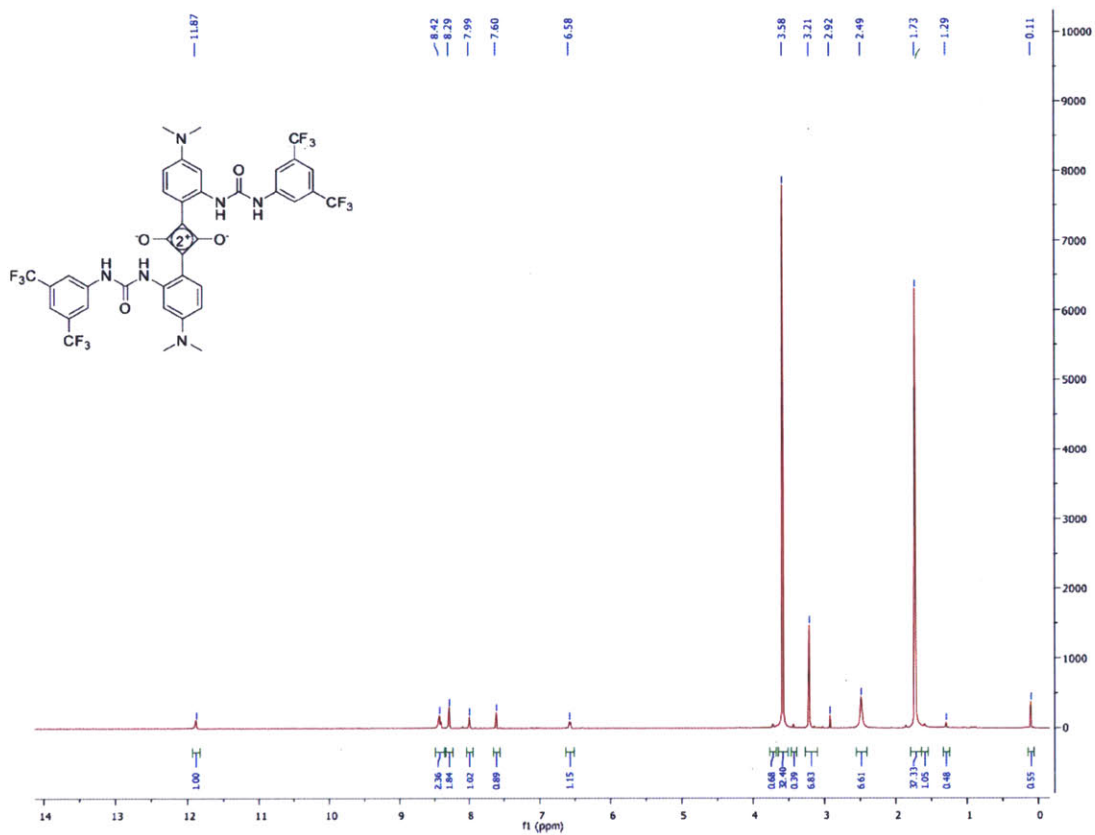
Figure 2.7.12. ^{1}H NMR spectrum of **SQ1** (THF-d_8).

*CRYSTAL DATA AND STRUCTURE REFINEMENT FOR **SQ1**:*

Identification code	x10009
Empirical formula	C41 H35 F12 N7 O5
Formula weight	933.76
Temperature	100(2) K
Wavelength	1.54178 Å
Crystal system	Triclinic
Space group	P-1
Unit cell dimensions	a = 7.9149(2) Å α= 89.6190(10)°.
	b = 13.8805(3) Å β= 82.0830(10)°.
	c = 18.1339(4) Å γ = 88.7430(10)°.
Volume	1972.76(8) Å^3
Z	2
Density (calculated)	1.572 Mg/m^3
Absorption coefficient	1.259 mm^{-1}
F(000)	956
Crystal size	0.12 x 0.04 x 0.03 mm^3
Theta range for data collection	3.18 to 66.91°.
Index ranges	-9<=h<=9, -16<=k<=16, -17<=l<=21
Reflections collected	34262
Independent reflections	6956 [R(int) = 0.0338]
Completeness to theta = 66.91°	98.9 %
Absorption correction	Semi-empirical from equivalents
Max. and min. transmission	0.9632 and 0.8636
Refinement method	Full-matrix least-squares on F^2
Data / restraints / parameters	6956 / 373 / 614
Goodness-of-fit on F^2	1.027

59

Final R indices [I>2sigma(I)]	R1 = 0.0397, wR2 = 0.1035
R indices (all data)	R1 = 0.0441, wR2 = 0.1078
Largest diff. peak and hole	0.477 and -0.397 e.Å^{-3}

2.8 References

(1) Pinnaduwage, L. A.; Boiadjiev, V.; Hawk, J. E.; Thundat, T. *Appl. Phys. Lett.* **2003**, *83*, 1471.

(2) Singh, S. *J. Hazard. Mater.* **2007**, *144*, 15.

(3) (a) Lai, H.; Leung, A.; Magee, M.; Almirall, J. R. *Anal. Bioanal. Chem.* **2010**, *396*, 2997. (b) Lorenzo, N.; Wan, T.; Harper, R. J.; Hsu, Y. L.; Chow, M.; Rose, S.; Furton, K. G. *Anal. Bioanal. Chem.* **2003**, *376*, 1212.

(4) (a) Jehuda, Y. *Forensic Applications of Mass Spectrometry*, Vol. 3, 2nd ed.; CRC Press: Boca Raton, 1995. (b) Röck, F.; Barsan, N.; Weimar, U. *Chem. Rev.* **2008**, *108*, 705.

(5) (a) Ewing, R. G.; Miller, C. J. *Field Anal. Chem. Technol.* **2001**, *5*, 215. (b) Eiceman, G. A.; Karpas, Z. *Ion Mobility Spectrometry*, 2nd ed.; CRC Press: Boca Raton, 2005.

(6) Liu, H. – B.; Chen, Y.; Bastiaans, G. J.; Zhang, X. – C. *Optics Express* **2006**, *14*, 415.

(7) (a) Sanchez, J. C.; Trogler, W. C. *J. Mater. Chem.* **2008**, *18*, 3143. (b) Andrew, T. L.; Swager, T. M. *J. Am. Chem. Soc.* **2007**, *129*, 7254.

(8) (a) Yang, J. S.; Swager, T. M. *J. Am. Chem. Soc.* **1998**, *120*, 5321-5322. (b) Yang, J. S.; Swager, T. M. *J. Am. Chem. Soc.* **1998**, *120*, 11864-11873.

(9) Lai, H.; Leung, A.; Magee, M.; Almirall, J. R. *Anal. Bioanal. Chem.* **2010**, *396*, 2997.

(10) Furton, K. G.; Myers, L. J. *Talanta* **2001**, *54*, 487.

(11) Dexter, D. L. *J. Chem. Phys.* **1953**, *21*, 836.

(12) Förster, T. *Ann. Phys.* **1948**, *2*, 55.

(13) (a) Treibs, A.; Jacob, K. *Angew. Chem. Int. Ed. Engl.* **1965**, *4*, 694. (b) Park, J. D.; Cohen, S.; Lacher, J. R. *J. Am. Chem. Soc.* **2002**, *84*, 2919. (c) Beverina, L.; Salice, P. *Eur. J. Org. Chem.* **2010**, 1207.

(14) (a) Doyle, A. G.; Jacobsen, E. N. *Chem. Rev.* **2007**, *107*, 5713. (b) Etter, M. C.; Panunto, T. W. *J. Am. Chem. Soc.* **1988**, *110*, 5896. (c) Etter, M. C.; Urbánczyk-Lipkowska, Z.; Zia-Ebrahimi, M.; Panunto, T. W. *J. Am. Chem. Soc.* **1990**, *112*, 8415.

(15) Swager, T. M. *Acc. Chem. Res.* **2008**, *41*, 1181.

(16) Toro, C.; De Boni, L.; Yao, S.; Ritchie, J. P.; Masunov, A. E.; Belfield, K. D.; Hernandez, F. E. *J. Chem. Phys.* **2009**, *130*, 214504.

(17) Anslyn, E. V.; Dougherty, D. A. *Modern Physical Organic Chemistry*; University Science Books: Sausolito, CA, 2006.

(18) Buttry, D. A.; Ward, M. D. *Chem. Rev.* **1992**, *92*, 1355.

(19) Our laboratory has observed that solvents such as toluene and THF are capable of swelling CP films.

(20) Moore, D. S. *Rev. Sci. Instrum.* **2004**, *75*, 2499.

(21) Studies were conducted at the Edgewood Chemical Biological Center (ECBC).

Chapter 3

Liquid Crystal Alignment Layers Using an Axis-Selective Di-π-Methane Rearrangement

3.1 Introduction to Liquid Crystals

Liquid crystalline materials (LCMs) have permeated all areas of human life. It is difficult to imagine a world without liquid crystal displays (LCDs); yet, this particular application of LCMs represents only a small portion of technologies that exploit liquid crystalline phases. LCMs have been used as thermometers,[1] optical switches,[2] wavelength tunable filters,[3] lasing media,[4] sensing materials[5] and much more.[6] The utility of LCMs is derived from the special liquid crystalline phases that these materials can exhibit under appropriate conditions. Liquid crystalline phases, from a qualitative perspective, are phases that exhibit some of the anisotropic properties of solids (orientational or positional order) yet are free flowing liquids. This seemingly paradoxical state of matter was first described by an Austrian botanist named Friedrich Reinitzer at the University of Graz in 1888.[7] While working with cholesteric molecules he observed that this material undergoes a thermal transition to yield an opaque liquid that subsequently melts to a clear liquid at higher temperatures. This observation was the catalyst for the understanding and development of LCMs.

The simplest liquid crystalline phase – the nematic phase – is schematically depicted in Figure 3.1. Molecules exhibiting this phase of matter possess orientational order but lack any positional order; in other words, the molecules are not correlated with each other. When nematic phases are formed on isotropic substrates, such as glass, many nematic domains form where the vectors that describe the orientational order (director) vary in direction across the mesophase (Figure 3.2). This is not an ideal situation as devices that utilize liquid crystalline phases require uniform alignment of the phase.[8] In order to induce alignment, a technique known as rubbing was developed in 1911.[9] In this process, a thin polymer film is rubbed in one direction using a cloth. The microscopic and molecular anisotropies that develop on the surface are believed to be

the origin of liquid crystal alignment on these films.[10] Despite the crudeness of this approach, it is the major industrial technique for producing aligned LCMs. There are a number of problems associated with the rubbing process such as: (i) generation of static charges in the device, (ii) incorporation of dust particles on the surface and (iii) it serves as a bottleneck in the production of LCMs.[11] In order to solve these problems, there has been considerable interest in developing non-contact alignment processes that utilize light .
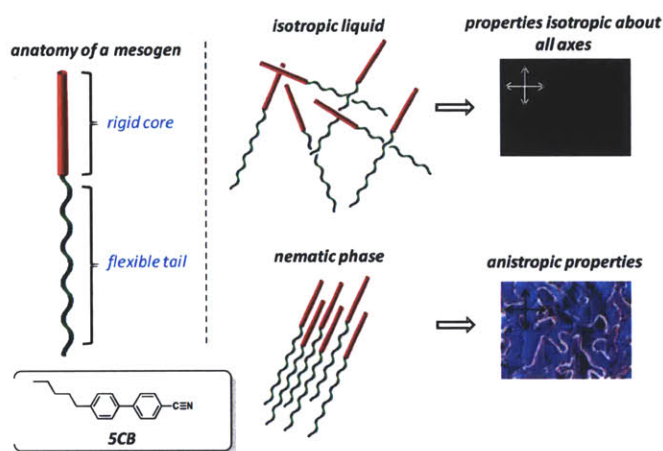
Figure 3.1. Schematic depictions of the structure of liquid crystal mesogens (left) and the nematic phase (right). Small inset (lower left) displays the molecular structure of 4-cyano-4'pentylbiphenyl (5CB).
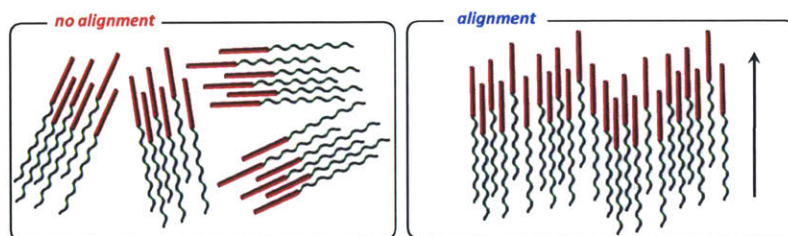
Figure 3.2. Schematic depictions of unaligned (left) and aligned (right) nematic liquid crystalline phases. The rod-like structure represents a liquid crystal mesogen such as 5CB. The black arrow on the right side represents the molecular director.

64

Non-contact alignment mechanisms that utilize light are collectively known as photoalignment mechanisms. The general approach is to coat a substrate with a photoresponsive polymeric film, and through polarized irradiation, generate anisotropy at the liquid crystal – polymer interface. The photoresponsive polymer films typically rely on simple photochemical transformations such as cis/trans isomerizations[12] and cycloaddition reactions.[13] The most commonly used transformations for photoalignment are shown in Figure 3.3.
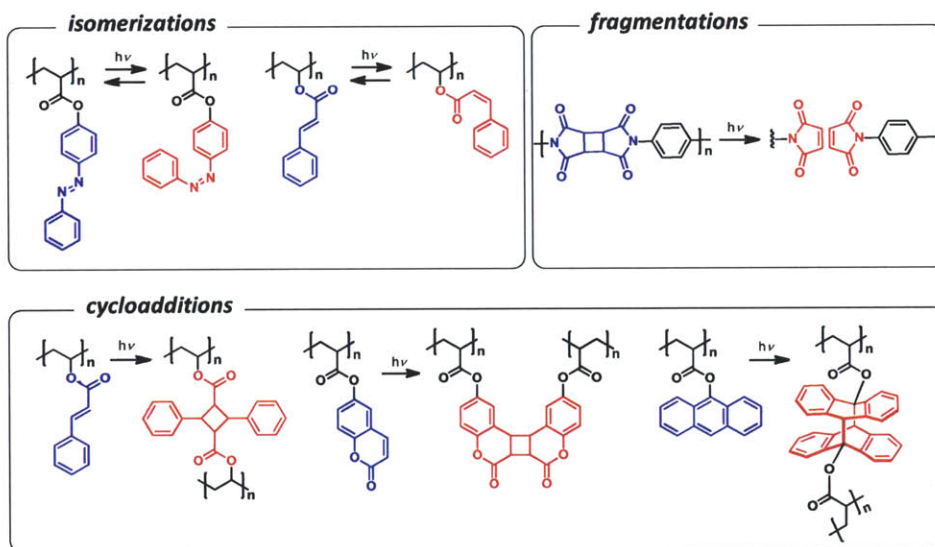
Figure 3.3. Various photochemical transformations that are applied in photoalignment mechanisms.[14]

The transformations outlined in Figure 3.3 are effective approaches for photoalignment; however, the listed reactions suffer from at least one of the following limitations: (i) the transformation is thermally reversible, (ii) more than one pathway is available, and/or (iii) extended irradiation destroys the alignment. To address these limitations, we sought to design robust photoalignment layers based on the di-π-methane rearrangement.

65

3.2 The Di-π-methane Rearrangement

The di-π-methane rearrangment is a high yielding photochemical transformation discovered by Zimmerman in 1966 (Figure 3.4).[15] The scope of this reaction and related reactions has been thoroughly reviewed.[16] The term di-π-methane refers to the arrangement of two vinylic moieties separated by a methylene unit, which is a general characteristic of substrates that undergo this rearrangment.
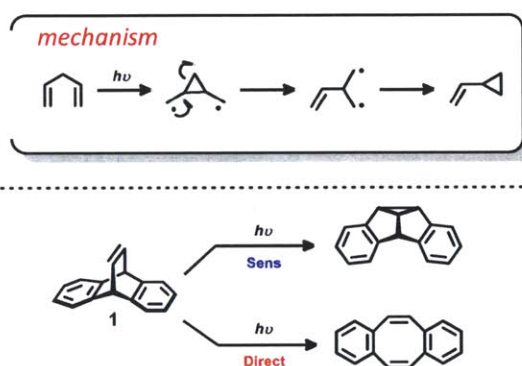
Figure 3.4. Overall transformation and mechanism of the di-π-methane rearrangement (top). Implications of the multiplicity of the di-π-methane rearrangement (bottom).

As shown in Figure 3.4, the overall transformation consists of converting a skipped diene system to an allylic cyclopropane moiety. In the case of unconstrained, freely rotating, divinyl groups (top, Figure 3.4), reaction via the excited singlet state yields the desired product. If the same substrate is reacted through a triplet manifold, the only observed products are the result of isomerization about the double bonds. Conversely, constrained divinyl moieties, as is the case with **1** (Figure 3.4), behave in the opposite fashion - triplet sensitization of **1** yields the desired product whereas direct irradiation yields dibenzocyclooctatetraene.[16] The multiplicity

66

dependence of this transformation with respect to dibenzobarrelene is essential to the work described in this chapter.

3.3 Approach and Design Considerations

The Swager group has exploited the intramolecular free volume (IFV) associated with triptycene-based structures to create polymers that are strongly aligned in liquid crystalline media.[17] This design principle served as inspiration for the construction of **P1** (Figure 3.5). The repeat unit of this polymer contains two functional units. The first unit, the diester substituted dibenzobarrelene structure, serves two purposes: (i) this structure exhibits a rigid carbocyclic structure similar to that of triptycene; as such, it is expected to form favorable interactions with an LC phase and (ii) the same structure also serves as a di-π-methane substrate. We hypothesized that the rearrangement would lead to a structure that exhibits a lower level of IFV and would therefore interact poorly with the LC phase. By using linearly polarized light to initiate the reaction, only chromophores with transition dipole moments oriented parallel to the polarized light source will undergo the transformation. The remaining chromophores would retain their IFV and lead to a net anistropy at the polymer LC phase and generate an alignment axis for the LC phase to couple with (Figure 3.6).
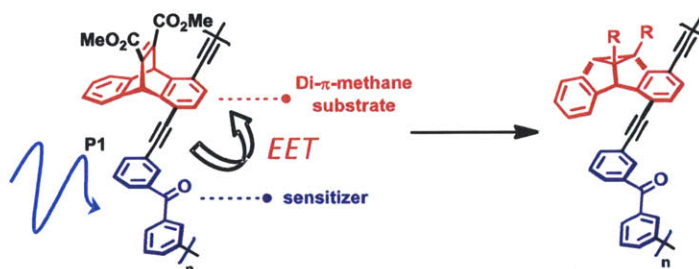
Figure 3.5. Molecular structure of **P1** and the resulting photoproduct of the di-π-methane rearrangement.

67

Because it is a rigid system, the rearrangement proceeds through a triplet manifold thereby requiring the presence of a triplet sensitizer. During photoexcitation with linearly polarized light, the benzophenone units (exhibiting the proper orientation with respect to the light source) are excited to the first singlet state and then quickly crossover to the first excited triplet state through intersystem crossing. We surmised that incorporation of sensitizer units directly into the backbone would lead to facile Dexter energy transfer thereby exciting the dibenzobarellene units to their triplet state followed by the di-π-methane rearrangement.
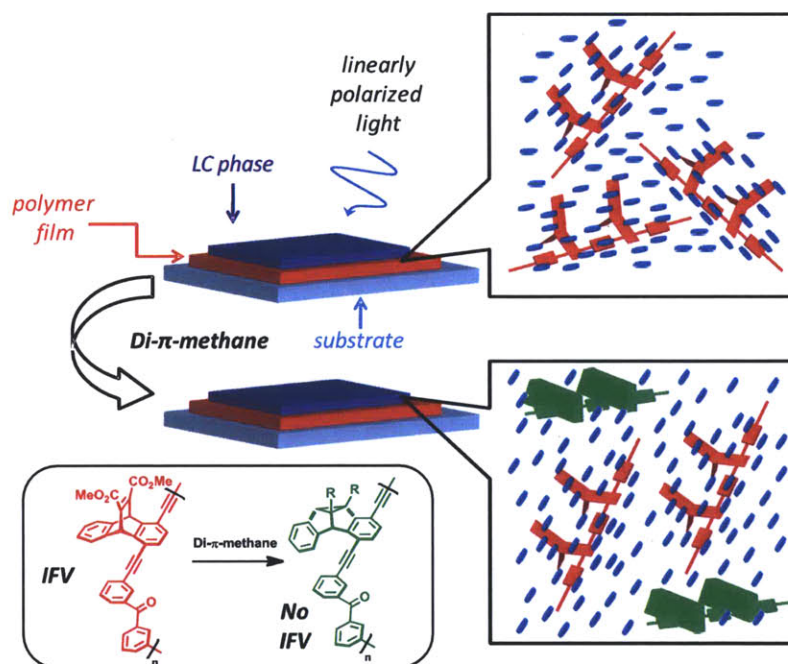
Figure 3.6. Schematic depiction of the proposed photoalignment mechanism using the di-π-methane rearrangement. Red (green) structures represent **P1** before (after) photolysis. Blue structures represent LC molecules.

3.4 Synthesis of Monomers, Model Compounds and Photoalignment Polymers

The core unit of **P1** is a diester-substituted dibenzobarellene compound as mentioned previously. The synthesis of this compound is shown in Scheme 3.1. The synthesis begins with the double addition of trimethylsilylacetylide to 1,4-anthraquinone followed by SnCl$_2$ mediated reductive aromatization to afford **2** in good yield. This compound underwent a facile Diels Alder reaction with DMAD followed by fluoride deprotection of the silyl groups to yield **3**. Double Sonogashira-Hagihara cross-coupling of **3** with **4** afforded the model compound **5**.
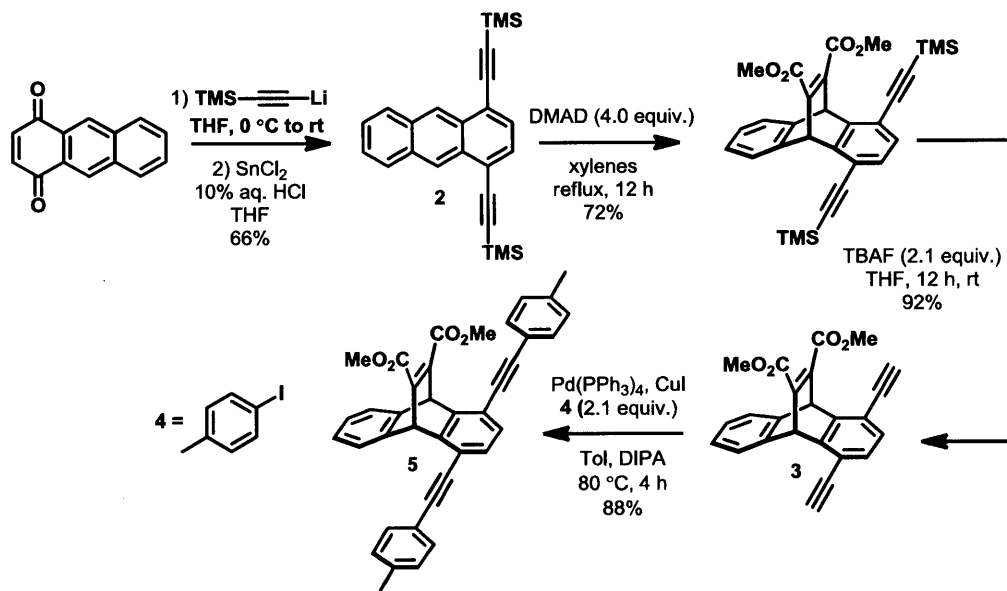
Scheme 3.1. Synthesis of model compound **5**.

Comonomers for the synthesis of **P1** and **P2** were synthesized according to Scheme 3.2. These comonomers were iodinated *meta* to the carbonyl group in order to limit the effective conjugation length of the resulting polymers. Typically, electronically deactivated arenes such as benzophenone and benzil are sluggish substrates for electrophilic halogenations; however, the use of concentrated sulfuric acid and *N*-iodosuccinimide (NIS) at low temperature successfully

iodinated both compounds in good yield. Presumably, the concentrated sulfuric acid is capable of protonating the succinimide groups thereby yielding a strongly electrophilic source of iodine.[18]
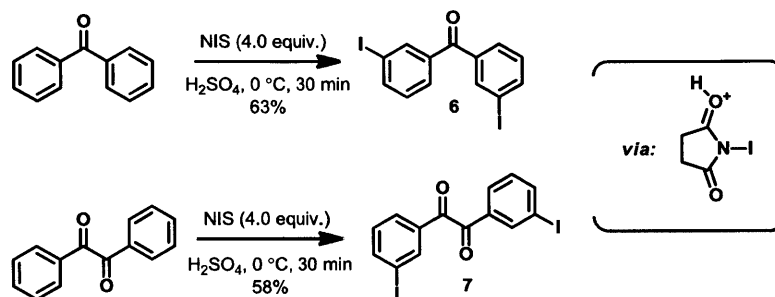
Scheme 3.2. Synthesis of comonomers **6** and **7**.

Polymers **P1** and **P2** were synthesized using standard Sonogashira-Hagihara cross-coupling chemistry as depicted in Scheme 3.3. In order to preserve the processability/solubility of the targeted polymers, the polymerization reactions were conducted for only 24-36 hours yielding number-average molecular weights (M_n) of 15,000 – 33,000 g/mol.
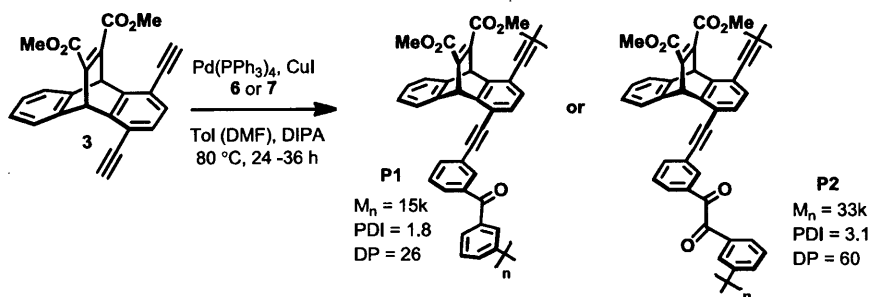
Scheme 3.3. Synthesis of photoalignment polymers **P1** and **P2**.

3.5 Photochemistry of Model Compound and Photoalignment Polymers

Polymers **P1** and **P2** contain di-π-methane substrates that each can yield two different regioisomers upon photolysis. To probe the regiochemical behavior of the dibenzobarrelene scaffold, the photochemistry of model compound **5** was investigated. As shown in Scheme 3.4,

the photolysis of **5** may give rise to racemic mixtures of two regioisomers. The regiochemistry of this transformation is controlled by the formation of the bridged diradical species shown in Scheme 3.4. There are two possibilities present, in one case the diradical could be centered on the lone arene ring (Diradical 2, Scheme 3.4). However, loss of aromaticity makes this diradical particularly unstable. We hypothesized that the extended conjugation of the ethynyl-bridged arene system would make this particular diradical (Diradical 1, Scheme 3.4) more stable and give rise to photoproduct *rac*-**DP1** as the major product.

Indeed, photolysis of **5** in chloroform using benzophenone as the triplet sensitizer gave rise to predominantly one set of new peaks as shown in Figure 3.7. It is noteworthy that the NMR spectrum in Figure 3.7 is of the crude mixture and that only signals from starting material and product can be observed. This point exemplifies the efficiency of the di-π-methane transformation and its possible utility as a photoalignment reaction. In order to unambiguously determine the regiochemistry of the rearrangement the major photoproduct was isolated by column chromatography. The product was analyzed via 2D NMR techniques and determined to be *rac*-**DP1.**
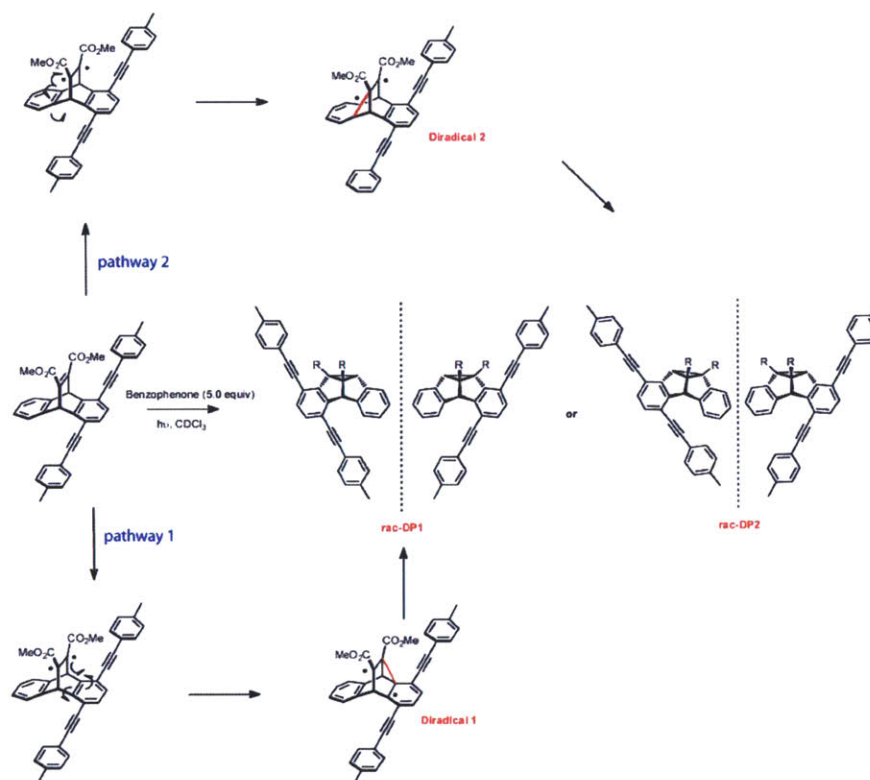
Scheme 3.4. Regiochemical possibilities during photolysis of model compound **5**.
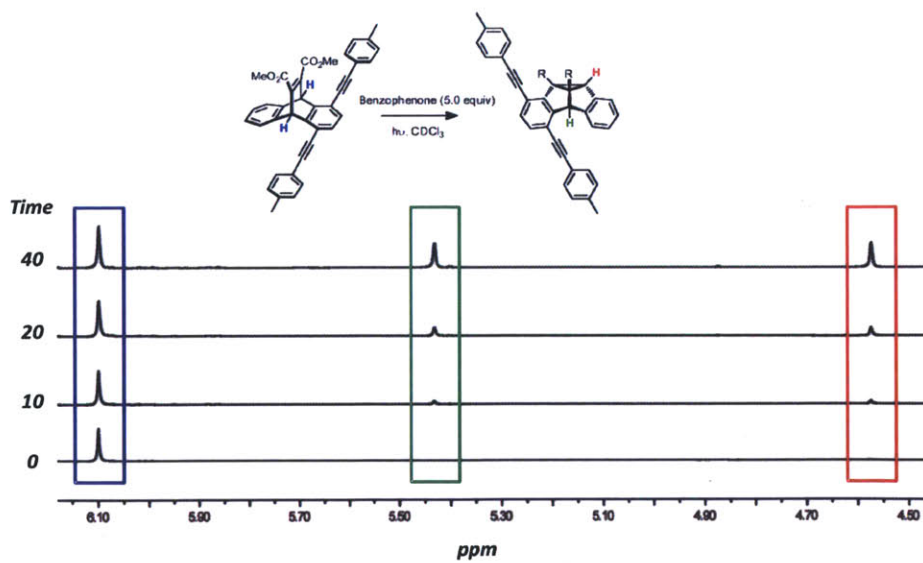
Figure 3.7. Stacked ^{1}H NMR spectra obtained during photolysis of **5**.

After investigating the photochemistry of model compound **5**, we turned our attention to the photochemistry of photoalignment polymers **P1** and **P2**. The reactions were carried out in $CDCl_3$ and monitored by ^{1}H NMR spectroscopy. The results of the photolysis of **P1** are shown in Figure 3.8.
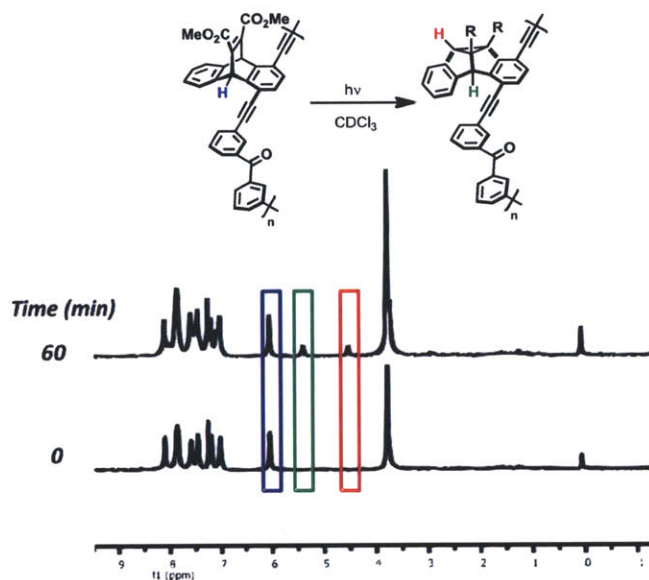
Figure 3.8. Stacked ^{1}H NMR spectra obtained during photolysis of **P1**.

As shown in Figure 3.8, the photolysis of **P1** in $CDCl_3$ cleanly yields the di-π-methane photoproduct. The new methine resonances at 5.5 and 4.5 ppm closely match the chemical shifts of the methines formed during the photolysis of model compound **5**. The generation of only two new methine peaks is indicative of the high regioselectivity of this transformation and is analogous to the observed regioselectivity of the model compound. It is noteworthy that the photolysis of **P1** was carried out in the presence of air. Typically, triplet sensitized photochemical transformations are carried out in degassed solutions as oxygen can easily quench the triplet state of the sensitizer.[19] In the case of **P1**, incorporation of the triplet sensitizer in the polymer backbone positions the sensitizer adjacent to the di-π-methane substrate and enhances

the rate of energy transfer. This enhancement alleviates the need to remove oxygen as the rate of energy transfer is faster than the diffusion rate of oxygen in solution. From a practical standpoint, this is an ideal situation as the photolysis of photoalignment films can be carried out in air as opposed to an inert atmosphere.

The photolysis of **P2** closely resembled that of **P1** (Figure 3.9). The major difference between these two polymers is the choice of the triplet sensitizer. Both benzil and benzophenone are efficient triplet sensitizers with intersystem crossing rates of near unity. However, the triplet energy of benzil is substantially lower than that of benzophenone ($E_{T,benzil}$ = 54 kcal/mol, $E_{T,benzophenone}$ = 69 kcal/mol).[19] This indicates that energy transfer from benzophenone to the di-π-methane substrate should be more exothermic and therefore more efficient than energy transfer from benzil. Interestingly, the rates of rearrangement for the two polymers are very similar (11% product formation **P2**, 17% product formation **P1** after 20 minutes of continuous irradiation) suggesting that the rate limiting step does not involve energy transfer.
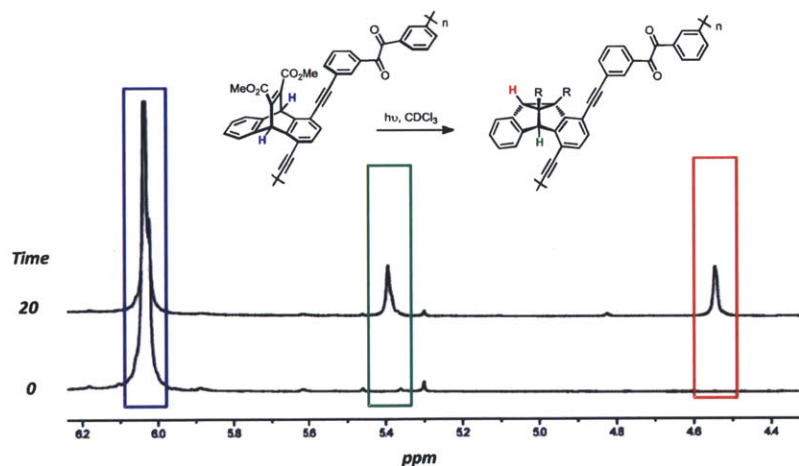

Figure 3.9. Stacked ^{1}H NMR spectra obtained during photolysis of **P2**.

74

Close inspection of the fluorescence spectra of **5**, **P1**, and **P2** reveals that the emission from **P1** exhibits a bathochromic shift of approximately 100 nm compared to model compound **5** and also lacks the well resolved vibrational structure characteristic of these chromophores. It is interesting that neither polymer exhibits any emission similar to that of **5** (despite using a λ_{ex} = 300 nm), this suggests that the emission from the dibenzobarrelene core is sufficiently quenched by the triplet sensitizer. This is consistent with an energy transfer cascade whereby excitation of the dibenzobarrelene core is followed by energy transfer (Dexter or FRET) to the sensitizer which then undergoes intersystem crossing to the lowest triplet state followed by back energy transfer (Dexter) to the dibenzobarrelene unit with subsequent rearrangement. The origin of the emission from **P1** is unknown and may be due to an impurity or defect site in the polymer backbone (alkyne homocoupling).
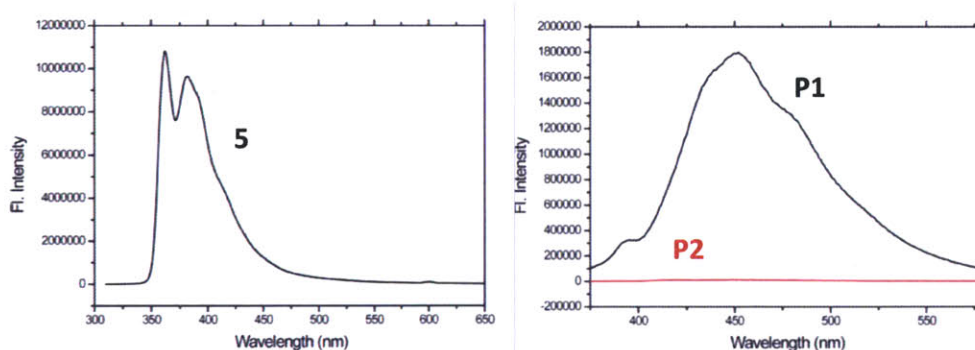
Figure 3.10. Fluorescence spectra of model compound **5** (left), **P1** and **P2** (right). Spectra were taken in dichloromethane solution using λ_{ex} = 300 nm with O.D. of 0.1 for all components.

3.6 Alignment of Liquid Crystal Phases using P1.

Benzil is known to react with oxygen during extended exposure to visible wavelengths greater than 400 nm to form peroxides.[20] This characteristic is not ideal for devices and required us to direct our attention towards **P1**. In order to test the alignment capabilities of **P1** we

fabricated simple LC devices as shown in Figure 3.11. The fabrication process begins with formation of a thin film of **P1** on a clean glass substrate followed by polarized irradiation. This process is repeated on a second substrate and the two slides are sandwiched together with 6 μm spacers and sealed with epoxy. The cells are then filled with the LC material at a temperature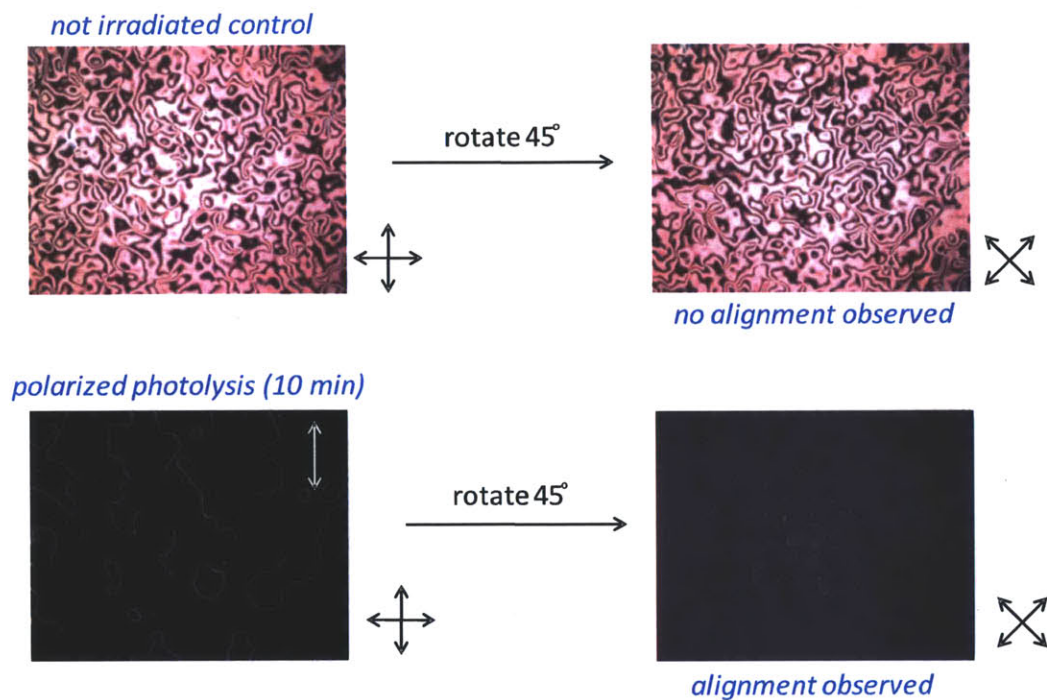 above the clearing point of the LC and allowed to slowly cool to the nematic phase. The alignment was observed via polarized optical microscopy (POM) on a rotating stage with crossed polarizers. In the case where the photoalignment layers are oriented parallel to each other we expect no light to pass through the cell when the LC director is parallel to either of the two polarizers when crossed. However, if the cell is rotated off-axis (45° angle relative to either polarizer), then we expect light to pass through the cell. Figure 3.12 exemplifies this situation.
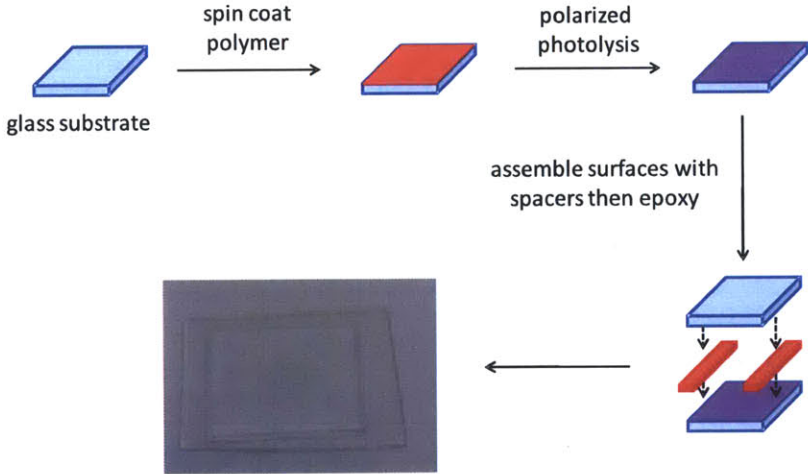

Figure 3.11. Schematic depiction of LC cell fabrication using photoalignment polymer **P2.**

not irradiated control

rotate 45°

no alignment observed

polarized photolysis (10 min)

rotate 45°

alignment observed

Figure 3.12. Optical micrographs of LC cells where the photopolymer **P1** has not been irradiated (top) or has been irradiated with polarized light (bottom). Irradiation was carried out for 10 minutes in air (LC = MLC 6884). Black arrows correspond to the orientation of the polarizers.

As can be seen in Figure 3.12, LC cells that have not been irradiated display no alignment whatsoever. This is indicated by the consistent brightness of the cells when rotated by the indicated amount. When the cells have been irradiated with polarized light the alternation between bright and dark states becomes evident and is consistent with alignment. To further probe the utility of this approach we attempted to create more elaborate patterns by using photomasks in conjuction with the polarized irradiation. Figure 3.13 displays an open-faced cell where a striped photomask was employed to generate alternating regions of irradiated and not-irradiated **P1**.
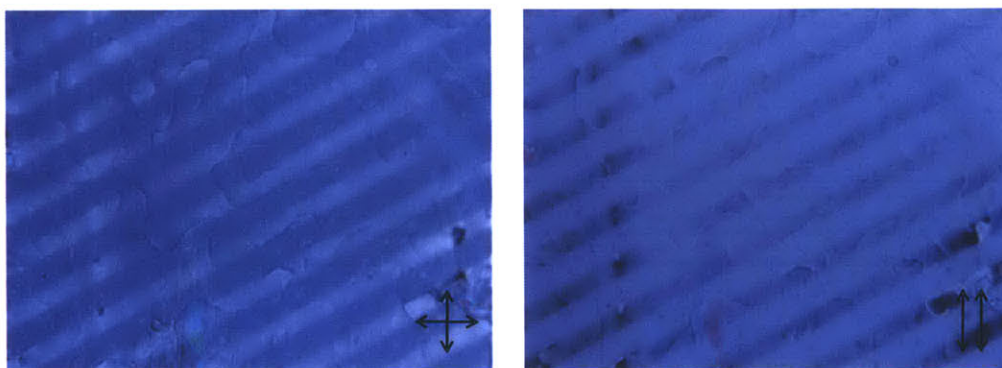
Figure 3.13. Optical micrographs of LC cells where the photopolymer **P1** has been irradiated through a polarizer and striped photomask. Irradiation was carried out for 10 minutes in air (LC = MLC 6884). The alternating stripes correspond to features of 100 μm. Black arrows correspond to the orientation of the polarizers.

We anticipated that the non-irradiated regions would exhibit no alignment; however, we were surprised to find that both irradiated and non-irradiated regions displayed significant alignment. Interestingly, Figure 3.13 shows that the two regions are aligned orthogonal to one another – a completely unexpected result. We hypothesize that this result may be due to swelling of the polymer in the irradiated regions which would generate a surface topography of alternating ridges and valleys. It has been shown previously that such surface patterns are capable of aligning LC mesogens.[21]

3.7 Conclusion.

In conclusion we have shown the design and synthesis of two new photoresponsive polymers that are capable of undergoing the di-π-methane rearrangement. The polymers contain triplet sensitizers within the polymer backbone that are capable of sensitizing the reaction via triplet-triplet Dexter energy transfer. In addition, these polymers are capable of aligning liquid

crystal mesogens by exploiting the IFV of dibenzobarrelene structures. Further work is currently underway in our laboratory to probe the scope of this approach.

3.8 Experimental Section.

MATERIALS AND METHODS: Toluene, CH_2Cl_2 and THF were purified by passage through solvent purification columns containing activated alumina. *N,N*-Dimethylformamide (DMF) was distilled from $MgSO_4$ and stored over 4Å molecular sieves. Diisopropylamine was distilled from CaH_2. All other reagents were obtained from commercial sources and used as received unless otherwise noted.

INSTRUMENTATION: NMR spectra were recorded on Varian Mercury 300 MHz, Varian Inova 500 MHz or Varian Inova 501 MHz spectrometers. Chemical shifts were reported in ppm and referenced to residual NMR solvent peaks ($CDCl_3$: δ 7.27 ppm for ^1H, δ 77.23 ppm for ^{13}C). High-resolution mass spectra (HRMS) were obtained at the MIT Department of Chemistry using a peak-matching protocol to determine the mass and error range of the molecular ion. Electrospray or direct analysis in real time (DART), operating in negative ion mode, were used as the ionization techniques. Melting points were measured on a Mel-Temp II apparatus (Laboratory Devices INC) and were not corrected. Number average molecular weights (M_n) and polydispersity (PDI) of polymers were obtained on a HP series 1100 gel permeation chromatography (GPC) system in THF and calibrated with polystyrene standards and utilizing both UV (450 nm) and refractive index detection. . UV-vis spectra were measured on an Agilent 8453 diode array spectrophotometer and corrected for background signal with a solvent filled cuvette. Fluorescence spectra were obtained using a SPEX Fluorolog-τ3 fluorimeter using right-

angle detection (solution measurements) or front-face detection (thin film measurements). Thin films containing **P1** and **P2** were fabricated by spin-coating (5000 RPM for 1 min) chloroform solutions of the appropriate concentrations (Specialty Coating Systems™ G3P-8 Spincoat). The films were then placed under vacuum to ensure complete removal of the residual solvent. Photolysis experiments were carried out using a BlueWave® 200 light curing system from Dymax. A FGUV W53199 UV filter from Thorlabs, Inc. was used generate 360 nm light output (36 mW/cm^2). Linearly polarized irradiation was achieved using a Glan-Taylor polarizer.

SYNTHETIC PROCEDURES AND CHARACTERIZATION:
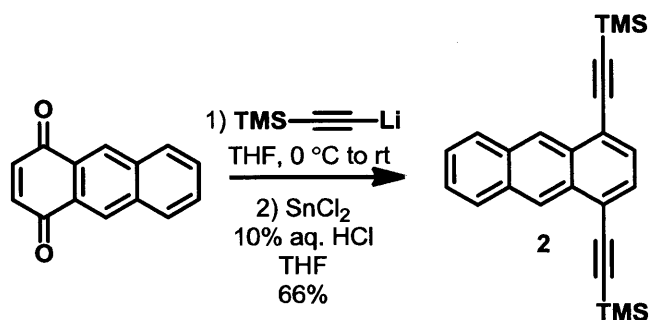
1,4-Bis[(trimethylsilyl)ethynyl]anthracene (2). Compound **2** was prepared based on a preparation described by Tannaci et al.[22] A flame dried flask was charged with dry THF (40 mL) and ethynyltrimethylsilane (1.42 g, 14.41 mmol). To this solution was added butyllithium (8.8 mL, 1.6 M) drop-wise over a period of 30 minutes at 0 °C under a nitrogen atmosphere. This solution was stirred and allowed to warm to room temperature (~1 hour). After 1 hour, 1,4-anthraquinone (1 g, 4.80 mmol) was added as a single solid portion to the stirring solution. The reaction mixture immediately turned purple upon addition of the solid. The solution was stirred at room temperature for 12 h at room temperature and monitored by TLC. To this solution was added saturated SnCl$_2$ in 10% aqueous HCl (10 mL). The solution immediately changed from a

purple to orange color and the reaction monitored by thin-layer chromatography. Upon completion, the reaction mixture was partitioned between water and hexanes. The organic phase was washed three times with water and passed through a plug of silica gel. The resulting yellow solid was further purified by recrystallization from ethanol to yield 1.2 g (66%) of a brilliant yellow solid. mp 169 °C. ^{1}H NMR (125 MHz, CDCl$_3$): δ 8.93 (s, 2H), 8.06 - 8.11 (m, 2H), 7.69 (s, 2H), 7.54 – 7.58 (m, 2H), 0.45 (s, 18H). ^{13}C NMR (501 MHz, CDCl$_3$): δ 132.90, 131.23, 130.45, 129.24, 126.93, 126.44, 122.44, 103.90, 102.59, 0.89.
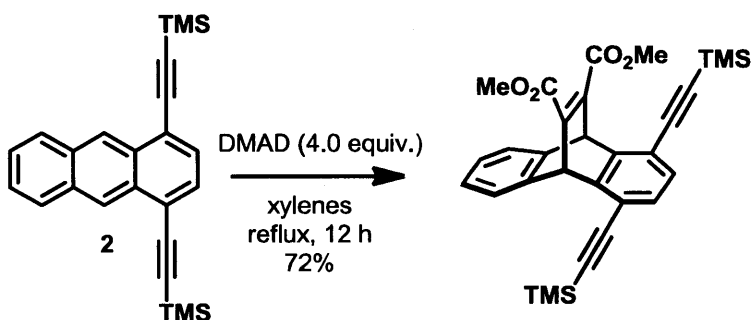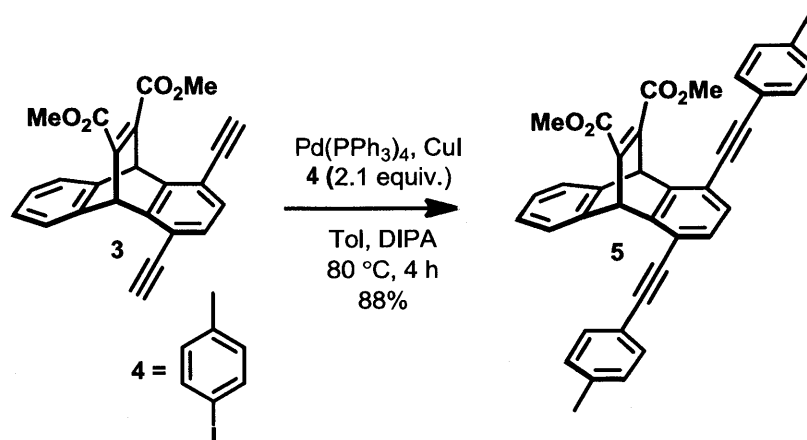

Dimethyl   1,4-bis[(trimethylsilyl)ethynyl]-9,10-dihydro-9,10-ethenoanthracene-11,12-dicarboxylate. The title compound was prepared using a procedure similar to that reported by McNeil et al.[23] To a flame dried 50 mL round-bottom flask was added compound **2** (1.0 g, 2.69 mmol), DMAD (1.53 g, 10.79 mmol), and 10 mL of dry o-xylenes. The reaction was refluxed under a nitrogen atmosphere for 12 h. The reaction was cooled to room temperature, concentrated in vacuo and purified by column chromatography using 90/10 hexanes/EtOAc. The material was then triturated with cold methanol to remove any residual DMAD. The off-white solid was dried *in vacuo* to yield .99 g (1.94 mmol) of the target compound. ^{1}H NMR (501 MHz, CDCl$_3$): δ 7.40-7.41 (m, 2H), 7.04-7.06 (m, 4H), 5.95 (s, 2H), 3.82 (s, 6H), 0.35 (s, 18H). ^{13}C NMR (125 MHz, CDCl$_3$): δ 166.16, 147.77, 146.902, 143.812, 128.65, 126.37, 124.95, 119.51,

102.48, 100.71, 53.14, 51.41, 0.71. MS (DART) calc for $C_{30}H_{32}O_4Si_2$ [M + H]⁻: 513.1912, found 513.1912.
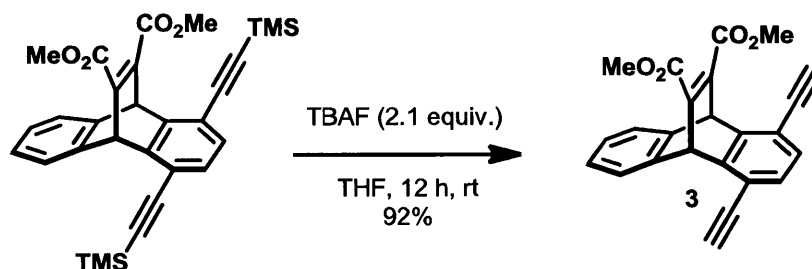

Dimethyl 1,4-diethynyl-9,10-dihydro-9,10-ethenoanthracene-11,12-dicarboxylate (3). To a flame-dried 50 mL round-bottom flask was added dry THF (20 mL) and dimethyl 1,4-bis[(trimethylsilyl)ethynyl]-9,10-dihydro-9,10-ethenoanthracene-11,12-dicarboxylate (0.5 g, 0.975 mmol) under a nitrogen atmosphere. TBAF (2.05 mL, 1.0 M) was added slowly via a syringe and allowed to stir overnight. The reaction mixture was concentrated *in vacuo* and purified by silica gel column chromatography using 2:1 (hexanes/CH_2Cl_2) to afford a off-white solid (0.33 g, 0.897 mmol, 92%). ^{1}H NMR (501 MHz, $CDCl_3$): δ 7.47-7.45 (m, 2H), 7.16 (s, 2H), 7.06-7.08 (m, 2H), 5.99 (s, 2H), 3.8 (s, 6H), 3.43 (s, 2H). ^{13}C NMR (125 MHz, $CDCl_3$): δ 165.83, 146.97, 146.70, 143.18, 128.90, 126.04, 124.56, 118.39, 82.58, 80.49, 52.81, 50.69. MS (DART) calc for $C_{24}H_{16}O_4$ [M + H]⁻: 369.1121, found 369.1135.

Dimethyl 1,4-bis (*p*-tolylethynyl)-9,10-ethenoanthracene-11,12-dicarboxylate (5). To a flame-dried 10 mL Schlenk flask was added dry toluene (5 mL), dry diisopropylamine (2 mL), compound **3** (0.05 g, 0.136 mmol), and compound **4** (0.062 g, 0.285 mmol) under a nitrogen atmosphere. The flask was evacuated and refilled with nitrogen three times followed by addition of a spatula tip of tetrakis(triphenylphosphine)palladium and CuI. The vessel was sealed and heated to 80 °C for 4 h with stirring under a nitrogen atmosphere. The reaction mixture was then cooled to room temperature, concentrated in vacuo and partitioned between CH_2Cl_2 and water. The organic phase was washed with saturated NH_4Cl (aq) solution followed by three washes with water. The organic phase was concentrated *in vacuo* and purified by silica gel column chromatography using 2:1 (Hexanes:CH_2Cl_2). The light brown powder was dried in vacuo to yield 0.66 g (0.119 mmol, 88%) of the title compound. ^{1}H NMR (501 MHz, CDCl$_3$): δ 7.53-7.54 (d, J = 7.85 Hz, 4H), 7.47-7.48 (m, 2H), 7.24-7.25 (d, J = 7.85 Hz, 4H), 7.17 (s, 2H), 7.05-7.07 (m, 2H), 6.07 (s, 2H), 3.83 (s, 6H), 2.43 (s, 6H). ^{13}C NMR (125 MHz, CDCl$_3$): δ 166.37, 147.74, 146.36, 143.94, 139.61, 132.34, 129.99, 128.73, 126.40, 125.01, 120.71, 119.60, 95.35, 86.46, 53.25, 51.54, 22.34. MS (DART) calc for $C_{38}H_{28}O_4$ [M + H]$^-$: 549.2060, found 549.2059.
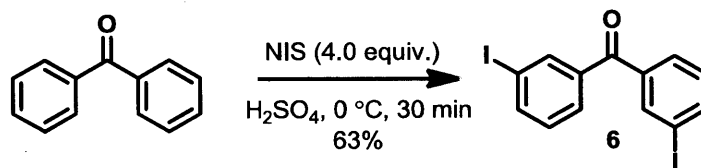
Bis(3-iodophenyl)methanone (6). The title compound was prepared by following the literature procedure reported by Chaikovskii et al.[18] To a round-bottom flask was added 30 mL of sulfuric acid (90%) and cooled to 0 °C with an ice bath. To this solution was added N-iodosuccinimide (2.25 g, 10 mmol) and the reaction was stirred until it became homogenous. To this solution was added benzophenone (0.46 g, 2.5 mmol) as a single solid portion and the solution was stirred for 4 h. The reaction mixture was then poured onto a 100 mL ice/water mixture and treated with Na_2SO_3 solution. The mixture was partitioned between CH_2Cl_2 and water and the organic phase was washed three times with water. The organic phase was concentrated *in vacuo* and the resulting solid purified by recrystallization (EtOH) to yield 0.69 g (1.58 mmol, 63%) of a white crystalline solid. mp 146 °C. ^{1}H NMR (501 MHz, $CDCl_3$): δ 8.12 (s, 2H), 7.93-7.95 (d, J = 7.48 Hz, 2H), 7.70-7.72 (d, J = 7.48 Hz, 2H), 7.23-7.26 (t, J = 8.39 Hz, 2H). ^{13}C NMR (125 MHz, $CDCl_3$): δ 194.18, 142.27, 139.47, 139.25, 130.77, 129.80, 94.96.
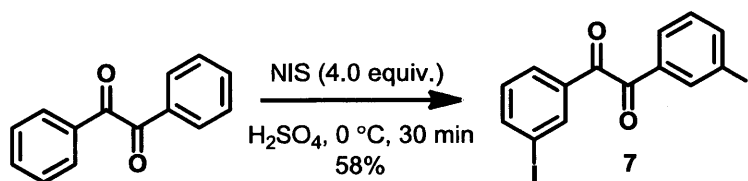

1,2-bis(3-iodophenyl)ethane-1,2-dione (7). The title compound was prepared using the same procedure and quantities described above. Yield = 0.70 g (58%). mp 127 °C. ^{1}H NMR (501 MHz, $CDCl_3$): δ 8.31 (s, 2H), 7.99-8.01 (d, J = 6.89 Hz, 2H), 7.89-7.92 (d, J = 6.89 Hz, 2H),

7.25-7.28 (t, J = 8.01 Hz, 2H. ^{13}C NMR (125 MHz, CDCl$_3$): δ 192.04, 144.03, 138.67, 134.55, 130.92, 129.44, 94.95.
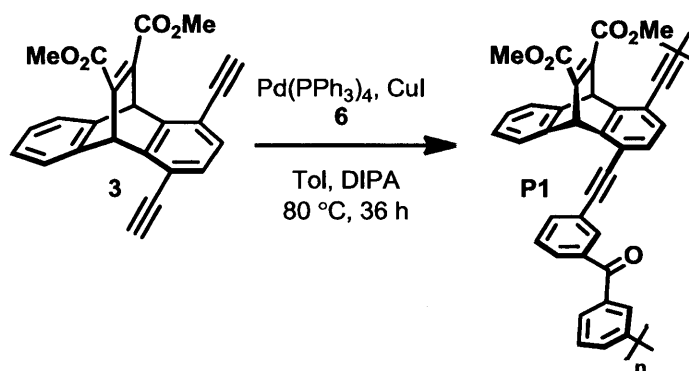
P1. To a flame-dried 25 mL Schlenk flask was added dry toluene (5 mL), dry diisopropylamine (3 mL), compound **3** (0.1 g, 0.271 mmol) and compound **6** (0.118 g, 0.271 mmol). The reaction vessel was subjected to one cycle of freeze-pump-thaw where during the freeze cycle a spatula tip quantity of tetrakis(triphenylphosphine)palladium and CuI was added. The reaction mixture was then subjected to two additional freeze-pump-thaw cycles and heated to 80 °C for 36 h under a nitrogen atmosphere. The solution was cooled to room temperature and reprecipitated directly into cold acetone (200 mL). The white polymeric material was partitioned between CHCl$_3$ and water, washed once with sat. NH$_4$Cl (aq) and washed three times with water. The organic phase was concentrated *in vacuo* to a volume of approximately 1 mL and reprecipitated from cold acetone to yield 0.09 g (61%) of a white powder. GPC gave M$_n$ = 15,000; PDI = 1.8, DP = 26. ^{1}H NMR (501 MHz, CDCl$_3$): δ 8.08 (broad, 2H), 7.84 (broad, 4H), 7.57 (broad, 2H), 7.44 (broad, 2H), 7.17 (broad, 2H), 7.00 (broad, 2H), 6.03 (broad, 2H), 3.77 (broad, 6H). ^{13}C NMR (125 MHz, CDCl$_3$): δ 166.18, 147.58, 146.81, 143.58, 138.29, 136.31, 133.65, 130.77, 129.39, 128.93, 126.51, 125.04, 124.36, 119.30, 94.11, 88.14, 53.25, 51.48.
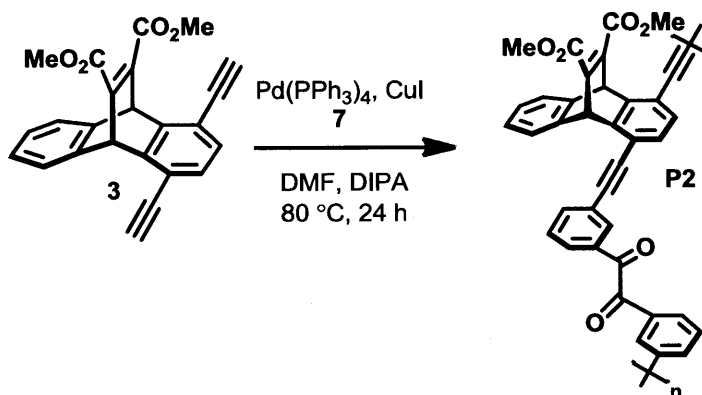
P2. To a flame-dried 25 mL Schlenk flask was added dry DMF (5 mL), dry diisopropylamine (3 mL), compound **3** (0.1 g, 0.271 mmol) and compound **7** (0.125 g, 0.271 mmol). The reaction vessel was subjected to one cycle of freeze-pump-thaw where during the freeze cycle a spatula tip quantity of tetrakis(triphenylphosphine)palladium and CuI was added. The reaction mixture was then subjected to two additional freeze-pump-thaw cycles and heated to 80 °C for 24 h under a nitrogen atmosphere during which time the target polymer appeared to crash out of the reaction. The vessel was cooled and the precipitate isolated by filtration. This white powder was taken up in $CHCl_3$ and washed with sat. NH_4Cl (aq) and water (3 times). The organic layer was isolated and concentrated to a volume of approximately 1 mL and then reprecipitated from cold methanol (200 mL) to yield 0.064 g (41%) of the target polymer. GPC gave M_n = 33,000; PDI = 3.1, DP = 60. ^{1}H NMR (501 MHz, $CDCl_3$): δ 8.3 (broad, 2H), 8.07 (broad, 2H), 7.97 (broad, 2H), 7.66 (broad, 2H), 7.51 (broad, 2H), 7.23 (broad, 2H), 7.10 (broad, 2H), 6.07 (broad, 2H), 3.85 (broad, 6H). ^{13}C NMR (125 MHz, $CDCl_3$): δ 193.70, 166.24, 147.66, 146.93, 143.63, 138.63, 133.73, 133.65, 130.76, 130.68, 130.10, 129.12, 126.7, 125.14, 119.33, 93.63, 88.68, 53.39, 51.54
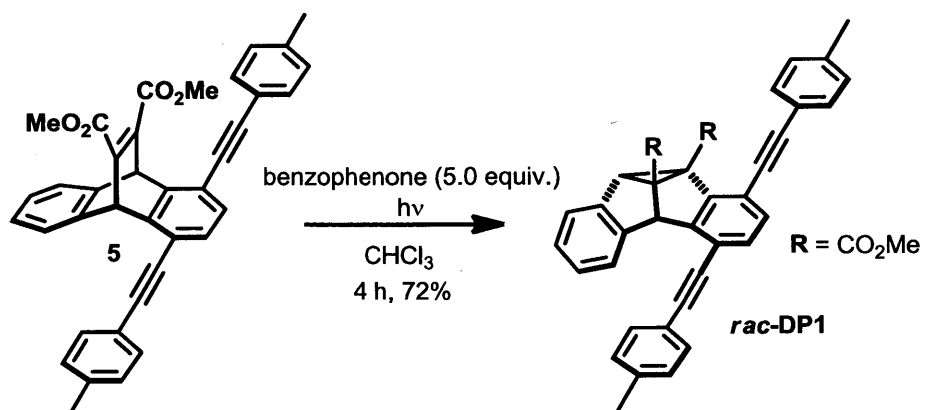
***rac*-DP1.** The title compound was synthesized by the bulk photolysis of compound **5** in $CHCl_3$ using benzophenone as a triplet sensitizer. To a rubber septum-stoppered quartz cuvette was added dry $CHCl_3$ (3.0 mL), compound **5** (0.05 g, 0.091 mmol) and benzophenone (0.083 g, 0.456 mmol). The cuvette was sparged with argon for 15 minutes and then irradiated with a lamp for 4 h. After photolysis, the reaction mixture was concentrated *in vacuo* and purified via silica gel column chromatography using hexanes/acetone (30:1).

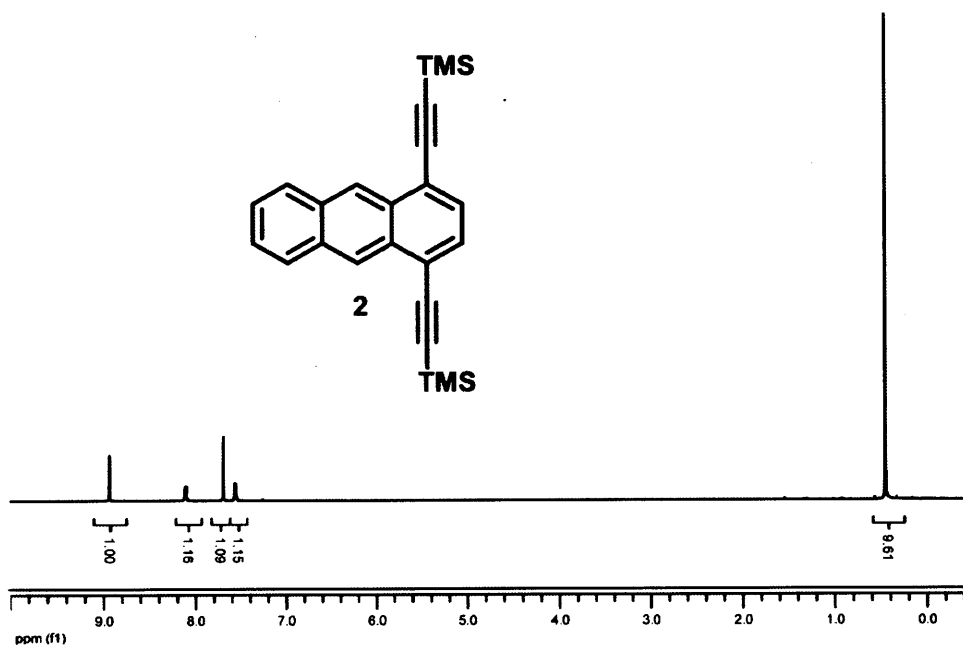**Figure 3.8.1.** ^{1}H NMR spectrum of **2** (500 MHz, CDCl$_3$).

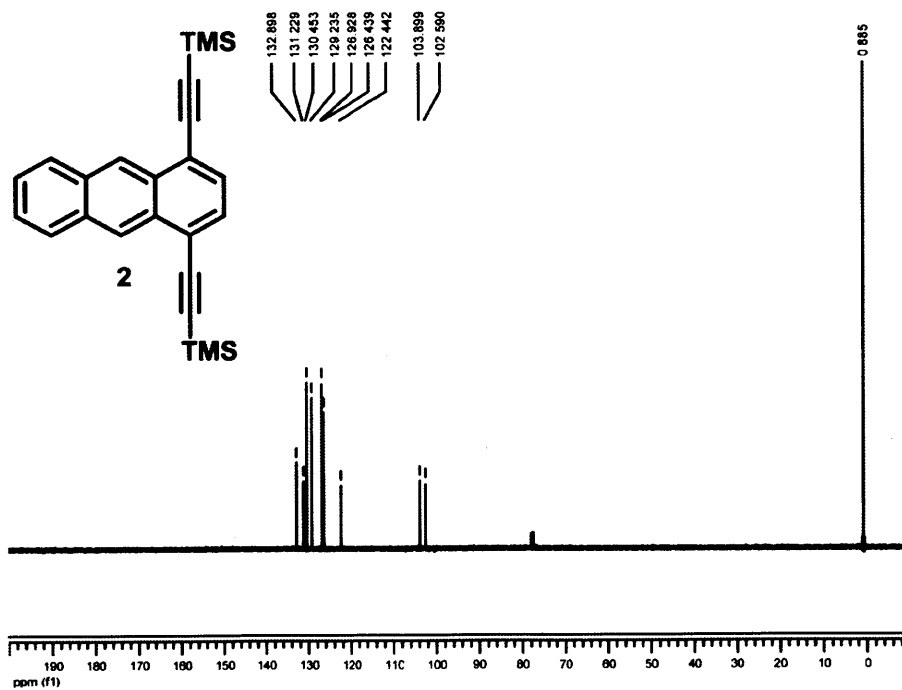**Figure 3.8.2.** ^{13}C NMR spectrum of **2** (125 MHz, CDCl$_3$).
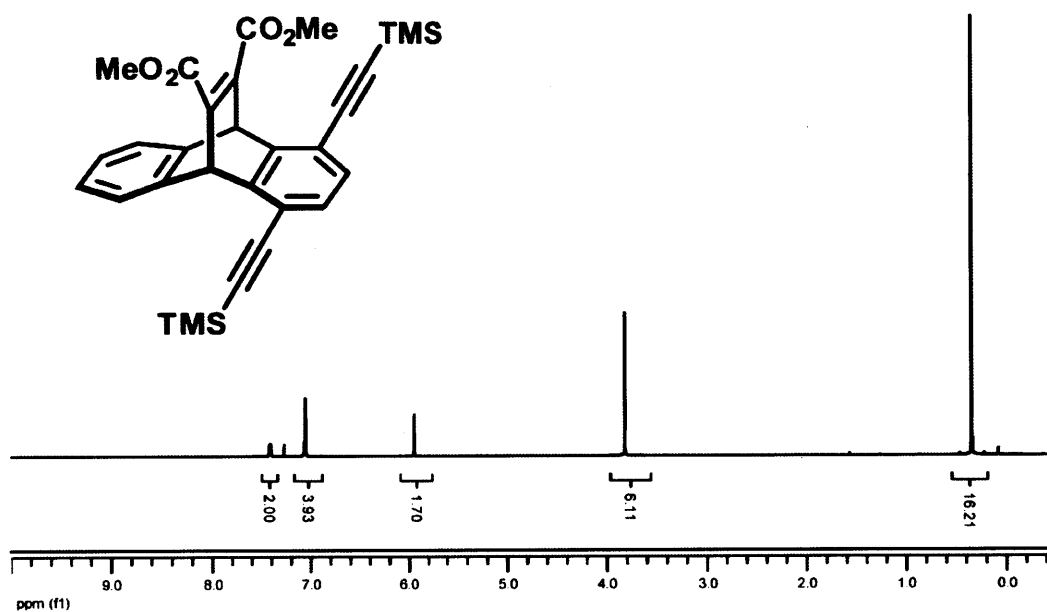
Figure 3.8.3. ^{1}H NMR spectrum of pictured compound (500 MHz, CDCl$_3$).
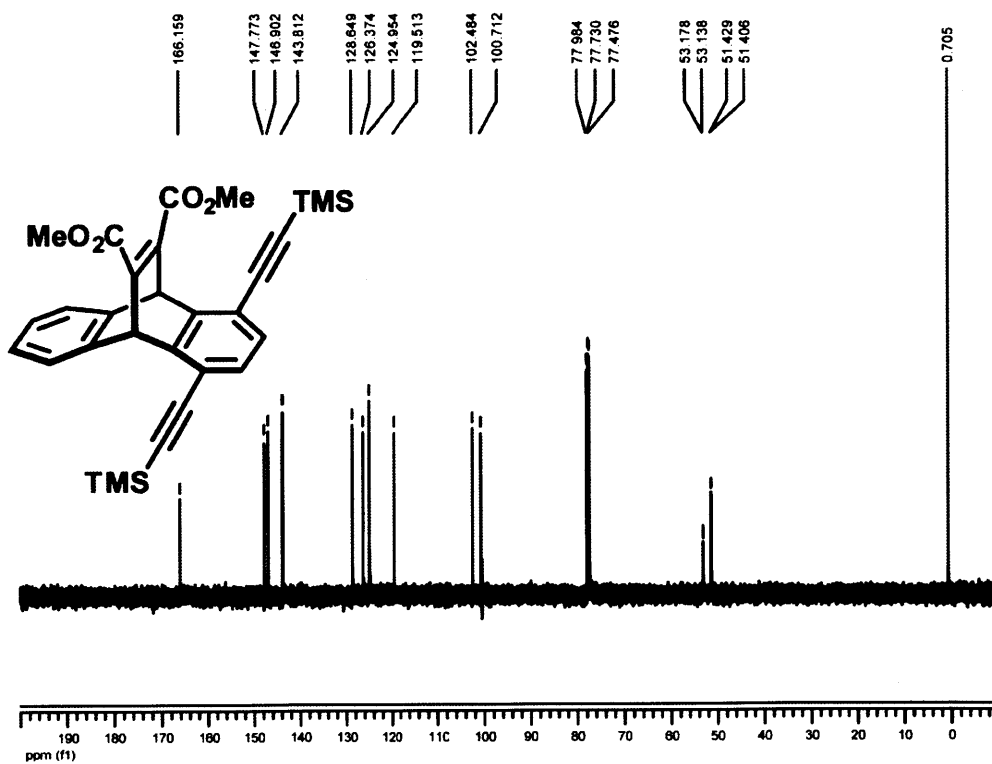

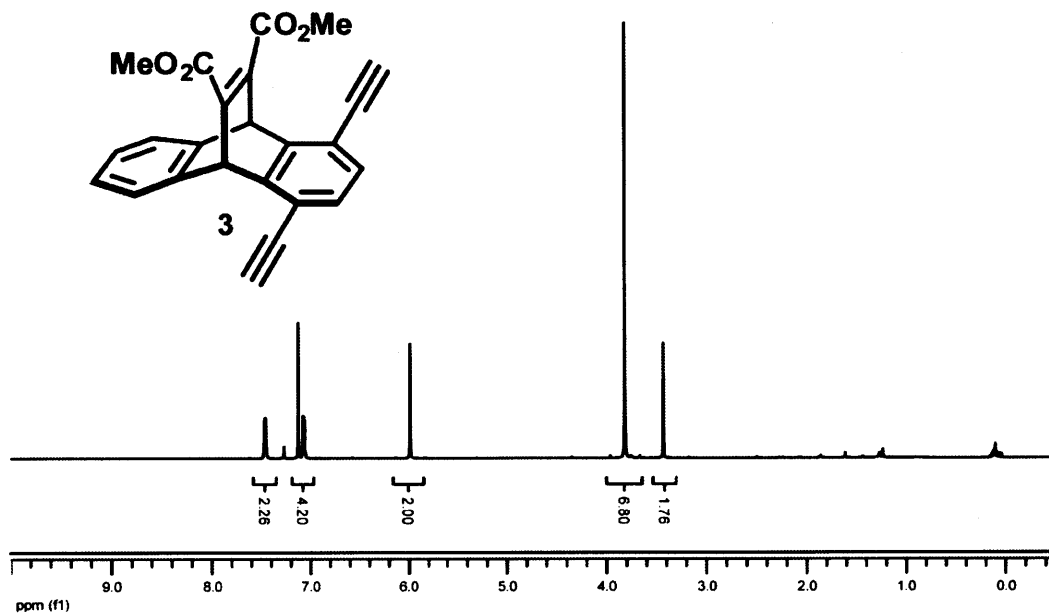**Figure 3.8.4.** ^{13}C NMR spectrum of pictured compound (125 MHz, CDCl$_3$).

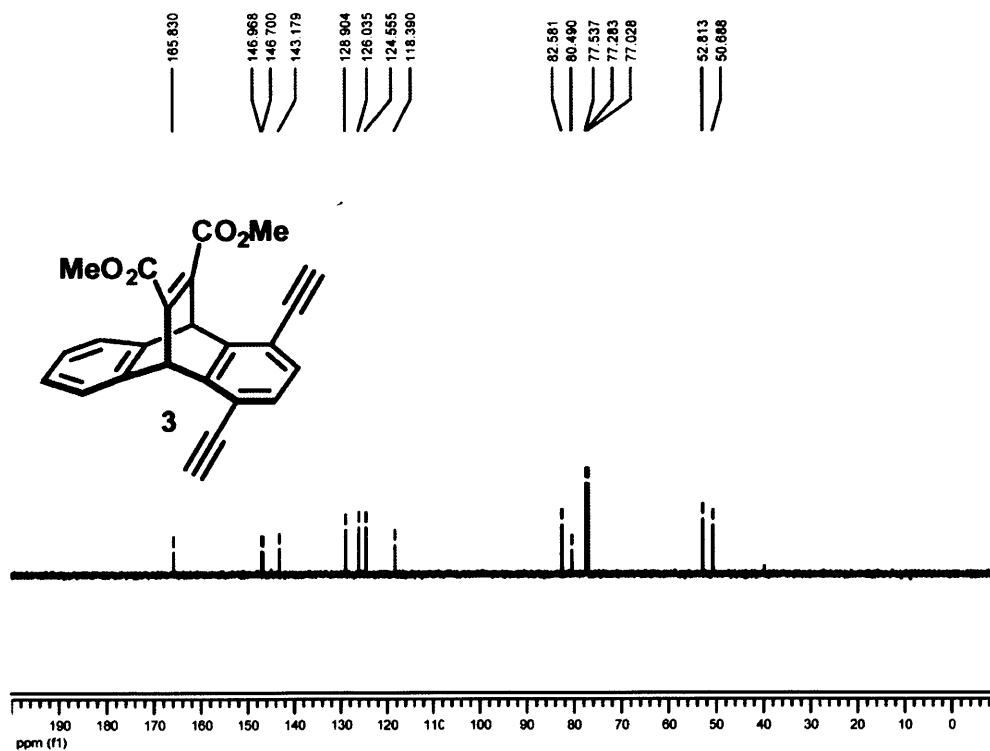**Figure 3.8.5.** ^{1}H NMR spectrum of **3** (500 MHz, CDCl$_3$).

Figure 3.8.6. ^{13}C NMR spectrum of **3** (125 MHz, CDCl$_3$).
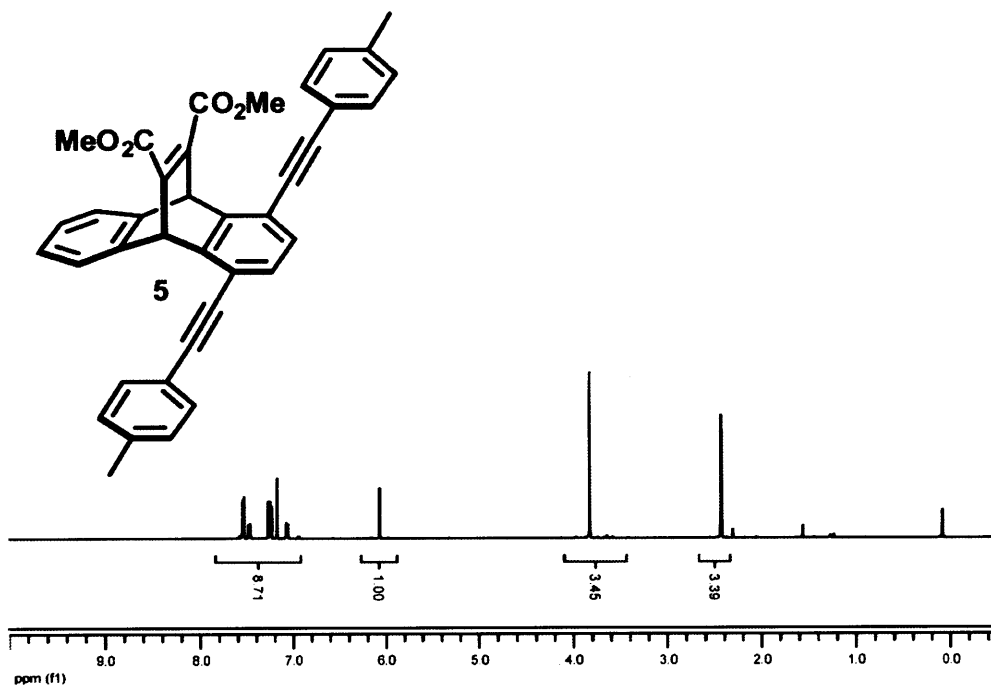
Figure 3.8.7. ^{1}H NMR spectrum of **5** (500 MHz, CDCl$_3$).
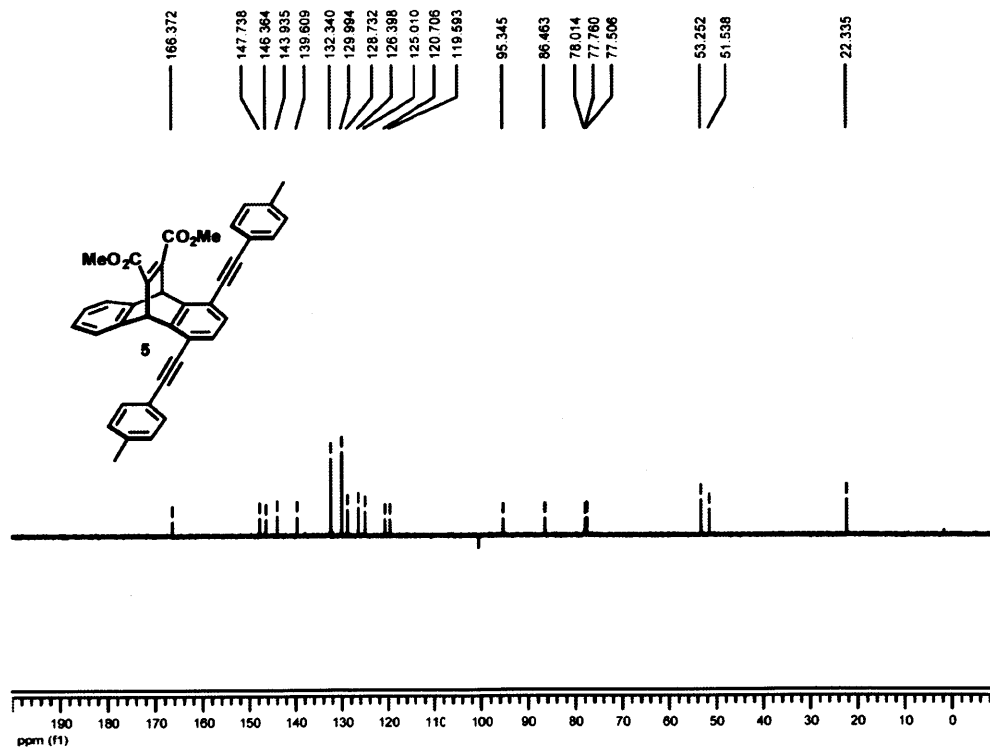
Figure 3.8.8. ^{13}C NMR spectrum of **5** (125 MHz, CDCl$_3$).
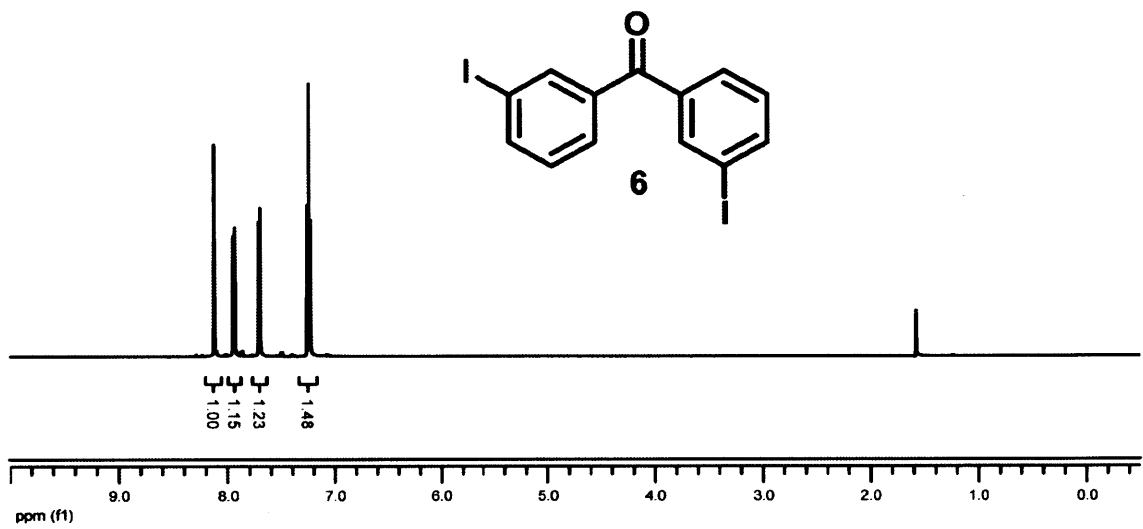
Figure 3.8.9. ^{1}H NMR spectrum of **6** (500 MHz, CDCl$_3$).
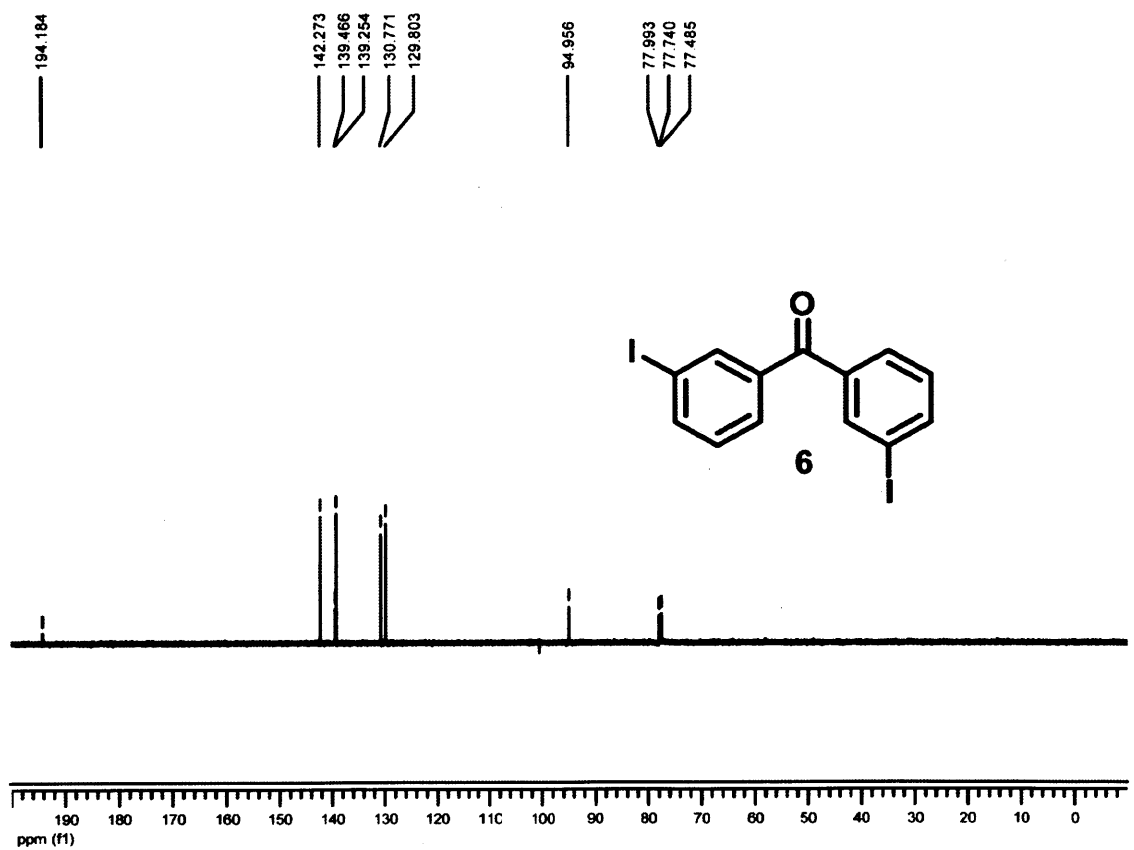
Figure 3.8.10. ^{13}C NMR spectrum of **6** (125 MHz, CDCl$_3$).
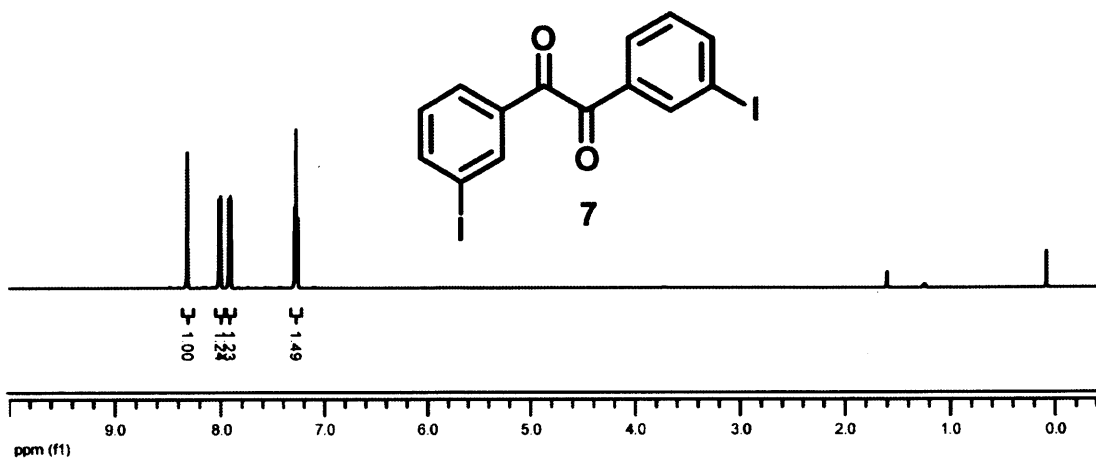
Figure 3.8.11. ^{1}H NMR spectrum of **7** (501 MHz, CDCl$_3$).
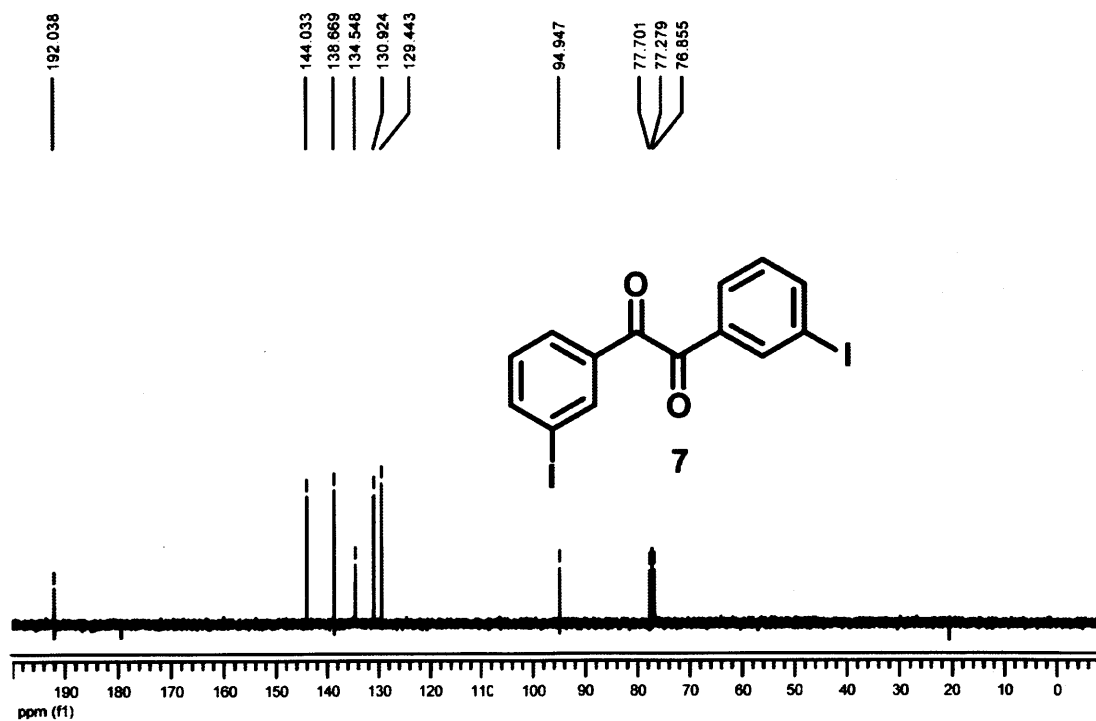
Figure 3.8.12. ^{13}C NMR spectrum of **7** (125 MHz, CDCl$_3$).
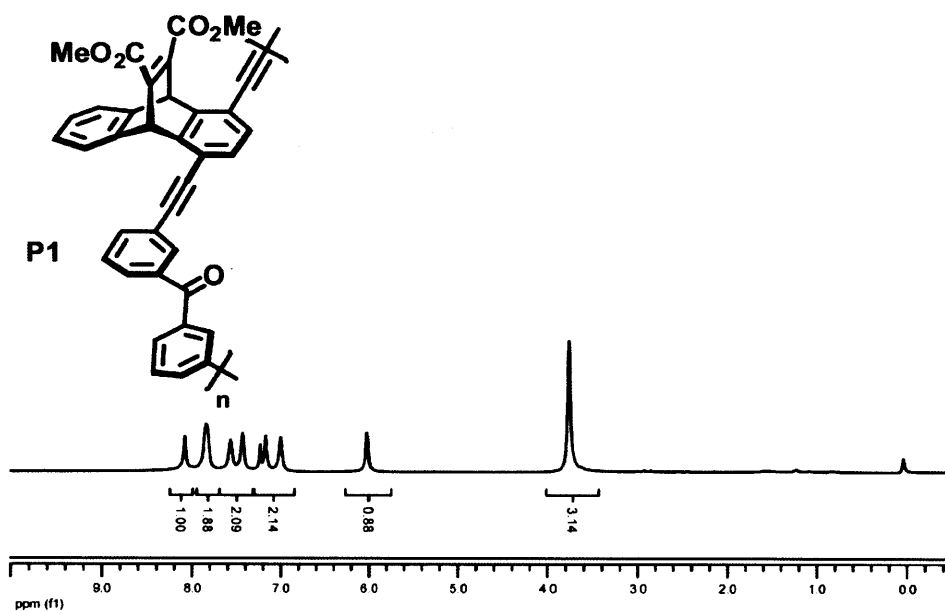
Figure 3.8.13. ^{1}H NMR spectrum of **P1** (500 MHz, CDCl$_3$).
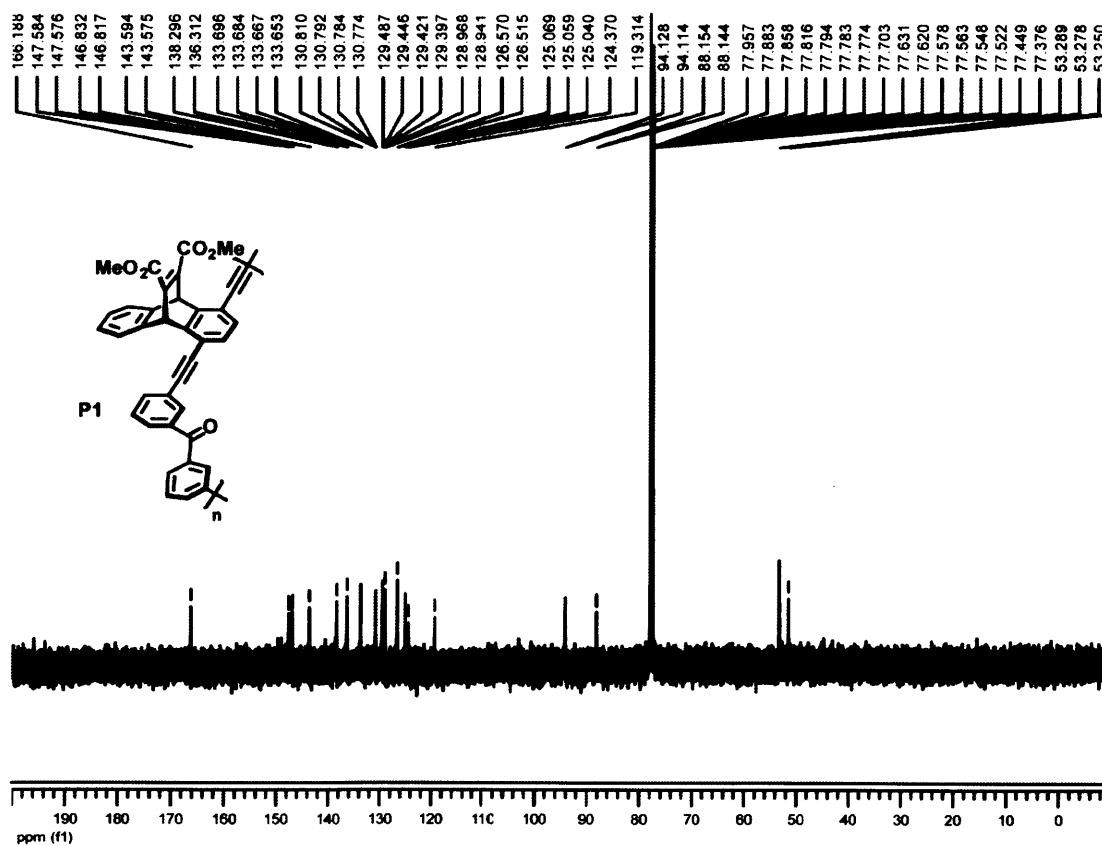
Figure 3.8.14. ^{13}C NMR spectrum of **P1** (125 MHz, CDCl$_3$).
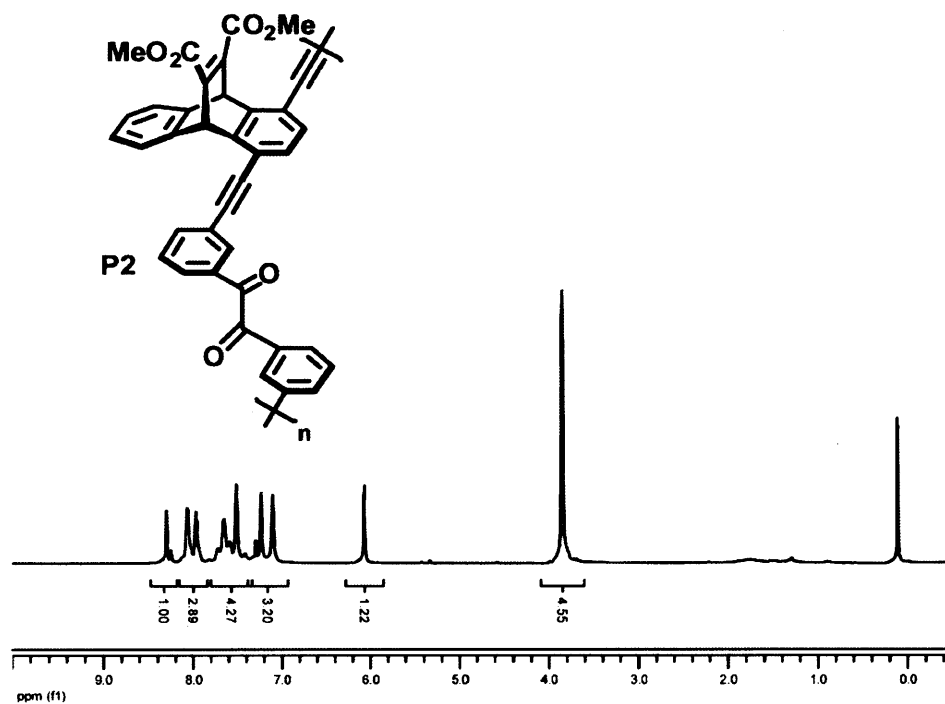
Figure 3.8.15. ^{1}H NMR spectrum of **P2** (500 MHz, CDCl$_3$).
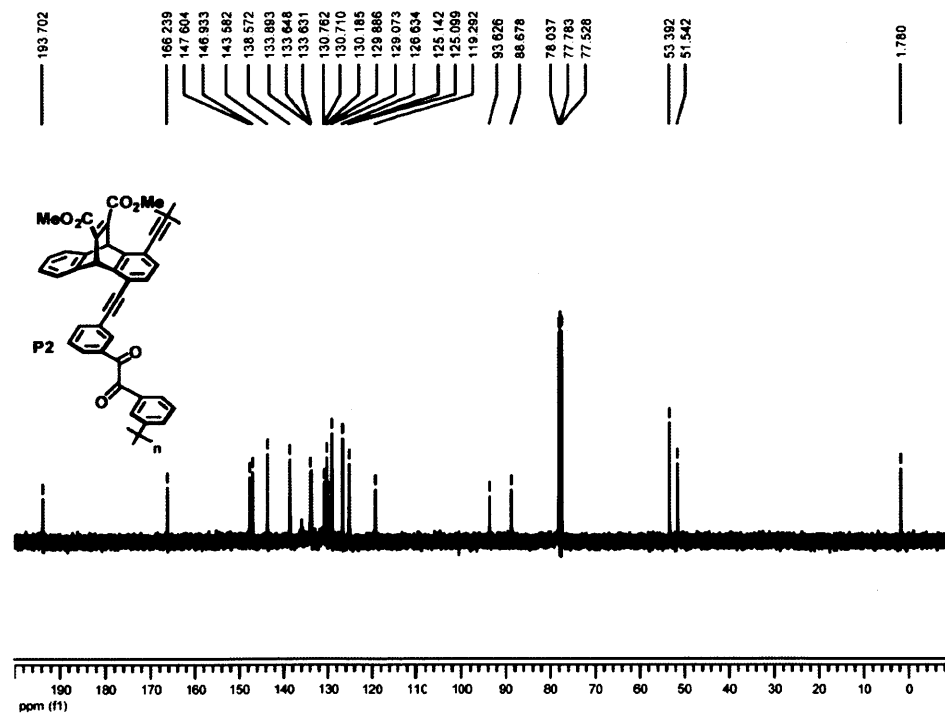
Figure 3.8.16. ^{13}C NMR spectrum of **P2** (125 MHz, CDCl$_3$).
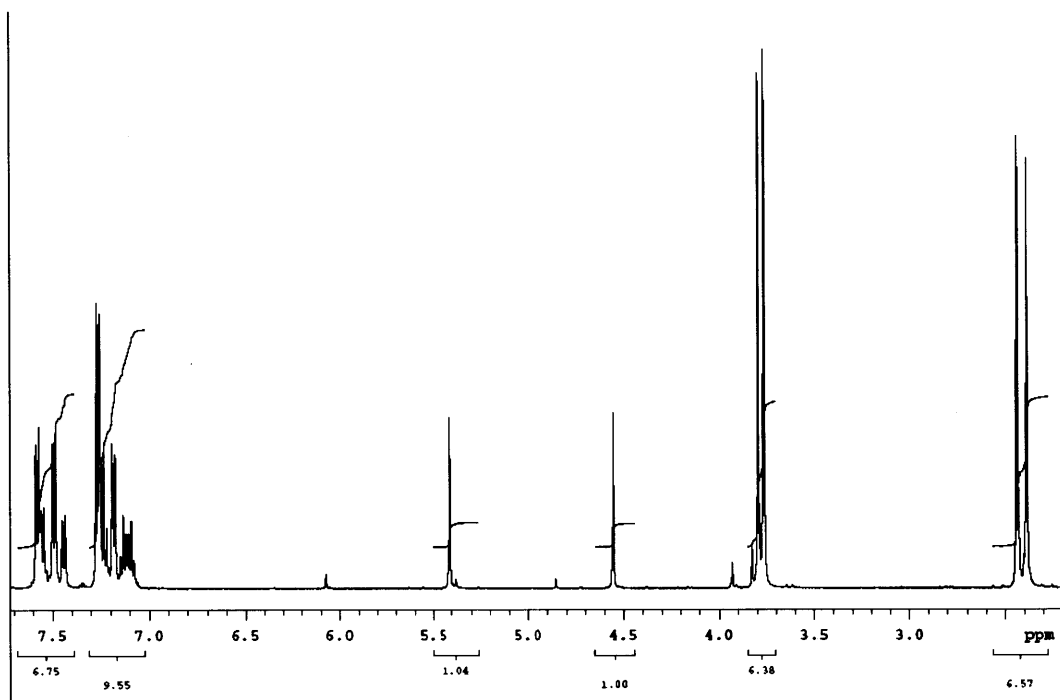
Figure 3.8.17. ^{1}H NMR spectrum of *rac*-**DP1** (500/ MHz, CDCl$_3$).
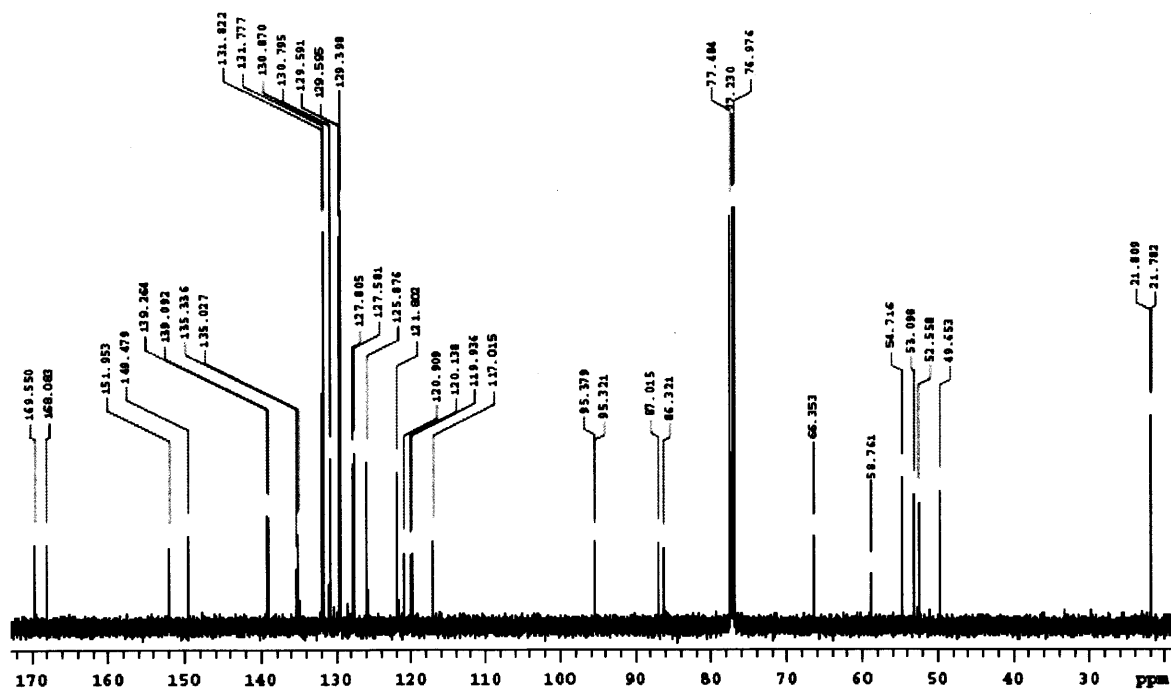
Figure 3.8.18. ^{13}C NMR spectrum of *rac*-**DP1** (125 MHz, CDCl$_3$).
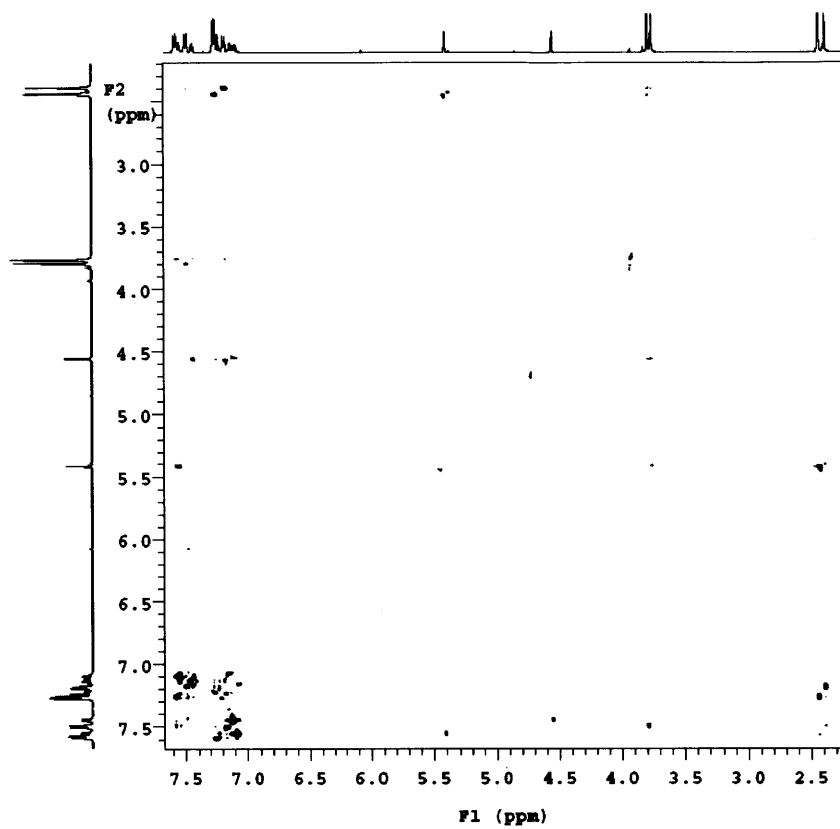
Figure 3.8.19. NOESY NMR spectrum of *rac*-**DP1** (500 MHz, CDCl₃).
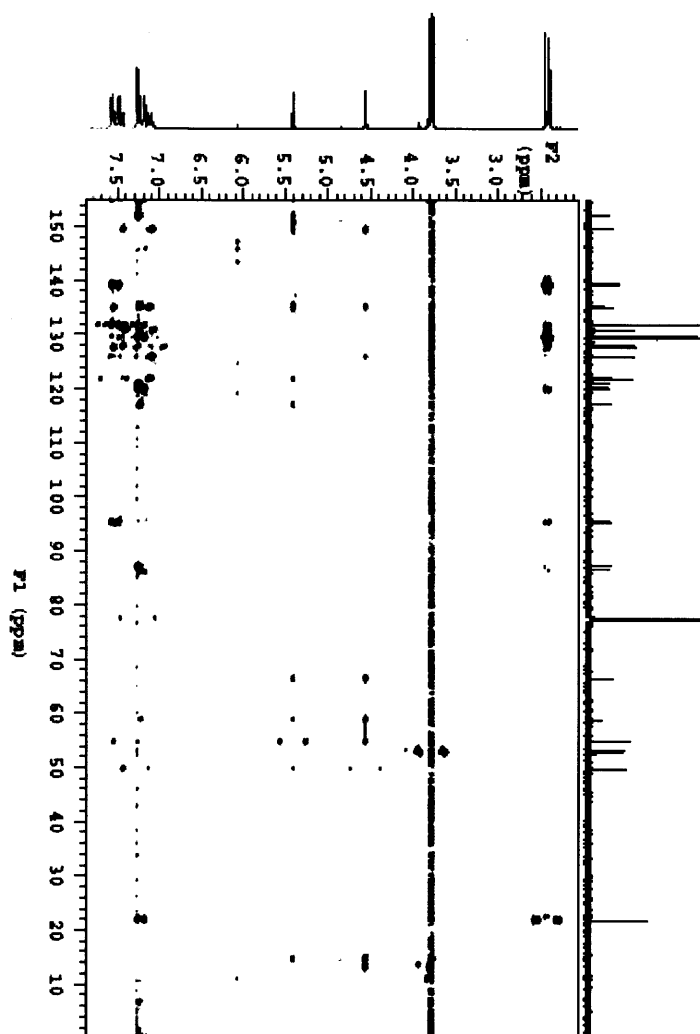
Figure 3.8.20. HMBC NMR spectrum of *rac*-**DP1** (500 MHz, CDCl₃).
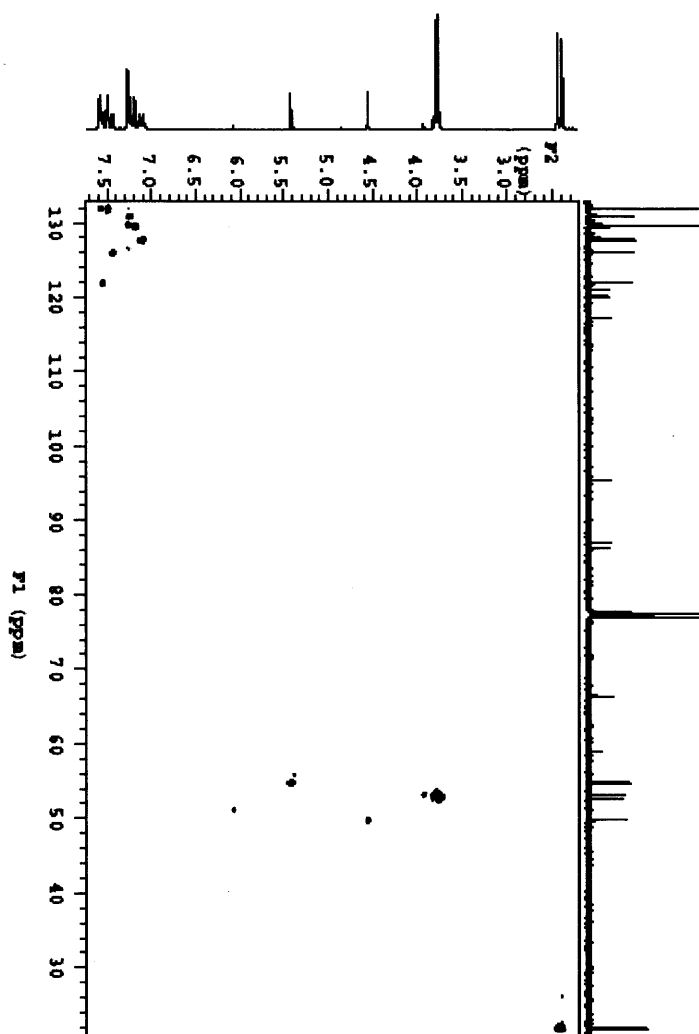
Figure 3.8.21. HSQC NMR spectrum of *rac*-**DP1** (500 MHz, CDCl₃).
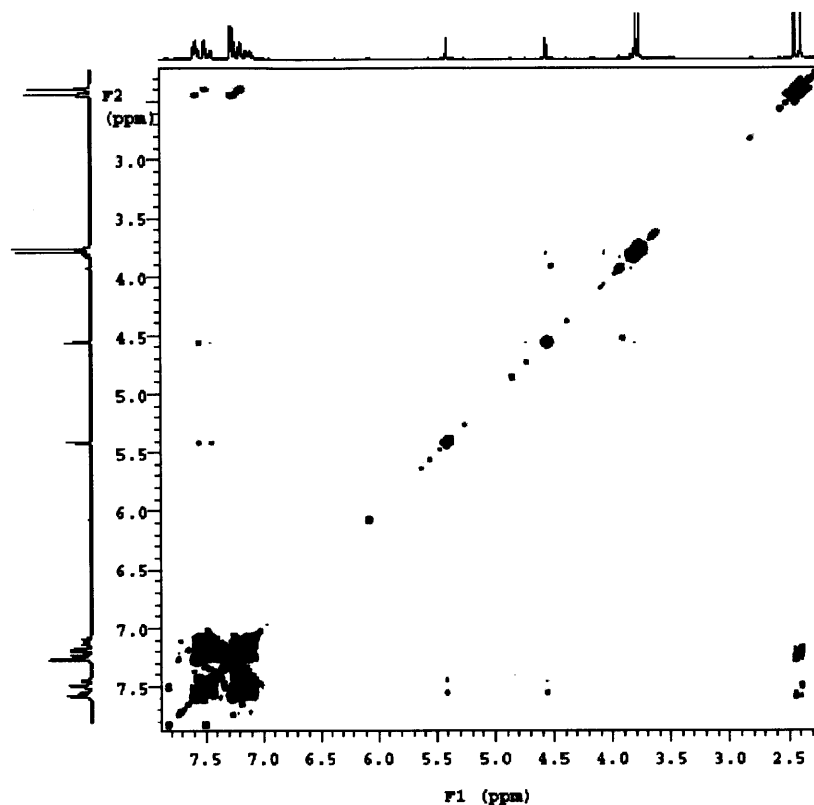
Figure 3.8.22. gCOSY NMR spectrum of *rac*-**DP1** (500 MHz, CDCl₃).

3.9 References

(1) Stasiek, J.; Stasiek, A.; Jewartowski, M.; Collins, M. W. *Optics & Laser Technology* **2006**, *38*, 243.

(2) d'Alessandro, A.; Asquini, R. *Mol. Cryst. Liq. Cryst.* **2003**, *398*, 207.

(3) Ohman, Y. *Nature* **1938**, *157*, 291.

(4) Kim, J.; Oh, C.; Escuti, M. J.; Hosting, L.; Serati, S. *Proc. SPIE* **2008**, *7093*, 709302.

(5) Poziomek, F. J.; Novak, T. J.; MacKay, R. A. *Mol. Cryst. Liq. Cryst.* **1973**, *27*, 175.

(6) Beeckman, J.; Neyts, K.; Vanbrabant, P. J. M. *Optical Engineering* **2011**, *50*, 081202-1.

(7) Reinitzer, F. *Monatsh. Chem.* **1888**, *9*, 421.

(8) Gelbart, W. M.; Barboy, B. *Acc. Chem. Res.* **1980**, *13*, 290.

(9) Mauguin, C. *Bull. Soc. Fr. Miner.* **1911**, *34*, 71.

(10) (a) Lee, K.-W.; Paek, S.; Lien, A.; Durning, C.; Fukuro, H. *Polymer Surfaces and Interfaces: Characterization, Modification, and Application*; Mittal, K. L.; Lee, K.-W.; Eds.; VSP: The Netherlands, 1996; p 1. (b) Geary, J. M.; Goodby, J. W.; Kmetz, A. R.; Patel, J. S. *J. Appl. Phys.* **1987**, *62*, 4100. (c) Seo, D.-S.; Muroi, K.; Isogami, T.; Matsuda, H.; Kobayashi, S. *Jpn. J. Appl. Phys.* **1992**, *31*, 2165. (d) van Aerle, N. A. J. M.; Barmentlo, M.; Hollering, R. W. J. *J. Appl. Phys.* **1996**, *80*, 431.

(11) Obi, M.; Morino, S.; Ichimura, K. *Chem. Mater.* **1999**, *11*, 656.

(12) The examples are too numerous to list. For a representative example see: Ichimura, K.; Suzuki, Y.; Seki, T. Hosoki, A.; Aoki, K. *Langmuir* **1988**, *4*, 1214.

(13) (a) Yaroshchuk, O.; Cada, L. G.; Sonpatki, M.; Chien, L.-C. *Appl. Phys. Lett.* **2001**, *79*, 30. (b) Zhang, C.-H.; Yang, Z.-H.; Ding, M.-X. *Liq. Cryst.* **2003**, *30*, 65. (c) Hafiz, H. R.; Nakanishi, F. *Nanotechnology* **2003**, *14*, 649.

(14) See the following and references cited therein: Yaroshchuk, O.; Reznikov, Y. *J. Mater. Chem.* **2012**, *22*, 286.

(15) Zimmerman, H. E.; Grunewald, G. L. *J. Am. Chem. Soc.* **1966**, *88*, 183.

(16) (a) Hixson, S. S.; Mariano, P. S. Zimmerman, H. E. *Chem. Rev.* **1973**, *73*, 531. (b) Zimmerman, H. E.; Pratt, A. C. *J. Am. Chem. Soc.* **1970**, *92*, 6259. (c) Zimmerman, H. E.; Armesto, D. *Chem. Rev.* **1996**, *96*, 3065.

(17) (a) Zhu, Z.; Swager, T. M. *J. Am. Chem. Soc.* **2002**, *124*, 9670. (b) Long, T. M.; Swager, T. M. *J. Am. Chem. Soc.* **2002**, *124*, 3826. (c) Hoogboom, J.; Swager, T. M. *J. Am. Chem. Soc.* **2006**, *128*, 15058.

(18) Chaikovskii, V. K.; Filimonov, V. D.; Skorokhodov, V. I.; Ogorodnikov, V. D. *Zhunal Organicheskoi Khimii* **2007**, *43*, 1285.

(19) Turro, N. J. *Modern Molecular Photochemistry*; University Science Books:Sausalito, CA, 1991.

(20) Lukáč, I.; Kósa, C. *Macromol. Rapid Commun.* **1994**, *15*, 929.

(21) Schenck, W.; Ko, D.-H.; Samulski, E. *J. Appl. Phys.* **2011**, *109*, 064301-1.

(22) Tannaci, J. F.; Kratter, I. H.; Rider, E. A.; McBee, J. L.; Miller, A. D.; Tilley, T. D. *Chem. Commun.* **2009**, 233.

(23) McNeil, A. J.; Müller, P.; Whitten, J. E.; Swager, T. M. *J. Am. Chem. Soc.* **2006**, *128*, 12426.

Chapter 4

Norbornadiene End-Capping of Cross-Coupling Polymerizations: A Facile Route to Triblock Polymers

4.1 Introduction

The previous chapters described the utility of PPEs in applications such as chemosensing and liquid crystal alignment. Scheme 4.1 displays the molecular structures of other classes of conjugated polymers that are used in device applications. The development of transition metal catalyzed carbon-carbon bond forming reactions has increased both the ease in which these materials are synthesized as well as the variety of available structures.[1] However, despite these advances, conjugated polymers continue to suffer from problems related to processability. The rigidity and self-associating properties of conjugated polymers limits the utility of these building blocks in materials applications exhibiting the full spectrum of mechanical properties.[2] Specifically, the low molecular weights of these materials limits the mechanical durability necessary to realize the often-stated goal of enabling flexible electronic/photonic devices.
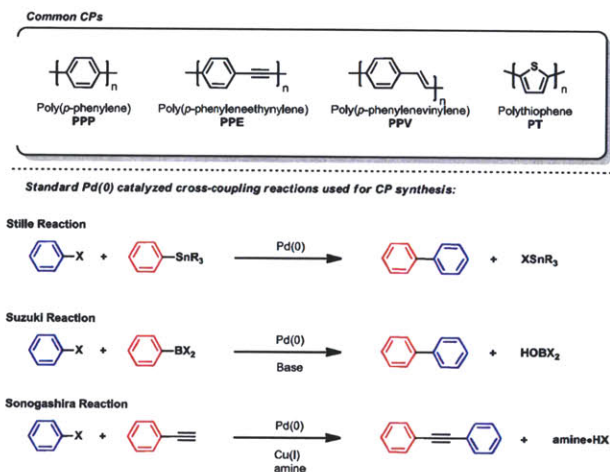
Scheme 4.1. Molecular structures of common conjugated polymers (top). Palladium catalyzed reactions that are employed in the synthesis of conjugated materials (bottom).

In order to retain the interesting optoelectronic characteristics of these polymers, while concomitantly maximizing their mechanical properties, groups have focused on the development of block copolymers that contain a conjugated segment.[3] This approach is best exemplified by the elegant work of McCullough[4], schematically shown in Scheme 4.2.
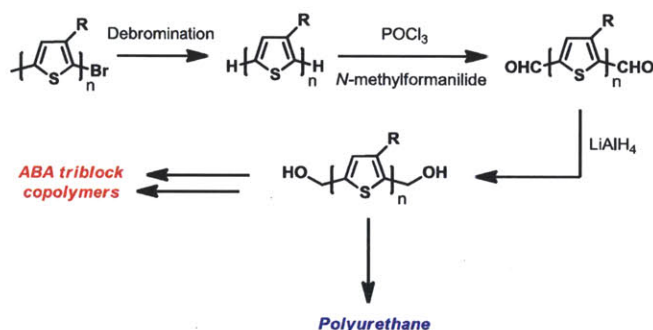
Scheme 4.2. Post-polymerization end-capping of PT using the Vilsmeier reaction.

In this work, PT is formed via the Grignard Metathesis reaction (GRIM) and the bromine end-groups are removed via a quenching procedure. This is then followed by a Vilsmeier reaction and subsequent reduction to generate reactive end-groups that can be converted to macroinitiators for further radical and condensation based polymerizations. This approach is mechanistically representative of standard approaches to triblock copolymer formation and typically requires at least one change in reaction conditions after polymer formation thereby necessitating additional purification and isolation cycles to generate a competent macroinitiator. We were interested in developing an end-capping reaction that is compatible with standard palladium-mediated cross-coupling reactions and would yield a macroinitiator in a single pot reaction thereby removing the numerous isolation/purification cycles.

104

4.2 The Hydroarylation of Norbornadiene

The proposed catalytic cycle for the hydroarylation reaction of norbornadiene is pictured in Scheme 4.3. The transformation is mechanistically similar to the Heck reaction with one major difference – the product of carbopalladation does not possess a properly oriented β-hydrogen atom for elimination to generate the product alkene.[5] Instead, formic acid is used as a hydride source to generate a palladium hydride species which subsequently undergoes reductive elimination to generate the hydroarylation product.[6]
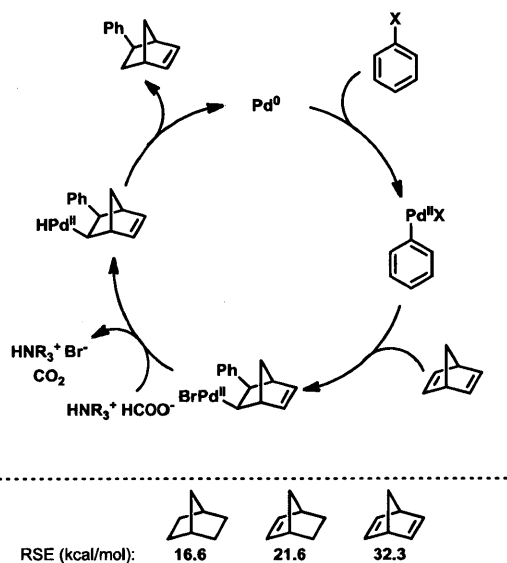
Scheme 4.3. Proposed catalytic cycle for the hydroarylation reaction (top). Ring strain energies associated with norbornane derivatives (bottom).

Some key features of this reaction are as follows: (i) the relief of ring strain associated with norbornadiene accelerates carbopalladation, (ii) the conditions are compatible with standard palladium catalyzed cross-coupling methods and (iii) the product norbornene is a competent monomer for ring opening metathesis polymerization (ROMP). This last feature is of utmost

In addition, the use of deuterium labeled formic acid (DCOOH) afforded the hydroarylated product with the deuterium label on the norbornene scaffold (Figure 4.1) as anticipated from the proposed catalytic cycle. Also, there is a small resonance associated with an aryl methine (6.8 ppm) suggesting that the major side product is hydrodehalogenation. However, this product accounts for only 3-18% of the product distribution based on the results shown in Scheme 4.4. This result, in conjunction with the model reactions, suggests that hydrodehalogenation of the aryl halide is slower than carbopalladation and should not interfere with the end-capping reaction.
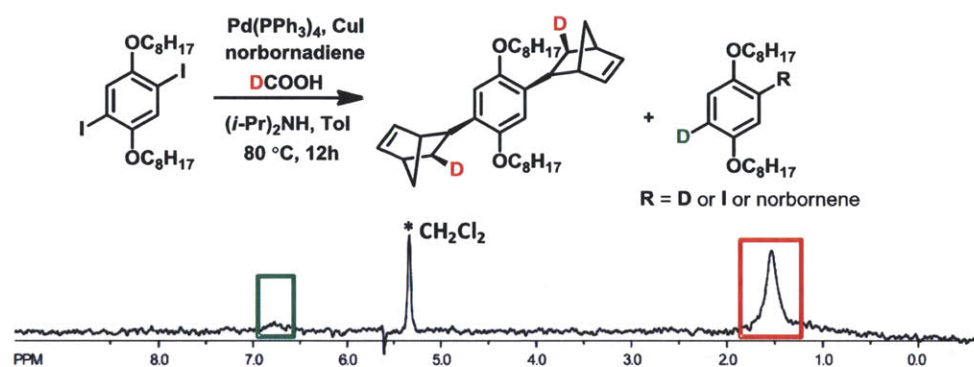
Figure 4.1. Crude ^{2}H NMR spectrum (bottom) (CH$_2$Cl$_2$) of the indicated transformation (top). Spectrum was taken after the removal of volatiles from the reaction mixture.

4.4 Polymer End-capping

With an efficient coupling reaction in hand we turned our attention to the end-capping of conjugated polymers. Scheme 4.5 displays the structures of the polymers that were end-capped in this work. The conditions that were employed for the end-capping of polymerization reactions mirrored those that were used in the model reactions. Small excesses of the dihaloarene were used to increase the percentage of conjugated polymer chains that were capped with an aryl

107

halide thereby facilitating the incorporation of norbornene units on both ends of a given polymer chain.
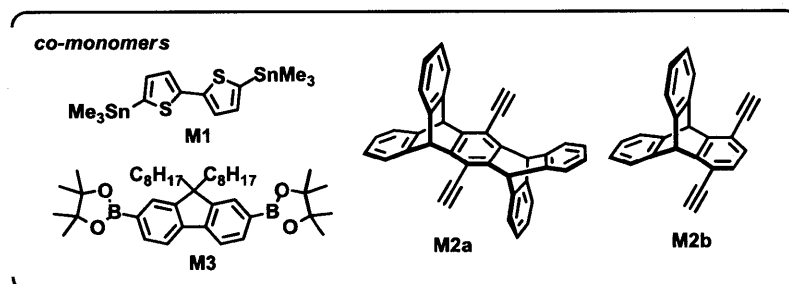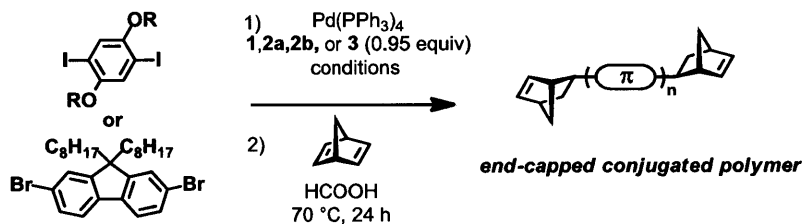
Scheme 4.5. Conditions used for the end-capping of cross-coupling polymerizations (top) and the resulting end-capped polymers synthesized in this work (bottom).

All end-capped polymers were characterized via ^{1}H and ^{13}C NMR spectroscopy as well as size-exclusion chromatography (SEC). Figure 4.2 displays the ^{1}H NMR spectrum of **P2**. The end-capped polymer displays the expected methines belonging to the norbornene end-groups

(red protons) as well as the bridgehead methines (green protons) of the triptycene unit and the α-methylenes (blue) of the dialkoxy comonomer. Of particular interest is the ratio of near end-cap α-methylenes of the dialkoxy monomer (small blue integral) to the norbornene methines (red protons). A perfectly efficient end-capping reaction would yield a ratio of 3:4 (red/blue); our ratio of 3:5 suggests that the reaction proceeded in a highly efficient manner.

Figure 4.2. ^{1}H NMR spectrum of **P2**. Included is the molecular structure of **P2** with the appropriate protons highlighted. The inset is a magnified portion of the spectrum.

Additional evidence for the efficient incorporation of norbornene end-caps comes from the behavior **P2** when exposed to a catalytic quantity of Grubbs' third generation catalyst (**G3**). Prior to addition of **G3**, **P2** exhibited a M_n of 10,400 g/mol (PDI = 1.7). The M_n increased to 20,400 g/mol (PDI = 3.7) after exposure to **G3** for 12 hours at room temperature indicating that **P2** is a competent macroinitiator.

(red protons) as well as the bridgehead methines (green protons) of the triptycene unit and the α-methylenes (blue) of the dialkoxy comonomer. Of particular interest is the ratio of near end-cap α-methylenes of the dialkoxy monomer (small blue integral) to the norbornene methines (red protons). A perfectly efficient end-capping reaction would yield a ratio of 3:4 (red/blue); our ratio of 3:5 suggests that the reaction proceeded in a highly efficient manner.
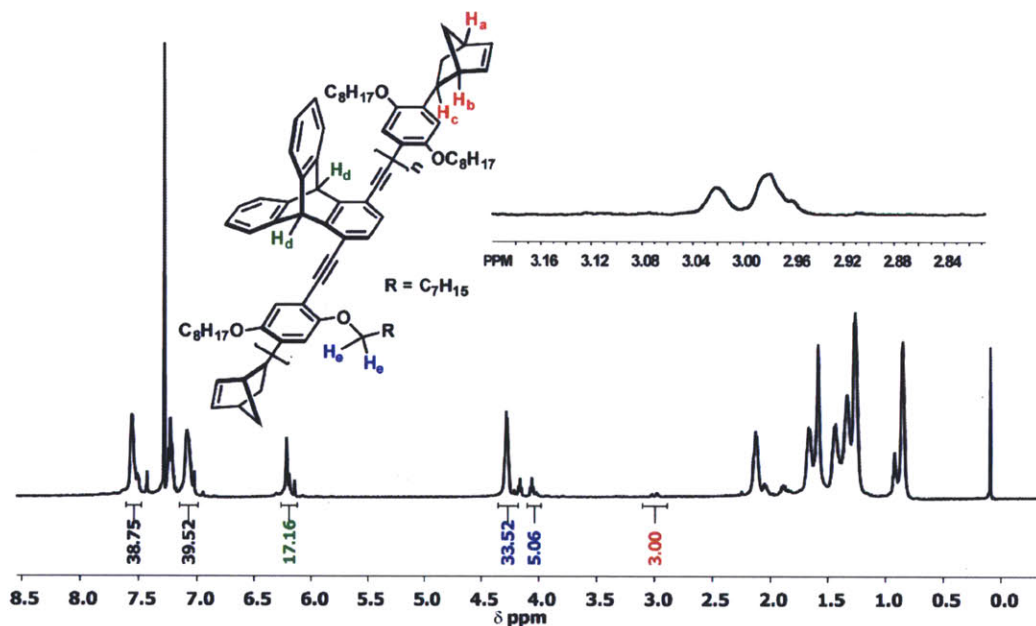

Figure 4.2. ^{1}H NMR spectrum of **P2**. Included is the molecular structure of **P2** with the appropriate protons highlighted. The inset is a magnified portion of the spectrum.

Additional evidence for the efficient incorporation of norbornene end-caps comes from the behavior **P2** when exposed to a catalytic quantity of Grubbs' third generation catalyst (**G3**). Prior to addition of **G3**, **P2** exhibited a M_n of 10,400 g/mol (PDI = 1.7). The M_n increased to 20,400 g/mol (PDI = 3.7) after exposure to **G3** for 12 hours at room temperature indicating that **P2** is a competent macroinitiator.

4.5 Formation of Triblock Copolymers

The formation of triblock copolymers from **P1** is schematically outlined in Figure 4.3 and is representative of our general strategy. The isolated macroinitiators **P1** was treated with stoichiometric quantities of **G3** for approximately 30 minutes at room temperature. The ruthenium-alkylidene terminated polymer was isolated by reprecipitation into cold hexanes and then redissolved in CH$_2$Cl$_2$. Subsequent exposure of this macroinitiator to a solution of norbornene resulted in the formation of high molecular weight triblock copolymer **PNB-*b*-P1-*b*-PNB**.
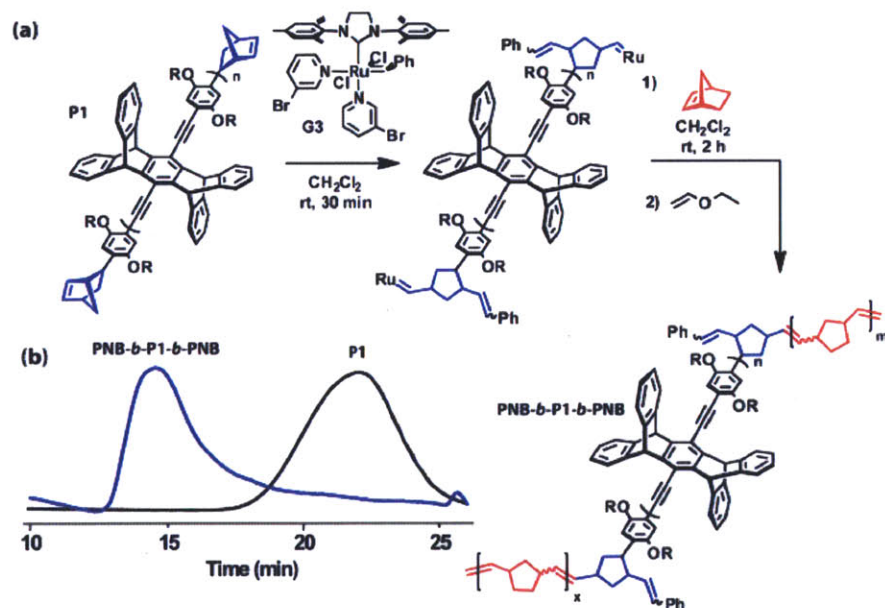
Figure 4.3. (a) Synthesis of **PNB-*b*-P1-*b*-PNB**. (b) THF SEC (UV detection 450 nm) traces of **P1** (black) and **PNB-*b*-P1-*b*-PNB** triblock copolymer (blue).

The SEC trace in Figure 4.3 confirms the following two points: (i) the vast majority of **P1** chains are end-capped with norbornene units and (ii) The ruthenium-alkylidene terminated

chains are competent macroinitiators for ROMP. The scope of this approach is shown in Scheme 4.6 and Table 4.1.

Scheme 4.6. Conditions and monomers used for the formation of triblock copolymers.

Table 4.1. Selected results of triblock copolymerizations[a].

CP	macroinitiator		Monomer	block copolymer	
	Mn^b (g/mol)	PDI		Mn^b (g/mol)	PDI
P1	130,900	2.5	5	511,200	6.3
P1	36,400	1.9	4	140,300	2.1
P3	29,000[c]	1.69	5	528,300	2.52
P4	23,600	1.8	6	26,900	4.0
P4	23,600	1.8	5	701,200	5.1

[a]Conditions: See Scheme 4.6 for general conditions, specific conditions are outlined in the Experimental Section. [b]Determined using SEC relative to polystyrene standards in THF. [c]This macroinitiator was formed using Grubbs' 2nd generation catalyst. **G3** exhibited significant oligomerization of the end-capped polymer.

As can be seen in Table 4.1, our approach yielded high molecular weight materials using three different strained alkenes. It has to be noted; however, that the formation of high molecular weight macroinitiators is not without limitations. Specifically, in some cases the end-capped polymers showed a tendency to oligomerize yielding intractable materials. The use of **G3** which exhibits an excellent initiation to propagation ratio was an effective solution to this problem.[8]

4.6 Applications of Macroinitiators

In addition to functioning as macroinitiators, the end-capped CPs can also act as cross-linkers to form functional plastics/rubbers. Polynorbornene (PHB), commercially known as Norsorex, is an elastomeric material with a tunable glass transition temperature (T_g) that can vary from 35 to -60 °C.[9] When the material is plasticized with an aromatic or hydrocarbon additive, the T_g drops below room temperature and the material behaves as an elastomer. We envisioned using **P1-P4** as cross-linkers for the formation of functionalized elastomers, materials that exhibit the mechanical properties of polynorbornene and the optical properties of the conjugated cross-linker.

The cross-linked materials were formed by treating a mixture of **P1** norbornene with a catalytic amount of **G3**. The polymerizations were carried out in Teflon® wells and the resulting plastics could be peeled from the wells. Figure 4.4 displays optical images of polynorbornene cross-linked with **P1** under both ambient and UV (365 nm) illumination. The material exhibits elastomeric behavior while also exhibiting the optical characteristics of **P1**. The material exhibited greater than 80% recovery after being uniaxially stretched to six times its initial length.

112
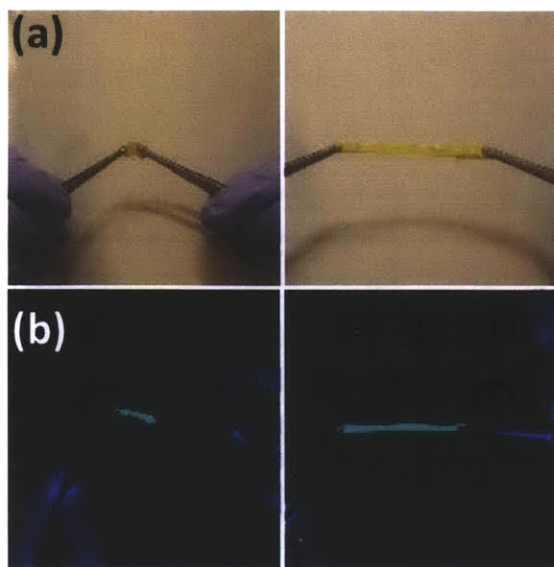
Figure 4.4. (a) Optical micrographs of PNB cross-linked with **P1** in unstretched (left) and stretched (right) states. (b) Optical micrographs with 365 nm excitation light of the same material in unstretched (left) and stretched (right) states.

P2 is a soluble conjugated polymer that exhibits red-shifted photoluminescence in thin films as a result of π-π interactions. We surmised that PNB rubber cross-linked with **P2** would exhibit photophysical perturbations as a result of swelling in the presence of organic solvents, possibly acting as a sensor for detection of volatile organic compounds (VOCs) in water. Figure 4.5 displays the photoluminescence spectra of this material in aqueous solutions with or without tetrahydrofuran (THF). In water, the film exhibits broad red-shifted emission consistent with interpolymer interactions such as π-π stacking. After addition of a small amount of THF (1% v:v) the emission shifts to shorter wavelengths suggesting that the material is swelling with concurrent loss of interpolymer interactions. In addition, exposure of the cross-linked material to the saturated vapor of THF shows a similar response and the emission decay at 450 nm is depicted in Figure 4.5c.
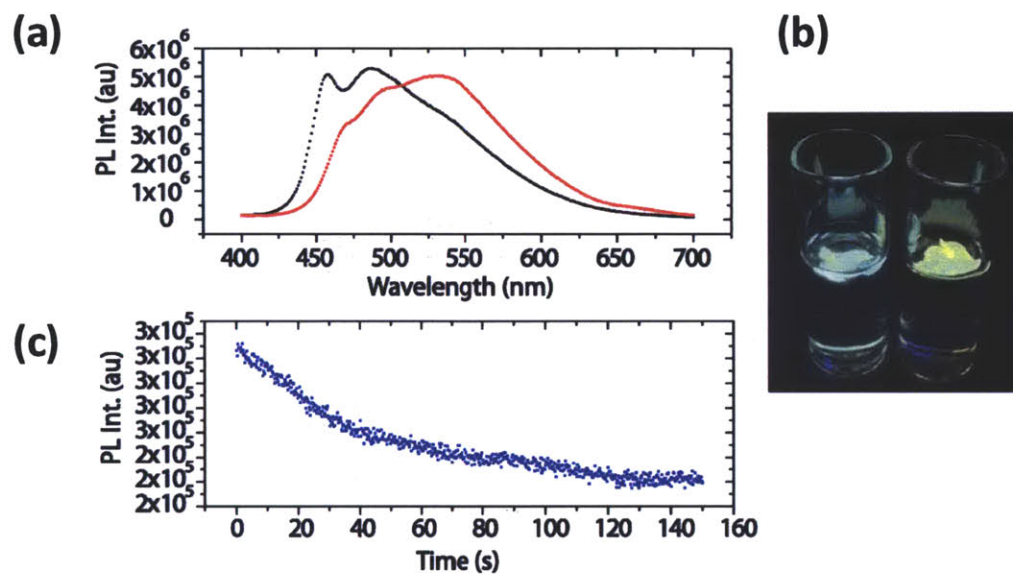
Figure 4.5. (a) Photoluminescence spectra of PNB cross-linked with **P2** in water (red) and 1% THF/water (v:v) (black). (b) Optical micrograph (UV excitation at 365 nm) showing PNB cross-linked with **P2** in water (right) and 1% THF/water (v:v; left). (c) Photoluminescence intensity decay (monitored at 450 nm) of the same film after exposure to the saturated vapor of THF.

4.7 Conclusion

To summarize, we have shown the utility of the hydroarylation of norbornadiene in the context of multiblock copolymer synthesis. The end-capping protocol is compatible with Stille, Sonogashira and Suzuki cross-coupling polymerizations – methods that are typically employed for the synthesis of CPs. This reaction can be carried out in a single pot fashion and generates end-capped polymers that can be subsequently transformed into ruthenium-alkylidene macroinitiators for the generation of tribock copolymers via ROMP. In addition, these end-capped materials can be used as cross-linking agents for the formation of functional rubber

114

scaffolds that exhibit the mechanical properties of the peripheral ROMP segments and the optical properties of the conjugated portion. These materials also displayed utility as possible sensor materials for VOCs. Further work is currently underway in our laboratory to use this method to generate highly functionalized conjugated polymer nanoparticles.

4.8 Experimental Section

MATERIALS AND METHODS: Toluene, CH_2Cl_2 and THF were purified by passage through solvent purification columns containing activated alumina. *N,N*-Dimethylformamide (DMF) was distilled from $MgSO_4$ and stored over 4Å molecular sieves. Diisopropylamine was distilled from CaH_2. Bicyclo[2.2.1]hepta-2,5-diene was distilled from alumina. Bicyclo[2.2.1]hept-2-ene was distilled from sodium. 1,4-bis((2-ethylhexyl)oxy)-2,5-diiodobenzene[10] (1), 1,4-bis(*n*-octyloxy)-2,5-diiodobenzene[11] (3), 1,4-bis(*n*-dodecyloxy)-2,5-diiodobenzene[12] (2), 5,5'-trimethylstannyl-2,2'-bithiophene[13] (M1), 2,7-bis(4,4,5,5-tetramethyl-1,3,2-dioxaborolan-2-yl)-9,9-dioctylfluorene[14] (M3), 2,3-*exo*-dicarboxylic acid dimethyl ester-7-oxabicyclo[2.2.1]hept-5-ene[15] (5), and 2,3-*exo*-bis(*tert*-butyldimethylsilyloxymethyl)-7-oxabicyclo[2.2.1]hept-5-ene[16] (6) and M2b[17] were prepared according to literature procedure. All other reagents were obtained from commercial sources and used as received unless otherwise noted.

INSTRUMENTATION: NMR spectra were recorded on Varian Mercury 300 MHz, Varian Inova 500 MHz or Varian Inova 501 MHz spectrometers. Chemical shifts were reported in ppm and referenced to residual NMR solvent peaks (CDCl$_3$: δ 7.27 ppm for ^{1}H, δ 77.23 ppm for ^{13}C). Mass spectra (MS) were obtained at the MIT Department of Chemical Instrumentation Facility (DCIF) using Bruker Daltonics APEX II 3T FT-ICR-MS. Melting points were measured on a

Mel-Temp II apparatus (Laboratory Devices INC) and were not corrected. Number average

molecular weights (M_n) and polydispersity (PDI) of polymers were obtained on a HP series 1100

gel permeation chromatography (GPC) system in THF and calibrated with polystyrene standards

and utilizing both UV (450 nm) and refractive index detection.

*SYNTHETIC PROCEDURES AND CHARACTERIZATION:*
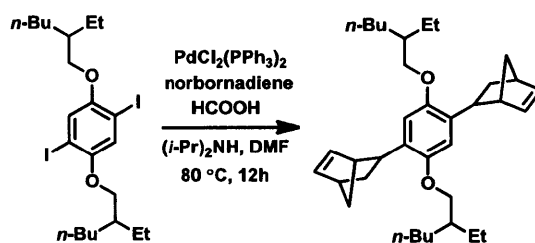
1,4-Bis(bicyclo[2.2.1]hept-5-en-2-yl)-2,5-bis((2-ethylhexyl)oxy)-benzene (MC1). Compound 1

(0.50 g, 0.85 mmol) and $PdCl_2(PPh_3)_2$ (II) (12.6 mg, 17.9 µmol) were placed in a Schlenk flask

with a stir bar. The flask was evacuated and backfilled with nitrogen three times before addition

of bicyclo[2.2.1]hepta-2,5-diene (0.40 mL, 3.93 mmol) DMF (4.0 mL) and diisopropylamine

(1.0 mL). This reaction flask was subjected to three cycles of freeze-pump-thaw. Formic acid

(0.20 mL, 5.30 mmol) was added slowly, and the reaction mixture was heated at 80 °C for

overnight. Then, the mixture was cooled to room temperature, diluted with CH_2Cl_2 and washed

with water and brine several times. After drying over $MgSO_4$, the solution was filtered, and the

solvent was distilled off under reduced pressure. Column chromatography of the crude material

on silica gel (CH_2Cl_2 :hexane (3:10)) provided the product as a viscous oil (0.431 g, 97%). ^{1}H

NMR (500 MHz, CDCl₃): δ 6.79 (s, 2H), 6.26 (dd, 2H, J= 5.61 Hz, J= 3.05 Hz), 6.19 (dd, 2H,

J= 5.61 Hz, J= 2.88 Hz), 3.85 (m, 4H), 2.97 (s, 2H), 2.93 (m, 2H), 2.90 (s, 2H), 1.71 (m, 2H),

1.63 (m, 4H), 1.59 (d, 4H, J= 7.85),1.56 - 1.41 (m, 8H), 1.37 - 1.31 (m, 8H), 0.97 - 0.91 (m,

12H). ^{13}C NMR (125 MHz, CDCl₃): δ 151.08, 137.53, 137.40, 132.26, 110.10, 70.44, 47.12,

116

46.27, 42.47, 40.09, 37.21,33.14, 31.00, 29.43, 24.35, 23.32, 14.35, 11.56. HR-MS (ESI): calcd for $C_{36}H_{54}O_2$ [M+Na]$^+$, 541.402; found 541.399.
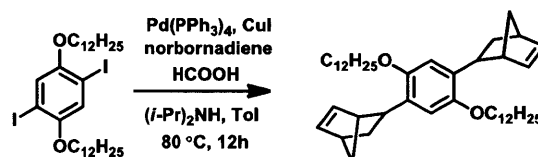
1,4-Bis(bicyclo[2.2.1]hept-5-en-2-yl)-2,5-bis(*n*-dodecyloxy)-benzene (MC2). This compound was synthesized by the same procedure as described for compound **MC1** using the following quantities of reagents: compound **2** (1.0 g, 1.43 mmol), bicyclo[2.2.1]hepta-2,5-diene (1.5 mL, 14.7 mmol), Pd(PPh$_3$)$_4$ (0) (40.0 mg, 35 μmol), CuI (20.0 mg, 0.10 mmol), formic acid (0.70 mL, 18.5 mmol), diisopropylamine (2.5 mL) and toluene (10.0 mL). Purification by column chromatography provided the product as a white solid (0.849 g, 93%). The final purification was achieved by recrystallization from acetone; mp 64 °C . ^{1}H NMR (500 MHz, CDCl3): δ 6.77 (s, 2H), 6.25 (dd, 2H, *J*= 5.64 Hz, *J*= 3.08 Hz), 6.17 (dd, 2H, *J* = 5.64 Hz, *J*= 2.75 Hz), 3.92 (t, 4H, *J*= 6.3 Hz), 2.95 (s, 2H), 2.92 - 2.89 (m, 4H), 1.76 (m, 4H), 1.64 (m, 2H), 1.57 (m, 4H), 1.50 - 1.43 (m, 6H), 1.36 - 1.26 (m, 32H), 0.89 (t, 6H, *J*= 6.94 Hz). ^{13}C NMR (125 MHz, CDCl3): δ 151.26, 137.51, 137.41, 132.63, 110.71, 69.03, 46.89, 46.31, 42.49, 37.16, 33.52, 32.15, 29.91, 29.89, 29.88, 29.85, 29.81, 29.62, 29.58, 26.43, 22.92, 14.36. HR-MS (ESI): calcd for $C_{44}H_{70}O_2$ [M+H]+, 631.545; found 631.545.
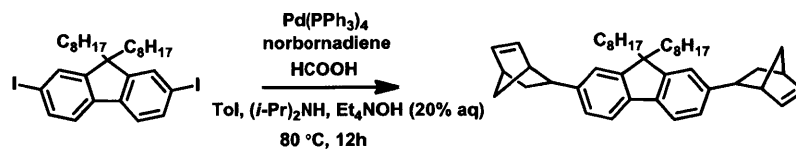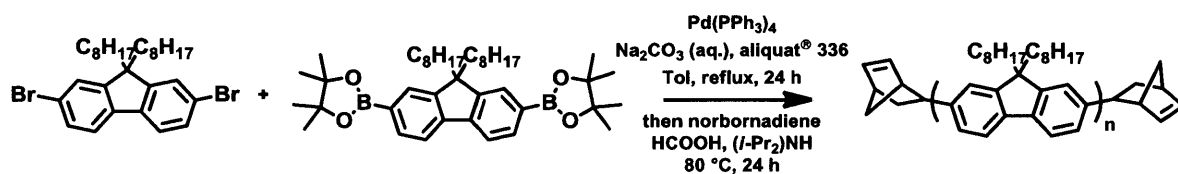
1,4-Bis(bicyclo[2.2.1]hept-5-en-2-yl)-9,9-dioctylfluorene **(MC3).** This compound was synthesized by the same procedure as described for compound **MC1** using the following quantities of reagents: 2,7-diiodo-9,9-dioctyl-fluorene (0.022 g, 0.034 mmol), bicyclo[2.2.1]hepta-2,5-diene (0.02 mL, 0.20 mmol), Pd(PPh$_3$)$_4$ (0) (1.0 mg, 0.86 μmol), aliquat® 336 (0.01 mL), tetraethylammonium hydroxide solution 20% in water (0.10 mL), formic acid (0.01 mL, 0.26 mmol), diisopropylamine (0.20 mL) and toluene (1.0 mL). Column chromatography of the crude material on silica gel (10% CH$_2$Cl$_2$ in hexane) provided the product as a viscous oil (0.016 g, 82%). ^{1}H NMR (500 MHz, CDCl$_3$): δ 7.57 (d, 2H, *J*= 7.63 Hz), 7.23 - 7.21 (m, 4H), 6.30 (dd, 2H, *J*= 5.64 Hz, *J*= 3.05 Hz), 6.20 (dd, 2H, *J*= 5.64 Hz, *J*= 2.90 Hz), 3.00 (s, 2H), 2.94 (s, 2H), 2.81 (m, 2H), 1.96 - 1.91 (m, 4H), 1.80 (m, 2H), 1.68 (m, 2H), 1.64 (d, 2H, *J*= 8.39 Hz), 1.46 (m, 2H), 1.23 - 1.07 (m, 20H), 0.83 (t, 6H, *J*= 7.17 Hz), 0.67 (m, 4H). ^{13}C NMR (125 MHz, CDCl$_3$): δ 151.07, 144.84, 138.90, 137.58, 126.16, 122.24, 119.16, 54.97, 48.82, 45.98, 44.19, 44.19, 42.57, 40.41, 34.05, 32.00, 30.13, 29.37, 29.30, 23.91, 22.84, 14.30. HR-MS (ESI): C$_{43}$H$_{58}$ [M]+, 574.453; found 574.452.
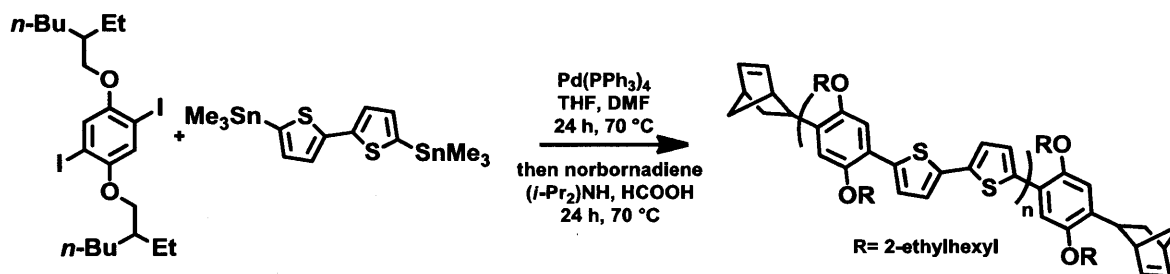
P4. Compound **1** (1.28 g, 2.19 mmol), compound **M1** (1.03 g, 2.08 mmol) and Pd(PPh₃)₄ (0)

(0.088 g, 76 µmol) were placed in a Schlenk flask with a stir bar. The flask was consecutively

evacuated and backfilled with argon three times prior to addition of DMF (20 mL) and THF (20

mL). This reaction flask was subjected to three cycles of freeze-pump-thaw, and the reaction

mixture was heated at 70 °C. After stirring for 24 h, THF (10 mL), diisopropylamine (0.60 mL),

bicyclo[2.2.1]hepta-2,5-diene (0.40 mL, 3.9 mmol) and formic acid (0.20 mL, 5.2 mmol) were

added successively. The mixture was stirred for another 24 h at 70 °C, cooled to room

temperature, diluted with CHCl₃, and washed with saturated ammonium chloride solution and

water. After drying over MgSO₄, the solution was filtered and the filtrate was passed through a

short column of silica gel with CHCl₃. The solvent was removed, and the residue was

redissolved in a small volume of CH₂Cl₂ and precipitated into stirred acetone. The precipitate

was separated, washed with acetone and dried *in vacuo*. This afforded 1.01 g of **P4** as a red solid.

^{1}H NMR (500 MHz, CDCl₃): δ 7.53 (br, d, 2H, *J*= 3.58 Hz), 7.29 (br, s, 2H), 7.24 (br, d, 2H, *J*=

2.78 Hz), 6.28, 6.22 (br, m, end group), 4.06 (br, d, 4H, *J*= 5.19 Hz), 3.00, 2.94 (br, end group),

1.94 (br, m, 2H), 1.72 - 1.49 (br, m, 8H), 1.41 (br, m, 8H), 1.04 - 0.94 (br, m, 12H). ^{13}C NMR

(125 MHz, CDCl₃): δ 149.60, 138.28, 237.81, 126.30, 123.35, 122.79, 111.96, 72.12, 39.95,

31.01, 24.36, 23.36, 14.40, 11.55.

P3. This polymer was synthesized by the similar procedure as described for **P4** at reflux condition for the polymerization and 80 °C for the end-capping reaction using the following quantities of reagent: 2,7-dibromo-9,9-dioctyl-fluorene (0.562 g, 1.02 mmol), compound **M3** (0.642g, 0.998 mmol), Pd(PPh$_3$)$_4$ (0) (3.0 mg, 2.6 μmol), 2M Na$_2$CO$_3$ (2.0 mL), aliquat® 336 (0.06 g), toluene (4.5 mL), bicyclo[2.2.1]hepta-2,5-diene (0.40 mL, 3.9 mmol), formic acid (0.20 mL, 5.3 mmol), diisopropylamine (0.50 mL). This afforded 0.722 g of **P3** as a bright yellow solid. ^{1}H NMR (500 MHz, CDCl$_3$): δ 7.86 (br, d, 2H, J= 7.86 Hz), 7.73 - 7.70 (br, m, 4H), 6.32, 6.22 (br, m, end group), 3.03, 2.97 (br, end group), 2.14 (br, 4H), 1.30 - 1.07 (br, m, 20H), 0.83 (br, t, 6H, J= 7.01 Hz), 0.70 (br, 4H). ^{13}C NMR (125 MHz, CDCl$_3$): δ 152.02, 140.69, 140.22, 126.37, 125.75, 121.70, 120.19, 55.57, 40.61, 32.03, 30.54, 30.27, 29.47, 24.13, 22.84, 14.31.
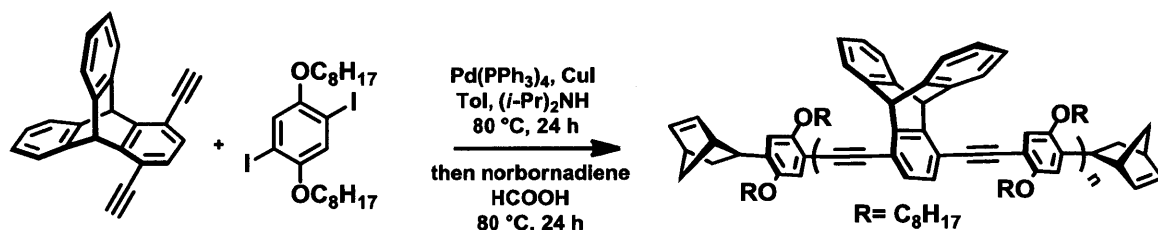
P2. This polymer was synthesized by the similar procedure as described for **P4** at 80 °C using the following quantities of reagent: **M2b** (0.201g, 0.665 mmol), compound **3** (0.370g, 0.632 mmol), Pd(PPh$_3$)$_4$ (0) (15 mg, 13 μmol), CuI (7 mg, 38 μmol), toluene (5 mL), diisopropylamine (1 mL), bicyclo[2.2.1]hepta-2,5-diene (0.2 mL, 2 mmol) and formic acid (0.1 mL, 2.6 mmol). This afforded 0.09g of orange solid. ^{1}H NMR (501 MHz, CDCl$_3$): δ 7.55 (br, 4H), 7.23 (br, 4H),

7.07 (br, 4H), 6.30 (br, endcap), 6.22 (br, 2H), 4.28 (br, 4H), 2.99 (br, endcap), 2.12 (br, 4H), 1.66 (br, 4H), 1.44 (br, 4H), 1.33-0.85 (m, 18H). ^{13}C NMR (125 MHz, CDCl$_3$): δ 154.38, 148.03, 145.55, 128.62, 126.07, 117.60, 100.50, 70.47, 32.55, 32.51, 30.51, 30.17, 29.99, 26.87, 26.83, 23.40, 23.34, 14.77.

R= C$_{12}$H$_{25}$
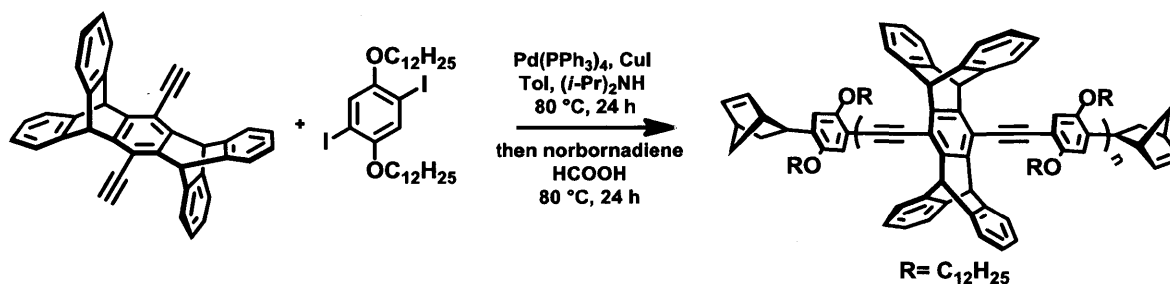
P1. This polymer was synthesized by the similar procedure as described for **P4** at 80 °C using the following quantities of reagent: compound **2** (0.176 g, 0.25 mmol), compound **M2a** (0.117 g, 0.24 mmol), Pd(PPh$_3$)$_4$ (0) (11 mg, 9.5 μmol), CuI (7.2 mg, 38 μmol), toluene (3.0 mL), diisopropylamine (0.80 mL), bicyclo[2.2.1]hepta-2,5-diene (0.20 mL, 2.0 mmol) and formic acid (0.10 mL, 2.6 mmol). This afforded 0.188 g of **P1** as a yellow solid. ^{1}H NMR (500 MHz, CDCl$_3$): δ 7.50 (br, 8H), 7.44 (br, 2H), 7.03 (br, 8H), 6.34, 6.26 (br, m, end group), 6.10 (br, 4H), 4.46 (br, 4H), 3.05, 3.03 (br, end group), 2.23 (br, 4H), 1.73 (br, 4H), 1.46 (br, 4H), 1.26 - 1.17 (br, 28H), 0.86 (br, 6H). ^{13}C NMR (125 MHz, CDCl$_3$): δ 145.29, 144.29, 125.48, 124.05, 70.38, 32.11, 30.18, 30.04, 29.89, 29.83, 29.79, 29.56, 26.53, 22.91, 14.36.

General Procedure for ROMP Homopolymerizations. Under nitrogen atmosphere in a glovebox, a solution of the desired monomer in CH$_2$Cl$_2$ (0.1 g/mL) was added rapidly and as one portion to a vigorously stirred solution of a desired concentration of either Grubbs' catalyst II or III in CH$_2$Cl$_2$. The resulting mixture was stirred at room temperature for a specified period of

time before being quenched by addition of an excess amount of ethyl vinyl ether. The resulting polymers were purified by precipitating into either methanol or hexane followed by drying *in vacuo*.

General Procedure for Block Copolymerizations. A solution of the norbornene endcapped CP (**P1**, **P2**, **P3**, or **P4**) in CH_2Cl_2 (concentration of solution depended on the CP's solubility) was added in one portion to a vigorously stirred solution of an excess of Grubbs' 3rd generation catalyst (~10 equiv.) in CH_2Cl_2 under nitrogen. The reaction mixture was stirred at room temperature for 30 min -2 h before precipitation into hexanes. Isolated macroinitiator was dried in vacuo and redissolved in CH_2Cl_2. To this solution, the ROMP monomer solution of norbornene, **5** or **6** in CH_2Cl_2 was added. The copolymerization was allowed to stir 20 h and quenched by addition of a drop of ethyl vinyl ether. The reaction mixture was poured into acetone or hexane to precipitate the block copolymer. Then, the polymer was dissolved in THF and reprecipitated in hexane and collected by a centrifuge, which was dried *in vacuo*. All protons of each block in copolymers corresponded to those of the appropriate homopolymers in 1H NMR spectra.

General Procedure for Cross-linked Rubber Formation. A teflon® well was filled with 1mL of a concentrated solution of norbornene in CH_2Cl_2 (0.5 g/mL) also containing 1 mL of 0.05 g/mL **P1**. To this solution was added in one portion (1 mL) a solution of (0.1 g/mL) **G3** catalyst. Immediately upon addition, the solution became viscous and finally 'gel-like'. After 1 hr, the material was removed from the well and dried *in vacuo*.
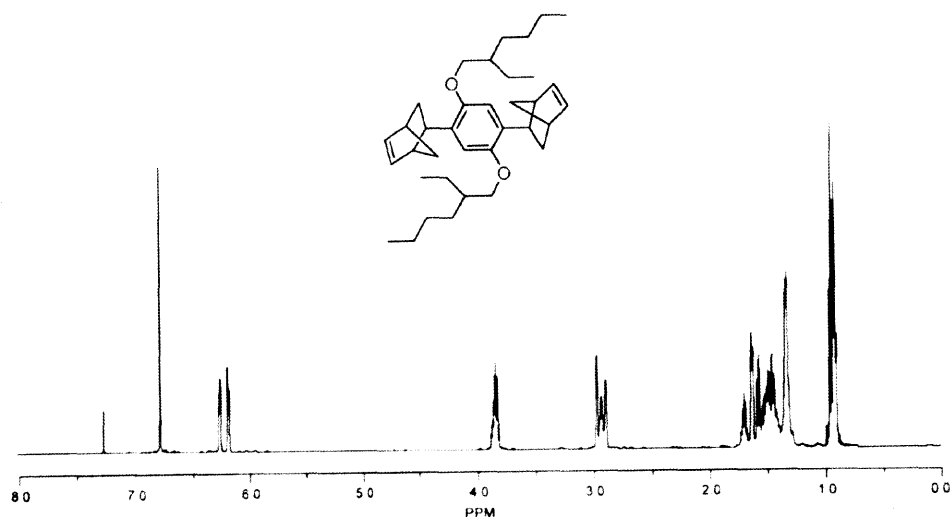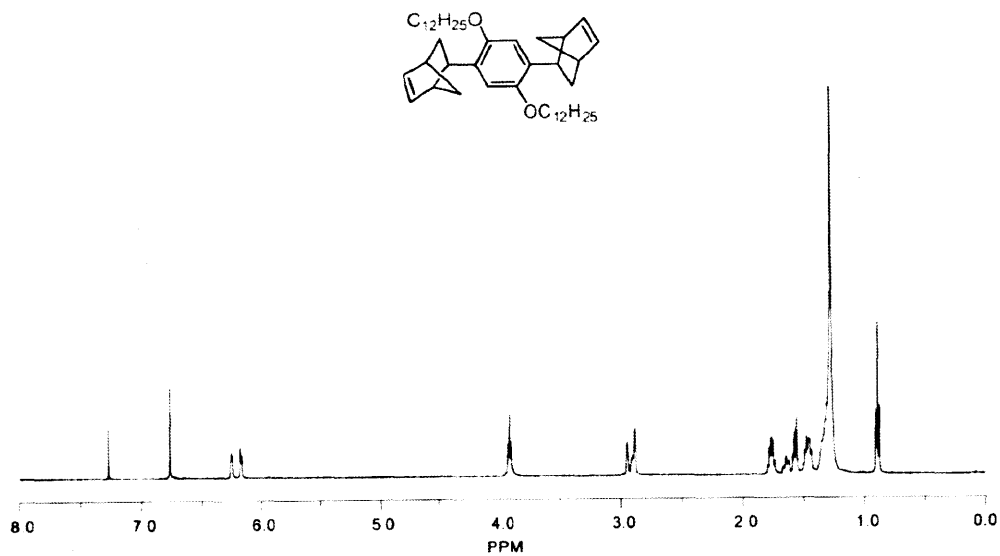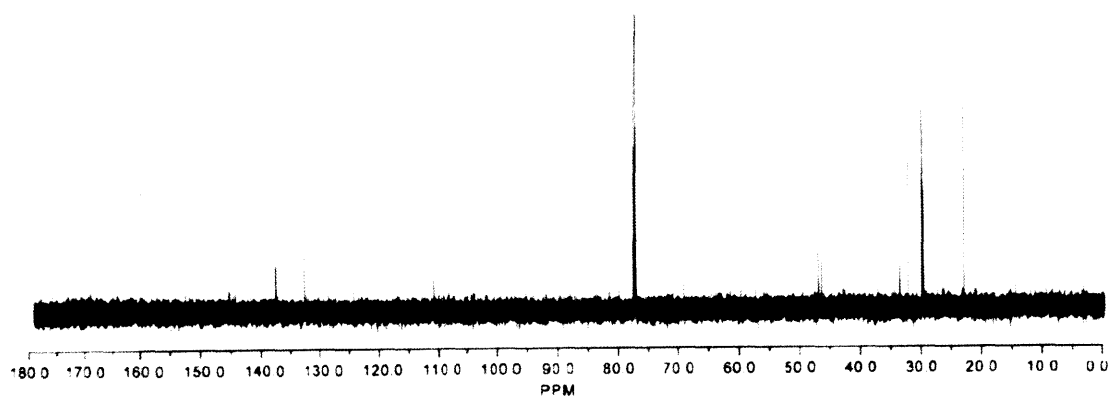
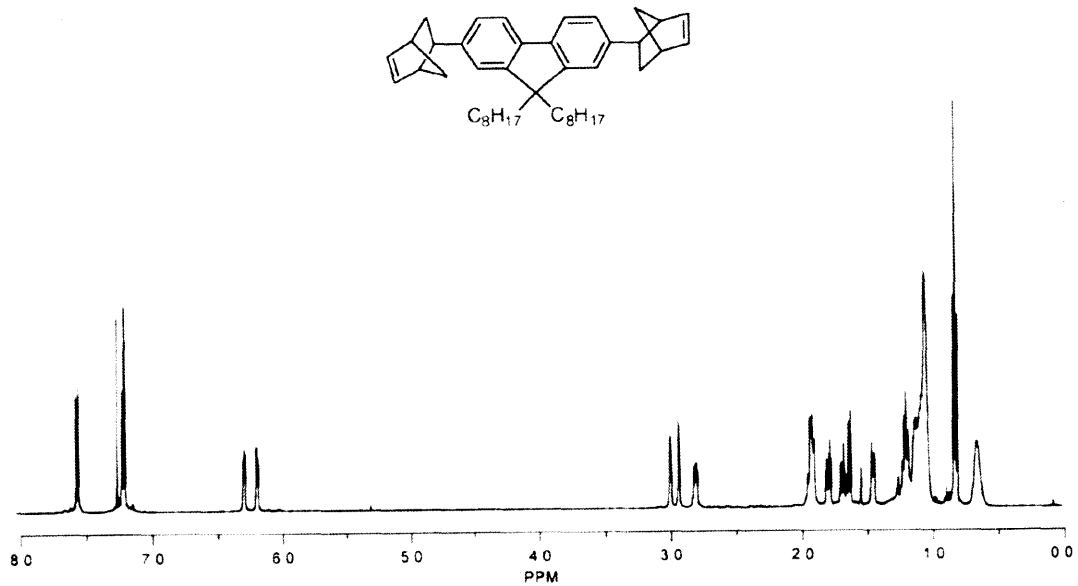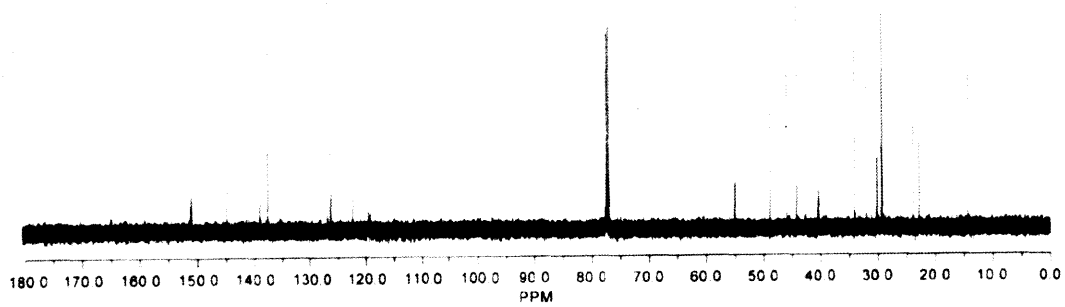**Figure 4.8.1.** ¹H NMR Spectrum of **MC1** (500 MHz, CDCl₃)
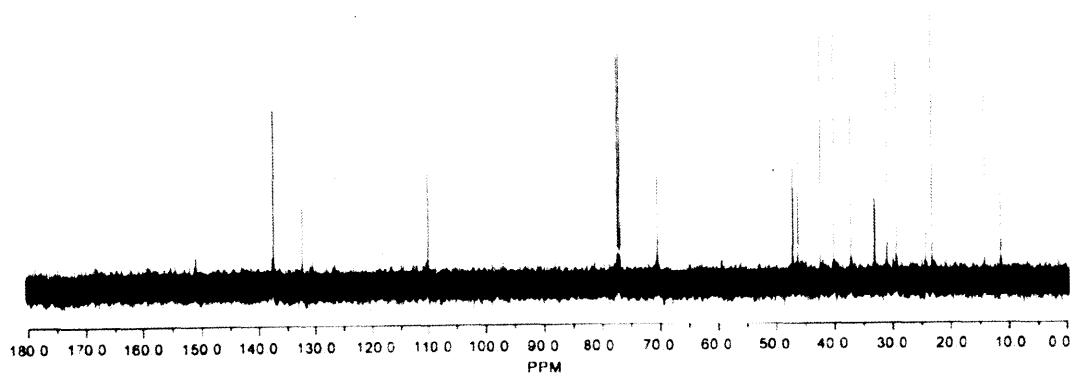
Figure 4.8.2. ¹³C NMR Spectrum of **MC1** (125 MHz, CDCl₃)

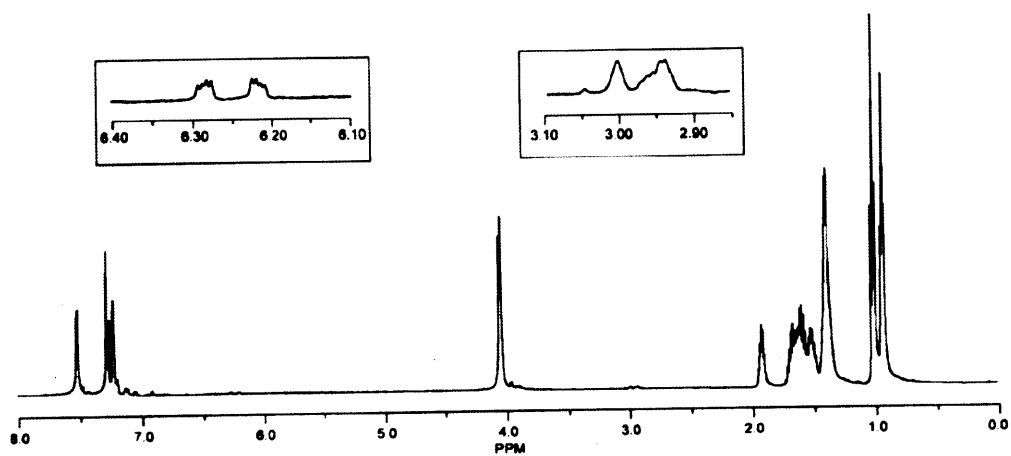**Figure 4.8.3.** ^{1}H NMR Spectrum of **MC2** (500 MHz, CDCl$_3$)

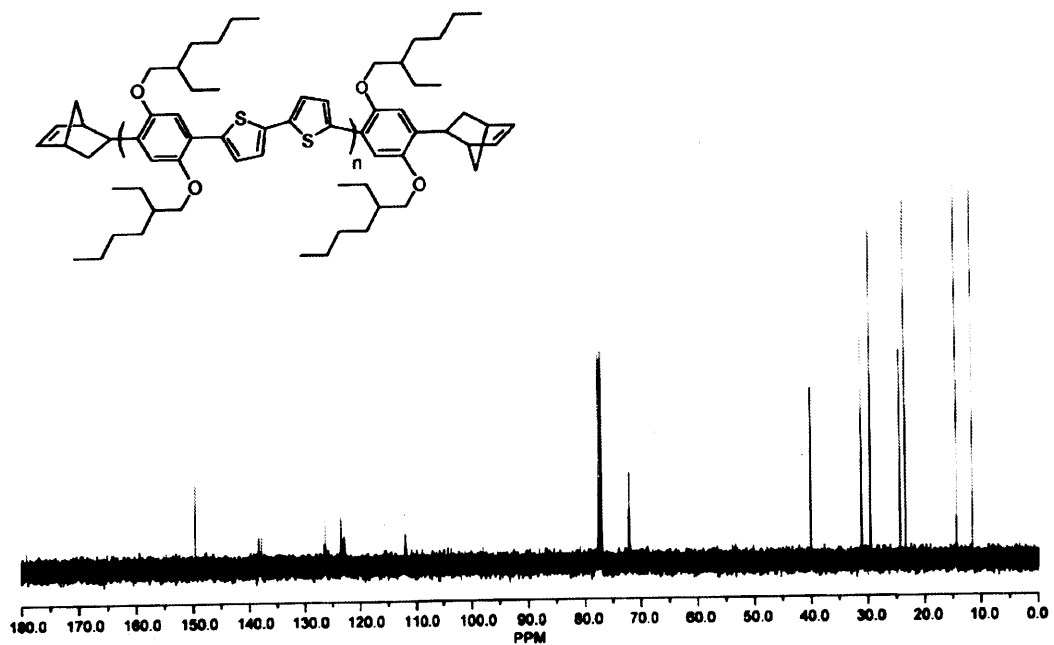**Figure 4.8.4.** ^{13}C NMR Spectrum of **MC2** (125 MHz, CDCl$_3$)

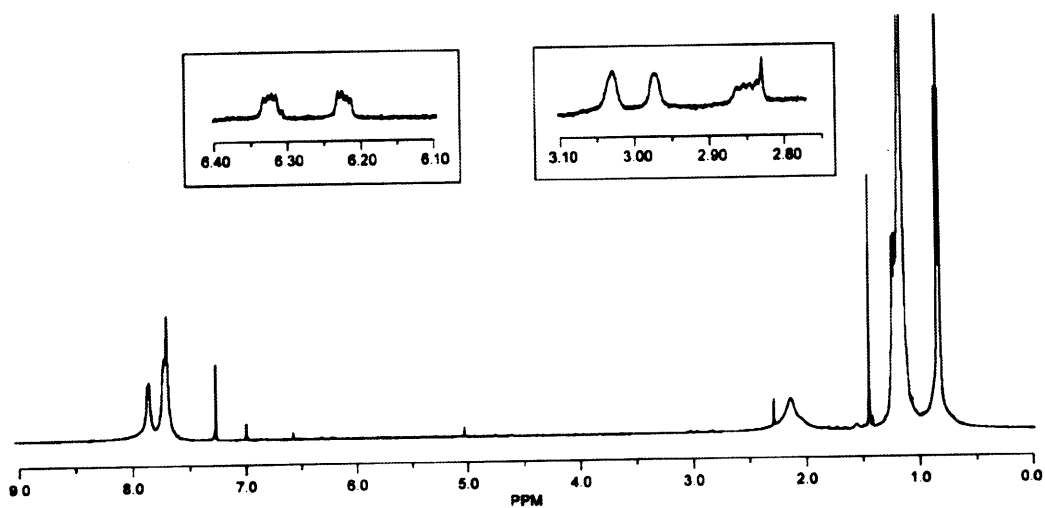**Figure 4.8.5.** ^{1}H NMR Spectrum of **MC3** (500 MHz, CDCl$_3$)

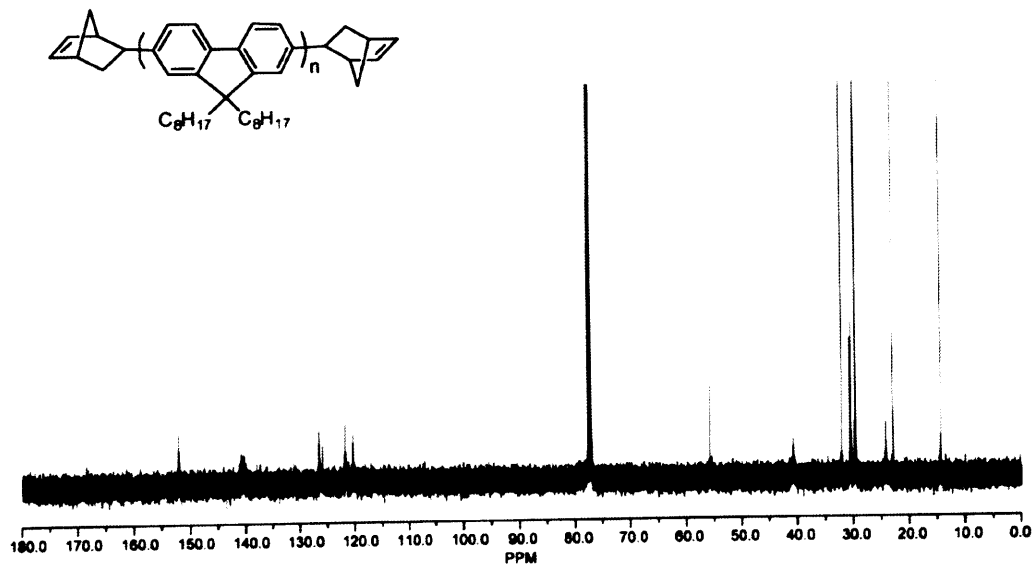**Figure 4.8.6.** ^{13}C NMR Spectrum of **MC3** (125 MHz, CDCl$_3$)

125

Figure 4.8.7. ^{1}H NMR Spectrum of **P4** (500 MHz, CDCl$_3$)

Figure 4.8.8. ^{13}C NMR Spectrum of **P4** (125 MHz, CDCl$_3$)

126

Figure 4.8.9. ^{1}H NMR Spectrum of P3 (500 MHz, CDCl$_3$)

Figure 4.8.10. ^{13}C NMR Spectrum of P3 (125 MHz, CDCl$_3$)
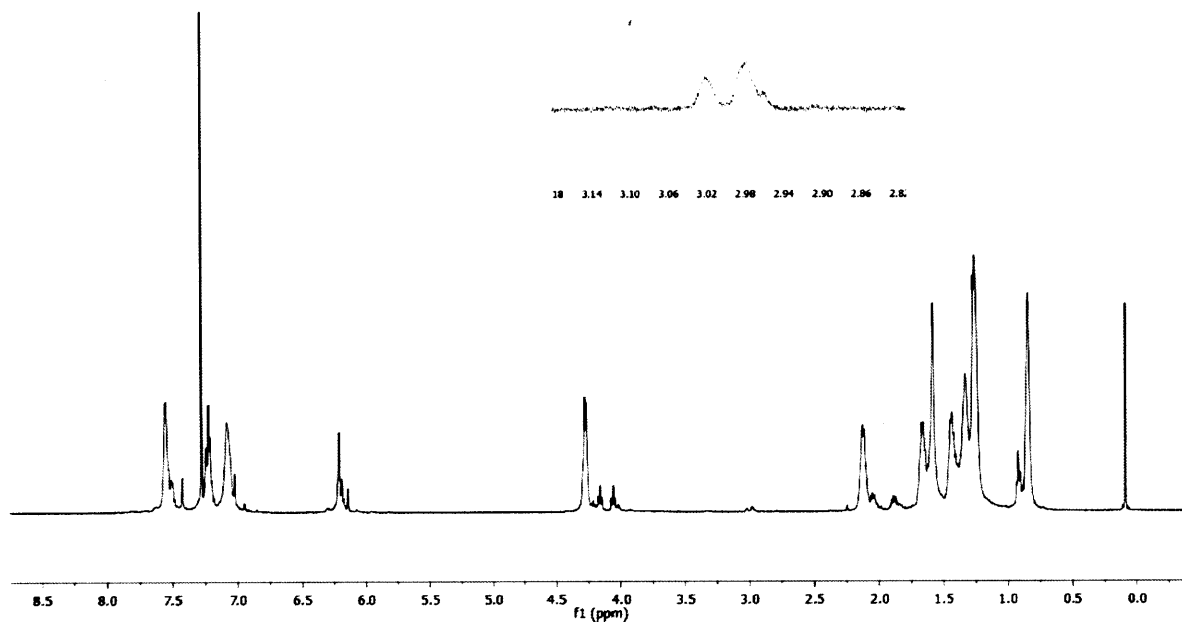
Figure 4.8.11. ^{1}H NMR Spectrum of **P2** (501 MHz, CDCl$_3$)
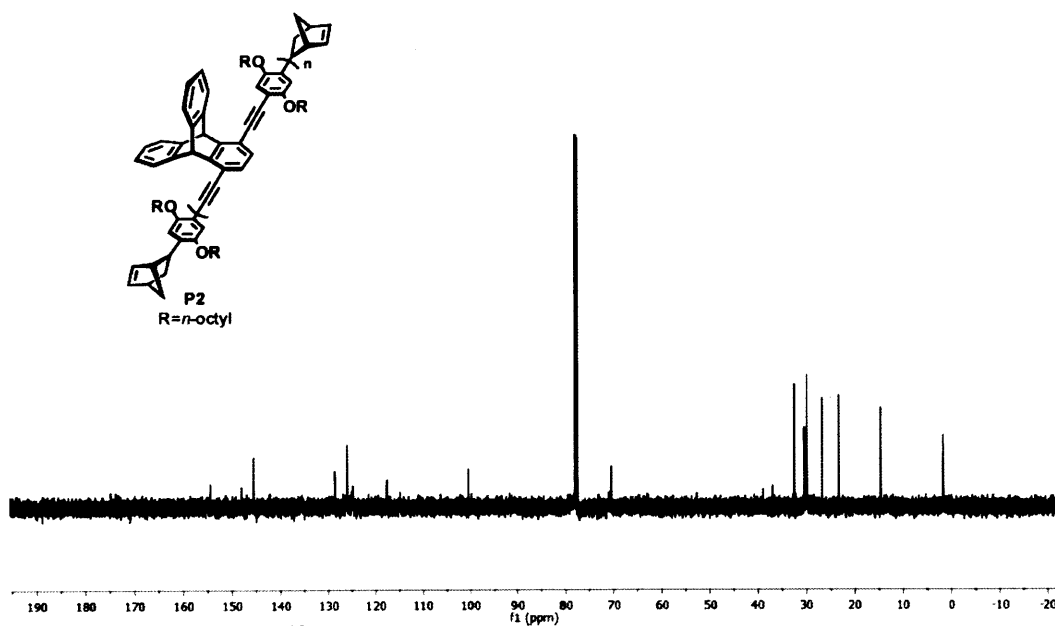
Figure 4.8.12. ^{13}C NMR Spectrum of **P2** (125 MHz, CDCl$_3$)
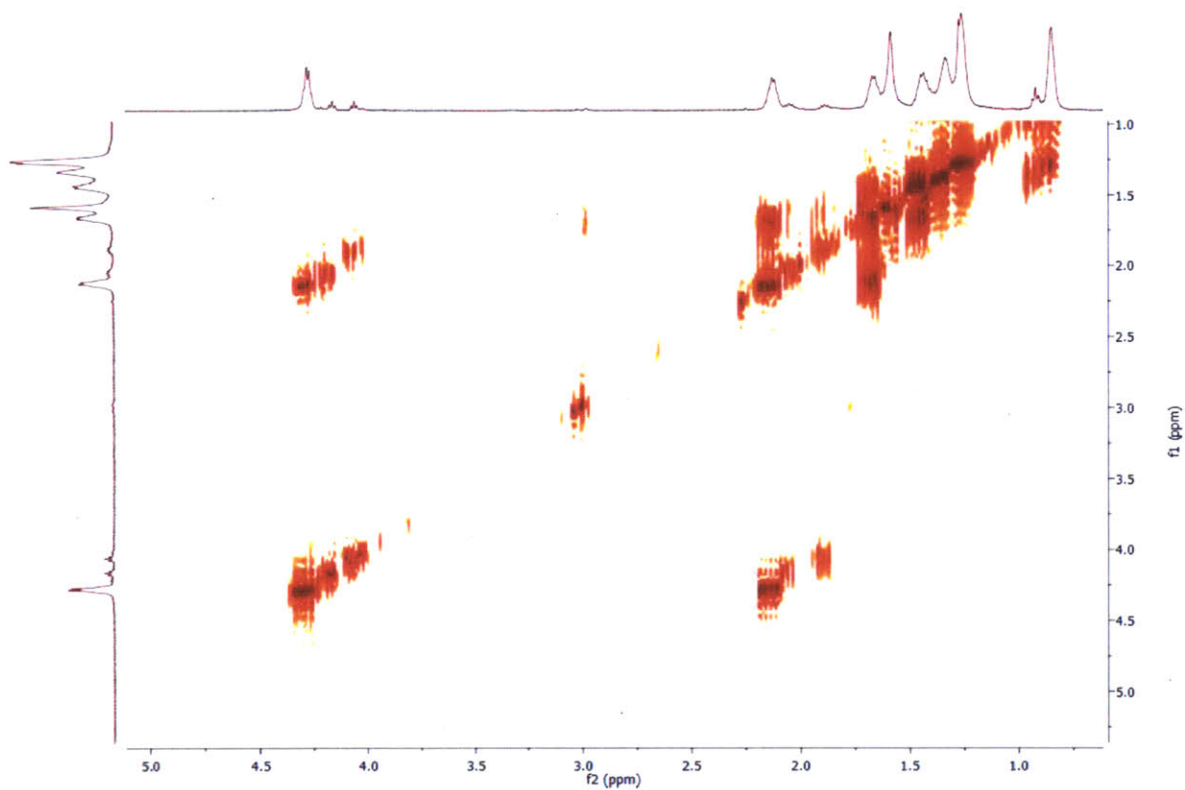
Figure 4.8.13. gCOSY Spectrum of **P2** (501 MHz, CDCl₃)
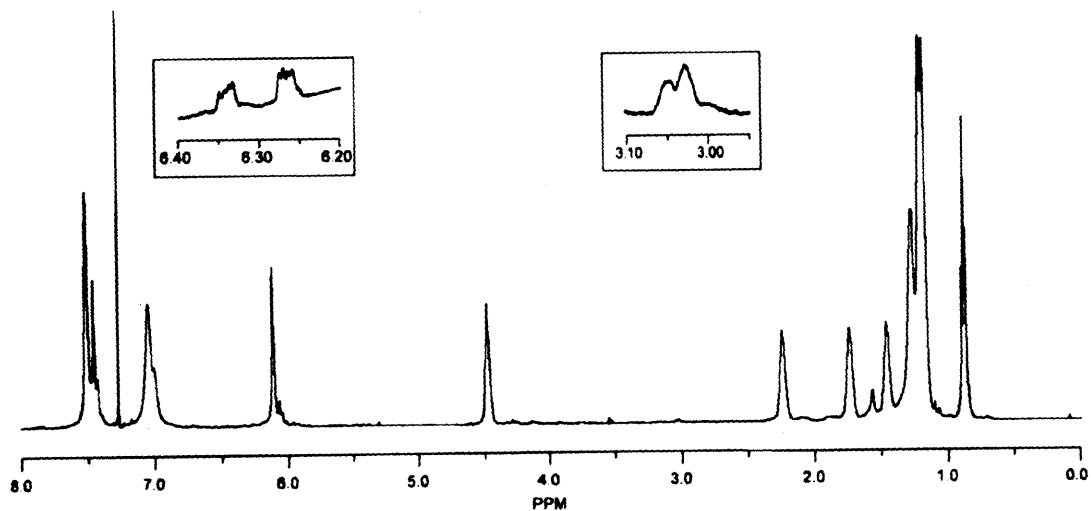
Figure 4.8.14. ^{1}H NMR Spectrum of **P1** (500 MHz, CDCl$_3$)
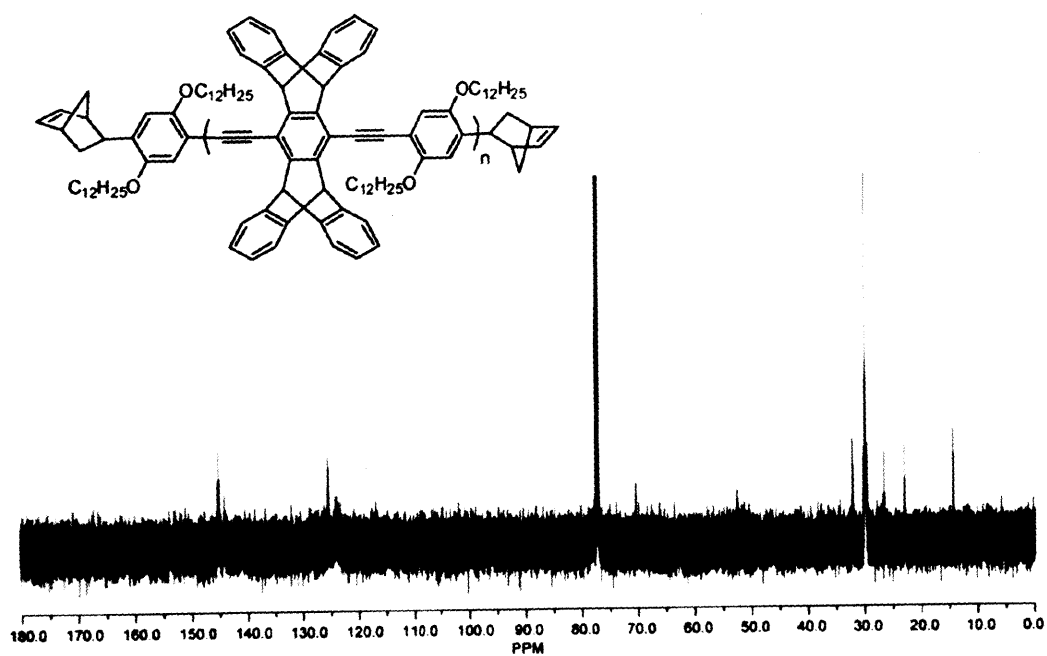
Figure 4.8.15. ^{13}C NMR Spectrum of **P1** (125 MHz, CDCl$_3$)

130
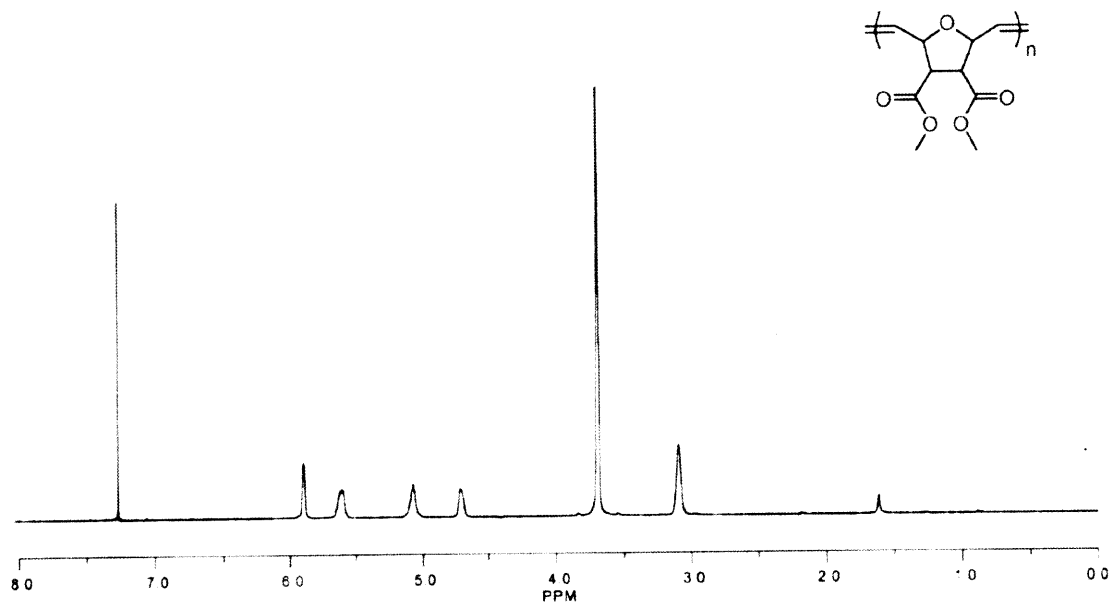
Figure 4.8.16. ^{1}H NMR Spectrum of **PNB5** (500 MHz, CDCl$_3$)
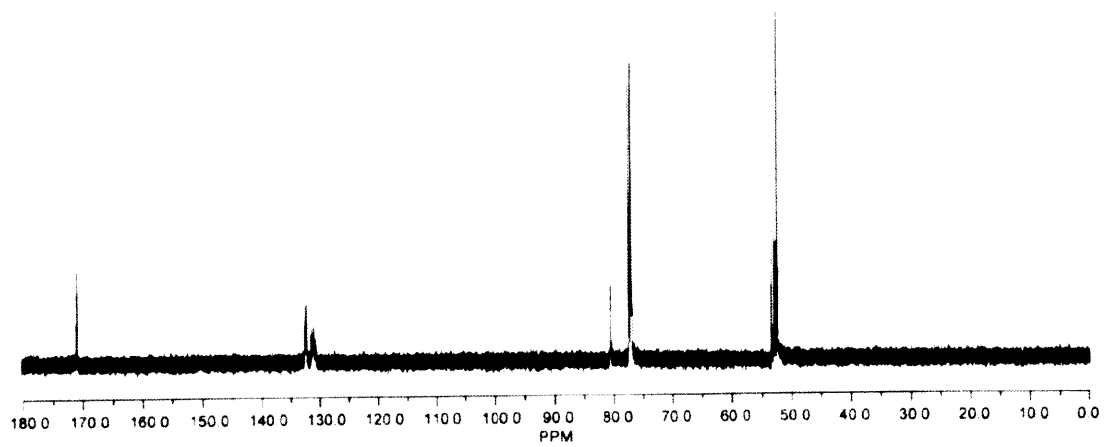
Figure 4.8.17. ^{13}C NMR Spectrum of **PNB5** (125 MHz, CDCl$_3$)
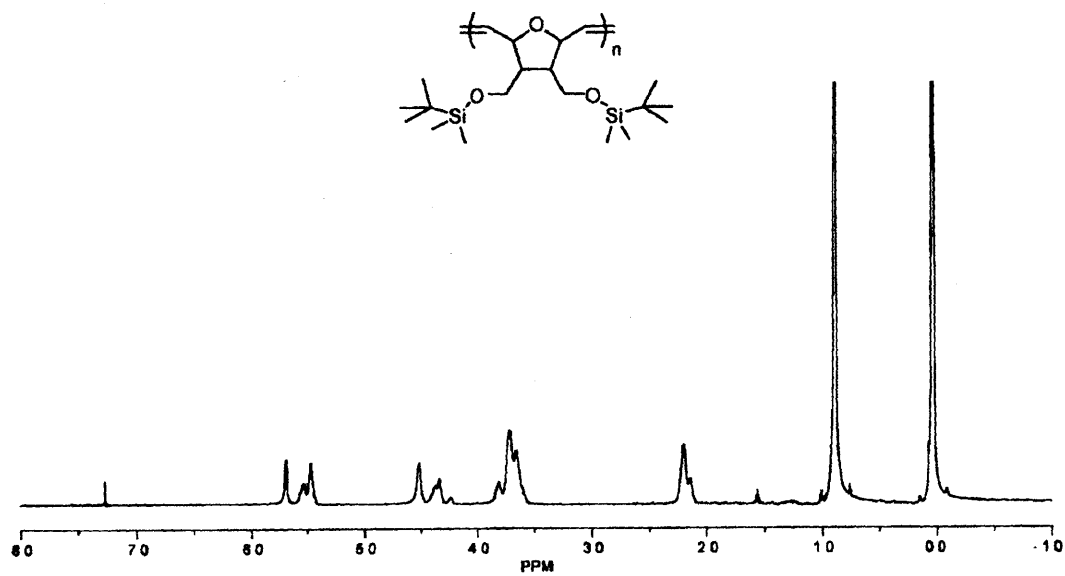
Figure 4.8.18. ^{1}H NMR Spectrum of **PNB6** (500 MHz, CDCl$_3$)
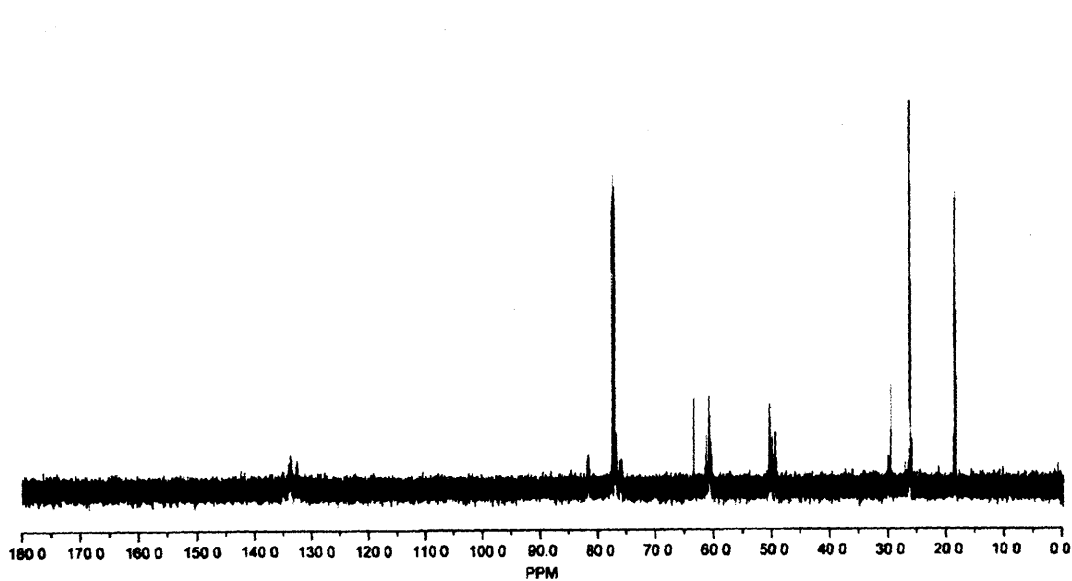
Figure 4.8.19. ^{13}C NMR Spectrum of **PNB6** (125 MHz, CDCl$_3$)

132

R= 2-ethylhexyl
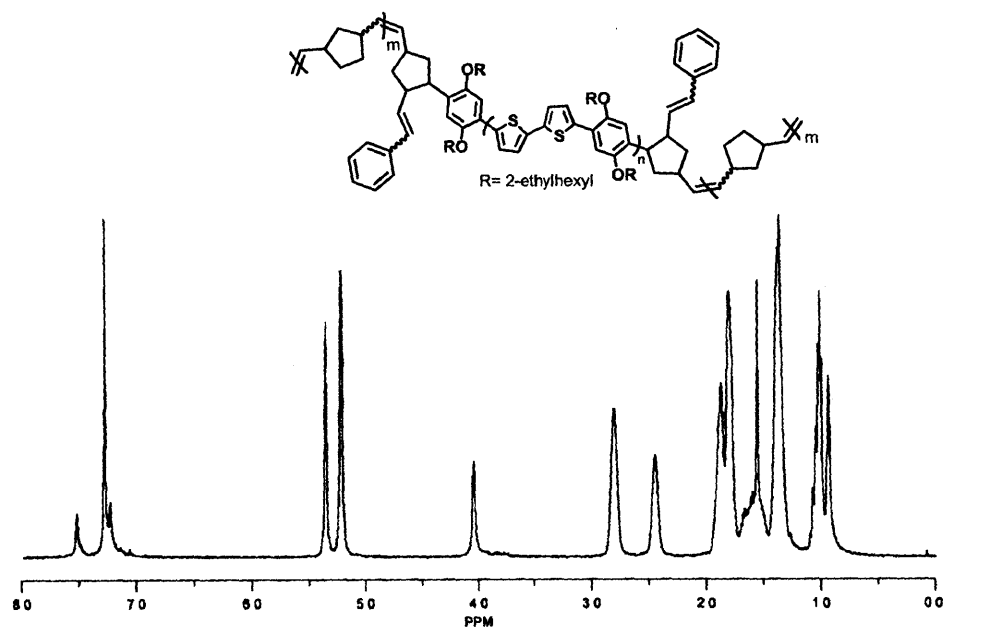
Figure 4.8.20. ^{1}H NMR Spectrum of PNB-**P4**-PNB (500 MHz, CDCl$_3$)

R= C$_8$H$_{17}$
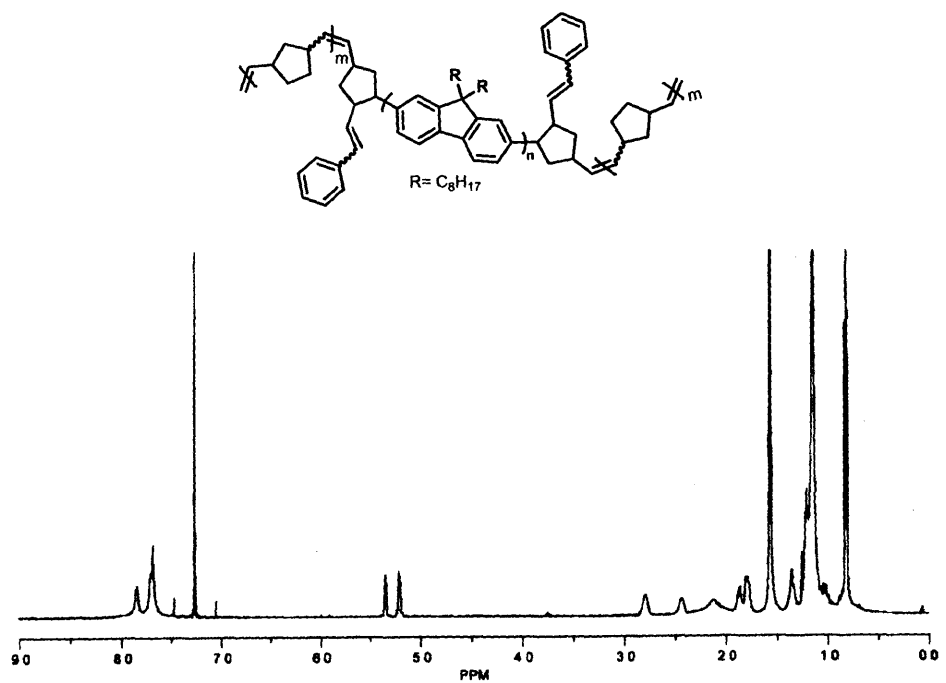
Figure 4.8.21. ^{1}H NMR Spectrum of PNB-**P3**-PNB (500 MHz, CDCl$_3$)

133

R= C$_{12}$H$_{25}$
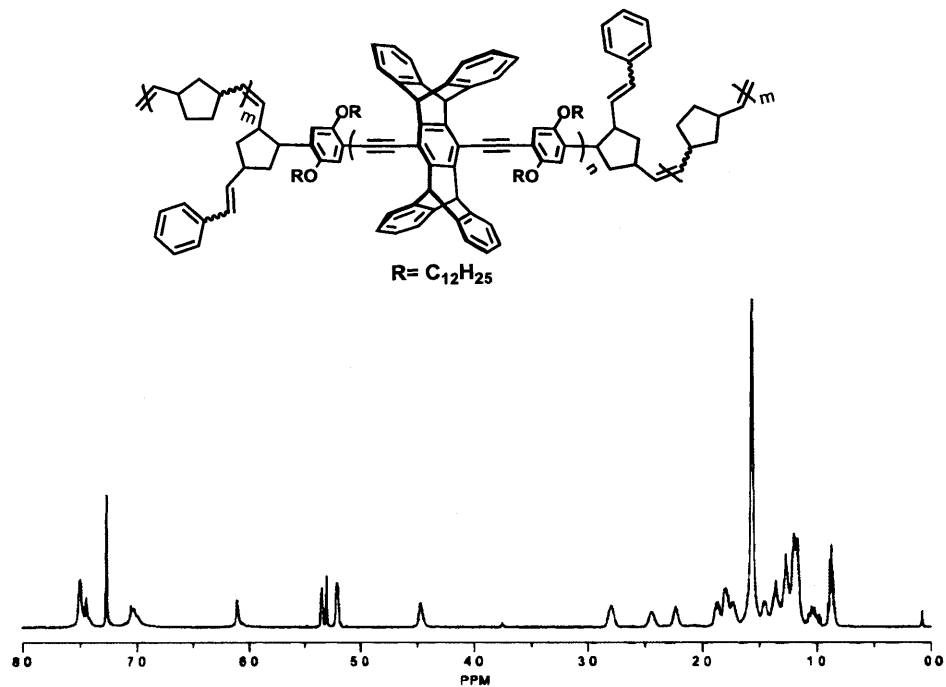
Figure 4.8.22. ^{1}H NMR Spectrum of PNB-**P1**-PNB (500 MHz, CDCl$_3$)

R= 2-ethylhexyl
R$_2$= CO$_2$Me
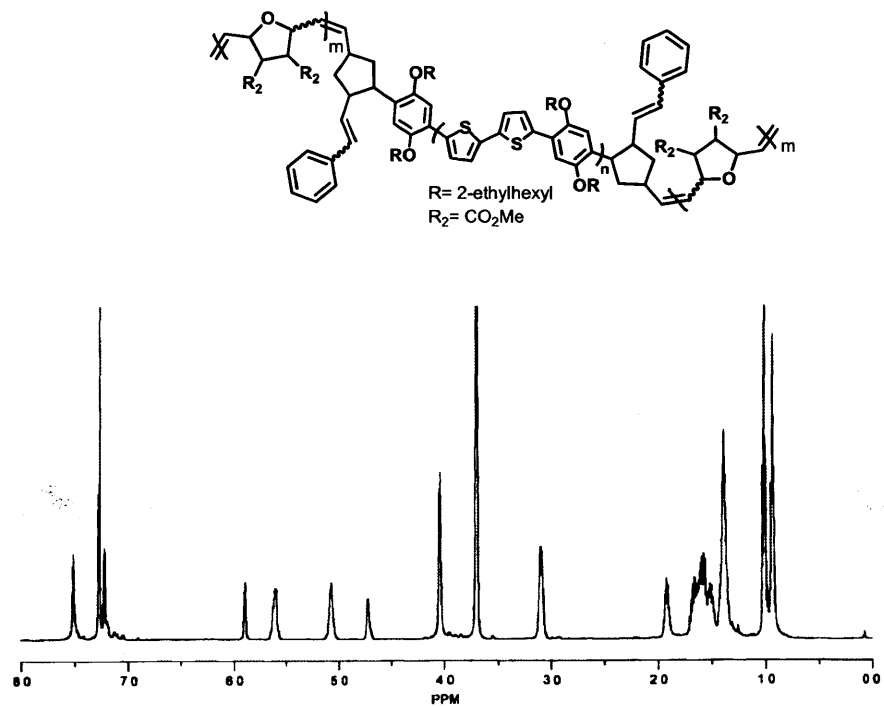
Figure 4.8.23. ^{1}H NMR Spectrum of **PNB5-P4-PNB5** (500 MHz, CDCl$_3$)

134

R= C8H17
R2= CO2Me
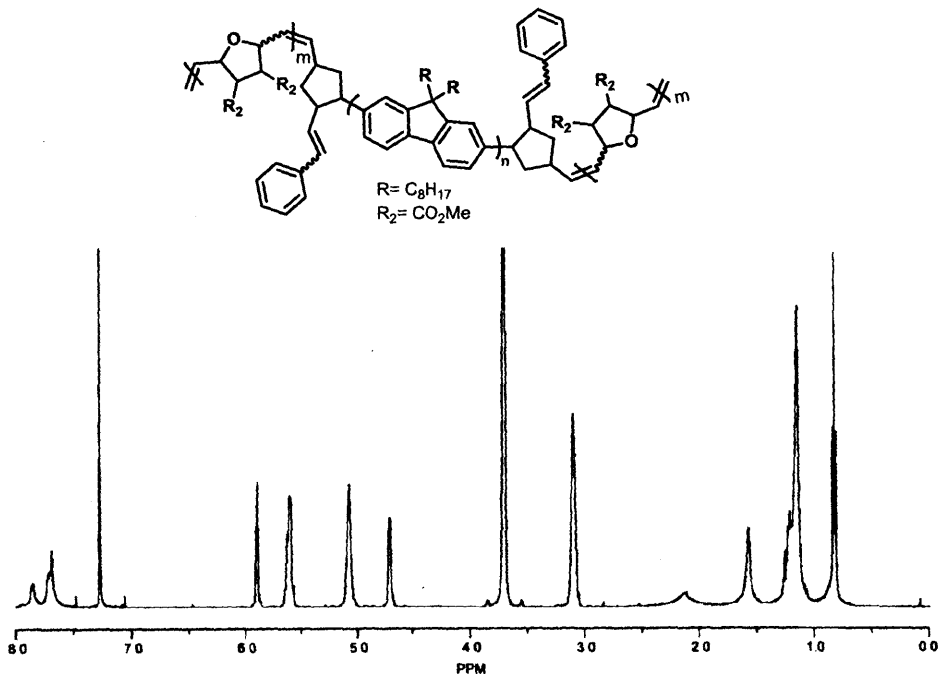
Figure 4.8.24. ^{1}H NMR Spectrum of **PNB5-P3-PNB5** (500 MHz, CDCl3)

R= C12H25
R2= CO2Me
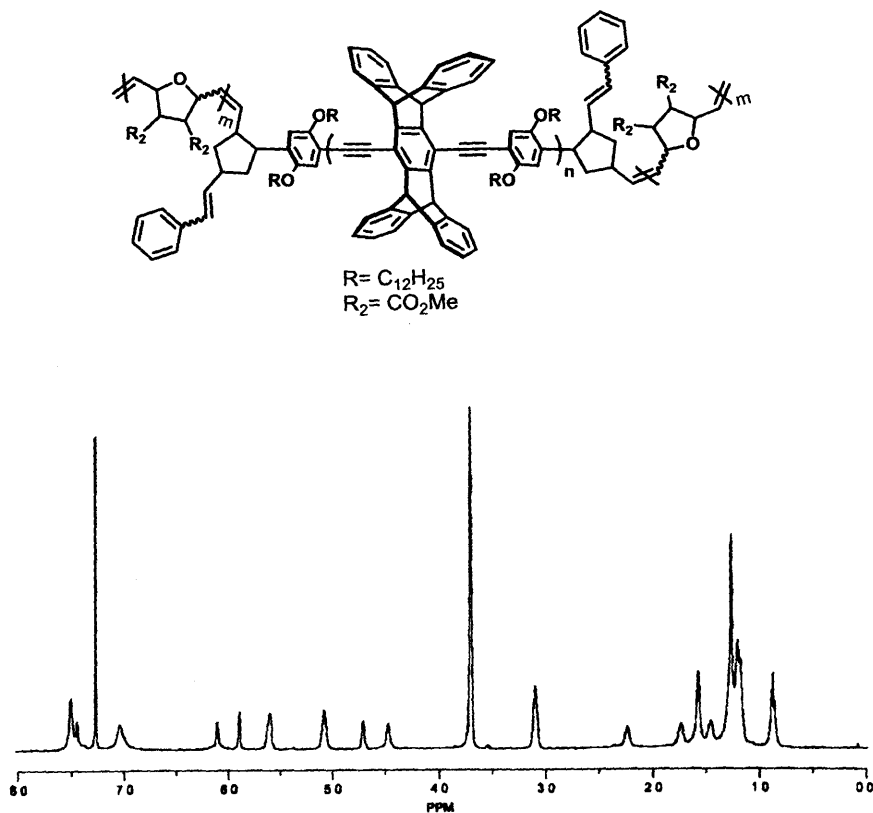
Figure 4.8.25. ^{1}H NMR Spectrum of **PNB5-P1-PNB5** (500 MHz, CDCl3)

135
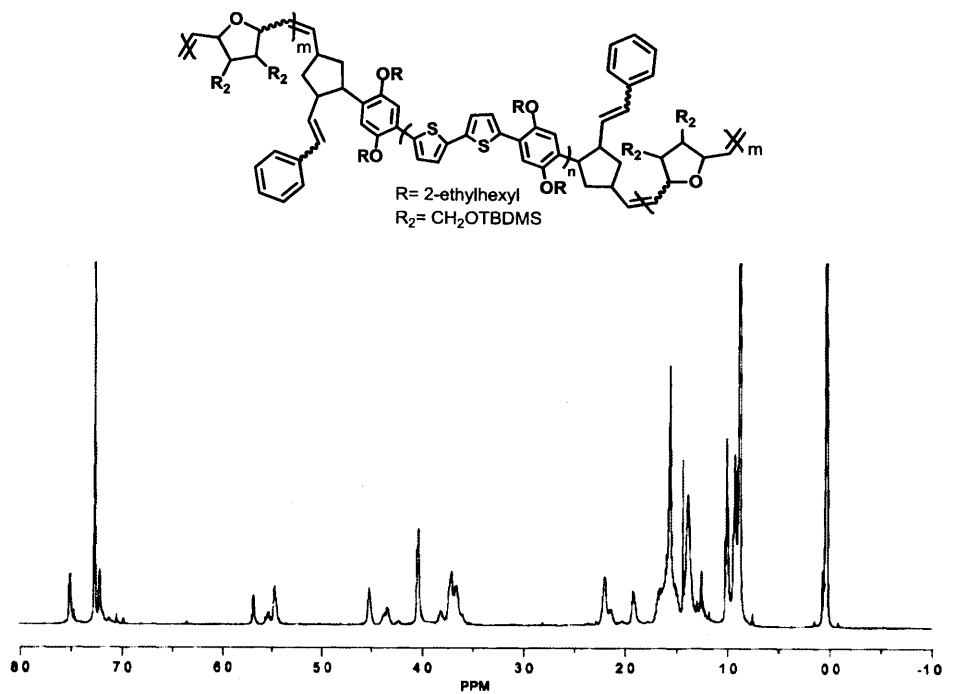
Figure 4.8.26. ^{1}H NMR Spectrum of **PNB6-P4-PNB6** (500 MHz, CDCl$_3$)

4.9 References

(1) For a review see: Cheng, Y.-J.; Yang, S.-H.; Hsu, C.-S. *Chem. Rev.* **2009**, *109*, 5868.

(2) (a) Rahman, M. H.; Liao, S.-C.; Chen, H.-L.; Chen, J.-H.; Ivanov, V. A.; Chu, P. P. J.; Chen, S.-A. *Langmuir* **2009**, *25*, 1667. (b) Gunes, S.; Neugebauer, H.; Sariciftci, N. S. *Chem. Rev.* **2007**, *107*, 1324. (c) Thompson, B. C.; Frechét, J. M. J. *Angew. Chem., Int. Ed.* **2008**, *47*, 58. (d) Kraft, A.; Grimsdale, A. C.; Holmes, A. B. *Angew. Chem., Int. Ed.* **1998**, *37*, 402. (e) *Electrochromism: Fundamentals and Applications*; Monk, P. M. S.; Mortimer, R. J.; Rosseinsky, D. R. Eds.; VCH: Weinheim, 1995. (f) Sapp, S. A.; Sotzing, G. A.; Reynolds, J. R. *Chem. Mater.* **1998**, *10*, 2101. (g) Swager, T. M. *Acc. Chem. Res.* **1998**, *31*, 201. (h) McQuade, D. T.; Pullen, A. E.; Swager, T. M. *Chem. Rev.* **2000**, *100*, 2537.

(3) For a recent discussion on the synthesis of block copolymers containing conjugated blocks, see the following and references cited therein: Brochon, C.; Hadziioannou, G. *ACS Symp. Ser.* **2009**, *1023*, 243.

(4) (a) Liu, J. S.; Sheina, E.; Kowalewski, T.; McCullough, R. D. *Angew. Chem., Int. Ed.* **2002**, *41*, 329. (b) Iovu, M. C.; Jeffries-EL, M.; Sheina, E. E.; Cooper, J. R.; McCullough, R. D. *Polymer* **2005**, *46*, 8582. (c) Iovu, M. C.; Craley, C. R.; Jeffries-EL, M.; Krankowski, A. B.; Zhang, R.; Kowalewski, T.; McCullough, R. D. *Macromolecules* **2007**, *40*, 4733.

(5) (a) Arcadi, A.; Marinelli, F.; Bernocchi, E.; Cacchi, S.; Ortar, G. *J. Organomet. Chem.* **1989**, *368*, 249. (b) Larock, R. C.; Johnson, P. L. *J. Chem. Soc., Chem. Commun.* **1989**, 1368.

(6) Cortese, N. A.; Heck, R. F. *J. Org. Chem.* **1977**, *42*, 1743.

(7) Trnka, T. M.; Grubbs, R. H. *Acc. Chem. Res.* **2001**, *34*, 18.

(8) Choi, T.-L.; Grubbs, R. H. *Angew. Chem., Int. Ed.* **2003**, *42*, 1743.

(9) Lee, L.-B. W.; Register, R. *Macromolecules* **2005**, *38*, 1216.

(10) Weder, C.; Wrighton, M. S. *Macromolecules* **1996**, *29*, 5157.

(11) Gu, T.; Nierengarten, J.-F. *Tetrahedron Lett.* **2001**, *42*, 3175.

(12) Bao, Z.; Chen, Y.; Cai, R.; Yu, L. *Macromolecules* **1993**, *26*, 5281.

(13) Kilbinger, A. F. M.; Feast, W. J. *J. Mater. Chem.* **2000**, *10*, 1777.

(14) Cho, S.; Grimsdale, A. C.; Jones, D. J.; Watkins, S. E.; Holmes, A. B. *J. Am. Chem. Soc.* **2007**, *129*, 11910.

(15) Brion, F. *Tetrahedron Lett.* **1982**, *23*, 5299.

(16) Arjona, O.; Medel, R.; Plumet, J.; Herrera, R.; Jiménez-Vázquez, H. A.; Tamariz, J. *J. Org. Chem.* **2004**, *69*, 2348.

(17) Zhu, Z.; Swager, T. M. *Org. Lett.* **2001**, *3*, 3471.

Jason R. Cox

Organic Materials Chemist

32 Providence St   Mobile: 508-579-3609
Unit #5   Email: *jrcox3@mit.edu*
Worcester, MA 01604

Education	MASSACHUSETTS INSTITUTE OF TECHNOLOGY (MIT)	CAMBRIDGE, MA
	Ph.D. in Organic Chemistry	JUNE 2012
	Advisor: Professor Timothy M. Swager (*tswager@mit.edu*)	

WORCESTER POLYTECHNIC INSTITUTE (WPI)   WORCESTER, MA
M.S. in Chemistry   JUNE 2009
Advisor: Dr. Venkat R. Thalladi (*vthalladi@gmail.com*)

WORCESTER POLYTECHNIC INSTITUTE (WPI)   WORCESTER, MA
B.S. in Chemistry with Distinction   JUNE 2005

Experience   MIT, DEPARTMENT OF CHEMISTRY   CAMBRIDGE, MA
Graduate Research Assistant   2008-PRESENT

- Focused on the rational design, synthesis and application of photoresponsive polymeric coatings capable of aligning nematic liquid crystalline phases.
- Designed and synthesized new organic chromophores with pendant receptors for trace detection of energetic materials in collaboration with Edgewood Chemical Biological Center (ECBC).
- Designed and synthesized organic electronic materials suitable as electron-accepting units in organic photovoltaic applications.
- Trained over 50 researchers in atomic force microscopy (AFM), fluorescence spectroscopy, and UV-Vis spectroscopy.
- Mentored 1 visiting undergraduate student in organic synthesis, purification and characterization.
- Familiar with NMR, GPC, FT-IR, AFM, and DSC analysis of polymers and small molecules.

UNITED STATES MARINE CORPS RESERVES   DEVENS, MA
Infantry Platoon Sergeant   2003-2011

- Supervised the training, welfare and combat operations of a platoon of infantry Marines.
- Redesigned the perimeter security systems of a forward operating base (FOB) during a combat deployment to Fallujah, Iraq.
- Designed and implemented a thermal sensor for the detection of improvised explosive devices (IEDs) while deployed to Fallujah, Iraq. This work resulted in a Navy Achievement Medal (NAM) and was featured by a number of media outlets.

Jason R. Cox

WPI, DEPARTMENT OF CHEMISTRY   WORCESTER, MA
Graduate Research Assistant   2005-2009

- Fabricated self-assembled monolayers (SAMs) capable of controlling the polymorphism of active pharmaceutical ingredients (APIs).
- Familiar with surface characterization using GATR-IR, contact angle goniometry and electrochemistry.
- Synthesized and characterized polymorphs of APIs using various crystallization techniques.
- Familiar with powder X-ray diffraction (PXRD), FT-IR, DSC and TGA analysis of organic solids. Specifically, in the identification of different polymorphs.
- Mentored 3 undergraduate students in the fabrication and applications of SAMs.
- Performed as a teaching assistant for four semesters of general chemistry.

Publications

- **Jason R. Cox**, Marta Dabros, Jeanne A. Shaffer, and Venkat R. Thalladi. "Selective Growth of the Anhydrous and Monohydrate Forms of Theophylline on Self-Assembled Monolayers." *Angew. Chem. Int. Ed.* **2007**, *46*, 1988.
- **Jason R. Cox**, Lori Ferris, and Venkat R. Thalladi. "Selective Growth of a Stable Drug Polymorph by Suppressing the Nucleation of Corresponding Metastable Polymorph." *Angew. Chem. Int. Ed.* **2007**, *46*, 4333.
- Trisha L. Andrew, **Jason R. Cox** and Timothy M. Swager. "Synthesis, Reactivity, and Electronic Properties of 6,6-Dicyanofulvenes." *Org. Lett.* **2010**, *12*, 5302.
- **Jason R. Cox**, Peter Müller, and Timothy M. Swager. "Interrupted Energy Transfer: Highly Selective of Cyclic Ketones in the Vapor Phase." *J. Am. Chem. Soc.* **2011**, *133*, 12910.
- **Jason R. Cox** and Timothy M. Swager. "The Di-π-Methane Rearrangement as a Vehicle for the Photoalignment of Liquid Crystal Mesogens." *Manuscript in preparation.*
- **Jason R. Cox**, Hyun A. Kang, and Timothy M. Swager. "Norbornene End-Capped Conjugated Polymers: Access to Tri-Block Coplymers via Ring-Opening Metathesis Polymerization." *Manuscript in preparation.*

Patents

- **Jason R. Cox**, Marta Dabros, and Venkat R. Thalladi. "Selective Growth of Stable Polymorphs." US Application 20110009623 (1/13/2011).

Conferences

- **Jason R. Cox** and Timothy M. Swager. "Interrupted Energy Transfer: Highly Selective of Cyclic Ketones in the Vapor Phase." Poster presentation in Gordon Research Conference (Polymers), Mount Holyoke College, MA, June **2011**.

Awards

- **Corning Fellowship (MIT)**   2009
- **Sigma Xi Membership (WPI)**   2008

Jason R. Cox

- **American Institute of Chemists Award (WPI)**   2008
- **Navy Achievement Medal (USMC)**   2008
- **GRAD 2007 for most outstanding research (WPI-campus wide)**   2007
- **Certificate of Commendation (USMC)**   2006
- **Combat Meritorious Promotion (USMC)**   2006
- **Presidential Major Qualifying Project Award for Thesis (WPI)**   2005

ACKNOWLEDGEMENTS

I must begin by thanking my advisor, Professor Timothy Swager, for instilling in me the passion and scientific creativity that is a staple of his personality and leadership style. His sense of humor and understanding have made the past four years some of my most memorable years.

I would also like to thank Professors Buchwald and Fu for serving on my committee. Their guidance and suggestions have been excellent and are greatly appreciated. Professor Joannopoulos has also served as a mentor during my time at the ISN and his commitment to ensuring the safety of our service members is unparalleled.

The research described in this thesis, and countless others, would not have been possible without the hard work of Kathy and Caitlin at Building 18 and Steve, Bill, John, Franklin, Maureen, Josh, Kurt, Marlisha, Ivan, Donna and Amy at the ISN.

The past four years in the Swager group have been amazing. I have to thank Brett, John, and Derek for all of the time spent at the board discussing chemistry, it will certainly be missed when I leave. My ISN-mates John, Yu Lin, Derek, Carlos, Stefanie, and Lionel have been excellent colleagues and I appreciate all of their advice/help in numerous endeavors over the years. I also would like to thank my colleagues at Building 18 - Jan, Olesya, Joel, Shuang, Eilaf, Birgit, Yossi, Dave, and Jeewoo – for all of their assistance and guidance.

Finally, I have to thank my beautiful wife Maegan and wonderful daughter Norah for all of their support and understanding these years. It has been such a long, long journey but I know the best years are yet to come!